

## **Oskarshamn site investigation**

### **Interpretation of airborne geophysical survey data**

**Helicopter borne survey data of gamma  
ray spectrometry, magnetics and EM from  
2002 and fixed wing airborne survey data  
of the VLF-field from 1986**

Carl-Axel Triumf, Hans Thunehed  
GeoVista AB

Leif Kero, Lena Persson  
Sveriges Geologiska Undersökning

October 2003

#### **Svensk Kärnbränslehantering AB**

Swedish Nuclear Fuel  
and Waste Management Co  
Box 5864  
SE-102 40 Stockholm Sweden  
Tel 08-459 84 00  
+46 8 459 84 00  
Fax 08-661 57 19  
+46 8 661 57 19



## **Oskarshamn site investigation**

### **Interpretation of airborne geophysical survey data**

### **Helicopter borne survey data of gamma ray spectrometry, magnetics and EM from 2002 and fixed wing airborne survey data of the VLF-field from 1986**

Carl-Axel Triumf, Hans Thunehed  
GeoVista AB

Leif Kero, Lena Persson  
Sveriges Geologiska Undersökning

October 2003

**Keywords:** Airborne geophysics, Interpretation, Magnetic total field, VLF, Multi-frequency EM, Spectrometry, Inversion, Two-layer earth, Helicopter-borne, Lineament, Magnetic susceptibility, Resistivity, Conductivity, Modelling, Lithology, Rock type, Structures, Overburden thickness, Soil type, Water depth, Euler deconvolution.

This report concerns a study which was conducted for SKB. The conclusions and viewpoints presented in the report are those of the authors and do not necessarily coincide with those of the client.

A pdf version of this document can be downloaded from [www\(skb.se](http://www(skb.se)

# Contents

<b>1</b>	<b>Introduction</b>	5
<b>2</b>	<b>Objective and scope</b>	7
<b>3</b>	<b>Equipment</b>	8
3.1	Description of equipment	8
<b>4</b>	<b>Execution</b>	9
4.1	Post-processing of air borne geophysical survey data	9
4.1.1	Gamma ray spectrometry from the helicopter borne survey of 2002	9
4.1.2	Magnetic total field from the helicopter borne survey 2002	11
4.1.3	Euler deconvolution of the magnetic total field data from the helicopter borne survey of 2002	14
4.1.4	Fixed-wing air-borne VLF (1986)	17
4.1.5	Helicopter borne multi-frequency EM (2002)	20
4.1.6	Helicopter borne VLF (2002)	31
4.1.7	Miscellaneous	32
4.2	Interpretation	36
4.2.1	Gamma ray spectrometry from the helicopter borne survey of 2002	36
4.2.2	Magnetic total field from the helicopter borne survey 2002	37
4.2.3	Electromagnetic data	37
<b>5</b>	<b>Results</b>	39
5.1	Identification of homogeneity areas at the ground surface from helicopter borne gamma ray spectrometry	39
5.1.1	Background	39
5.1.2	Identified areas with homogeneous distribution pattern and content of K, U and Th in helicopter borne gamma ray spectrometry	39
5.2	Identification of homogeneity volumes and lineaments from helicopter borne measurements of the magnetic total field	51
5.2.1	Background	51
5.2.2	Qualitative interpretation of data over the magnetic total field from the helicopter borne survey 2002	52
5.2.3	Quantitative interpretation of data over the magnetic total field from the helicopter borne survey 2002	59
5.3	Identification of homogeneity volumes and lineaments from airborne EM-measurements	65
5.3.1	Background	65
5.3.2	Interpretation of multi-frequency EM-data from the helicopter-borne survey 2002	65
5.3.3	Interpretation of VLF-data from the helicopter-borne survey 2002	75
5.3.4	Interpretation of VLF-data from the fixed-wing airborne survey 1986	77
5.4	Discussion	78
	<b>References</b>	79

<b>Appendix A</b>	Euler deconvolution of magnetic total field data from the helicopter borne measurements at Simpevarp (in Swedish)	81
<b>Appendix B</b>	Specifikationer för fortsatt arbete med tolkningsmetoder för flyg-EM data	91

# 1 Introduction

This document reports the results gained in the interpretation of airborne geophysical survey data which is one of the activities performed within the site investigation at Oskarshamn.

The interpretation activity reported is part of a frame work of surveys containing also preceding activities of similar nature. One early activity in the site investigation was the identification of possible lineaments and lithological inhomogenities which was carried out in the late 2002, with the aim to select a priority site west of the Simpevarp peninsula /1/. Part of that activity was based on preliminary processed data from the helicopter borne survey of 2002 /2/ and from an air borne photo session from 2001 /3/. During winter/spring of 2003 a complementary identification of lineaments in the Simpevarp area by the interpretation of topographical data took place /4/. It covered the majority of the regional model area as defined in /5/.

The interpretation activity reported here involves a more profound processing and interpretation of the helicopter borne geophysical survey data as compared to the activities described above. This processing and interpretation, together with an interpretation of earlier collected fixed-wing VLF-data, was conducted by GeoVista AB and Sveriges Geologiska Undersökning (SGU) during the spring and summer of 2003. It followed the instruction and guidelines from SKB (activity plan AP PS 400-03-010 and method description MD 211.003 and 120.001, SKB internal controlling documents) under the supervision of Leif Stenberg, SKB.

The location of the interpreted area is shown in Figure 1-1.

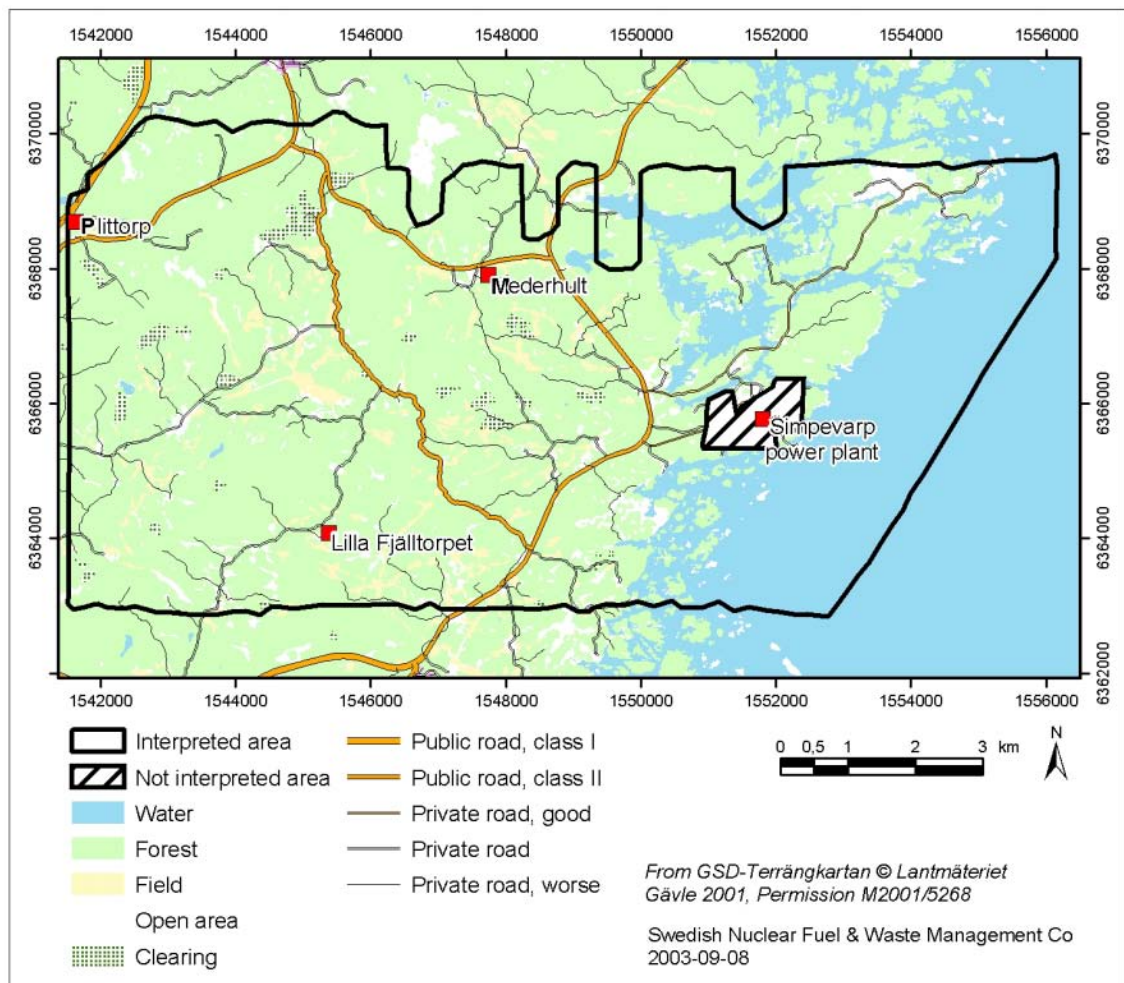


**Figure 1-1.** Location of the interpreted area.

## **2    Objective and scope**

The primary objective of the “Interpretation of airborne geophysical survey data” was to identify, extract and describe the following:

- Lineaments in the geophysical airborne survey data for the structural part of the site descriptive model.
- Surfaces or volumes on and in the ground with homogeneous characteristics regarding petrophysical parameters for future work regarding the geological part of the site descriptive model, both for quaternary geology and bedrock.
- Geometrical information such as thickness of overburden, depth to anomaly sources, dips of anomaly sources etc.

The interpretation work covered the entire area surveyed with helicopter in 2002 /2/.

The results of the interpretation are supposed to be used in future joint interpretation work within the site investigation, where among other data sets from geological field observations and identified lineaments from topography /4/ will be included.

# **3 Equipment**

## **3.1 Description of equipment**

The processing and interpretation work has a pure desk-top study character based on the use of computers with appropriate software. The software used for filtering, transformation, visualisation and Euler deconvolution of geophysical data was the Oasis Montaj (Geosoft Inc). Interpolation to regular grids was made with Oasis Montaj (Geosoft Inc) and Surfer (Golden Software Inc). AGC filtering of electromagnetic data was performed with MathCAD (Mathsoft Inc). The software for inversion of multi-frequency data into a two-layer model was developed at GeoVista AB, see Appendix B (in swedish). The different methods for the processing of VLF-data are developed at Uppsala University and SGU /6/, /7/, /8/. For the 2D-inversion of the VLF profiles, the inversion code Rebocc /9/ was used. Magnetic modelling of profile data was performed with GMM (GeoVista AB). The interpretation and presentation of results was made with MapInfo (MapInfo Corp) and ArcView (ESRI).

## **4 Execution**

In general the processing and interpretation of airborne geophysical survey data follows the SKB internal controlling documents (activity plan AP PS 400-03-010 and method description MD 211.003 and 120.001). Though the guidelines in the method descriptions are followed in general, personal judgements are necessary to introduce in both processing and interpretation. As a consequence some of the steps defined in the ideal process have not been carried out while new ones have been introduced. These deviations, if considered significant, are commented in the text.

The processing and interpretation of air borne geophysical survey data within this reported activity include the following major sub activities:

- post-processing of helicopter borne geophysical survey data,
- interpretation of helicopter borne geophysical survey data,
- interpretation of data from an air borne VLF survey using two transmitter stations (the survey was carried out in 1986),
- preparation of processing results and interpretation results for the data archives of SKB,
- reporting,
- delivery of the products.

### **4.1 Post-processing of air borne geophysical survey data**

#### **4.1.1 Gamma ray spectrometry from the helicopter borne survey of 2002**

The data from the helicopter borne gamma ray spectrometry were delivered as a Geosoft XYZ-file "Simpevarp Radiometrics NS.XYZ". Data are described in /2/.

Geosoft grid-files were created from the xyz-files which were then processed according to Table 4-1. The resulting grids were exported into MapInfo and ArcView. The processed grids which were used in the interpretation are shown in Figures 4-1 and 4-2.

**Table 4-1. Post-processing of helicopter borne gamma ray spectrometry.**

Processed primary data	Post-processing	Resulting GIS image
Simpevarp Radiometrics NS.XYZ	Interpolation of the three channels K, U and Th with Geosofts Bigrid, gridcell size 8 m. Low-pass filtering Butterworth filter, filter order 1, cut-off wave number 0.005 cycles/m. Colour composite K – green, U – blue, Th – red	smp_spec_composite_lp_005.tab (MapInfo-tif) smp_spec_composite_lp_005.tfw (ArcView-tif)
Simpevarp Radiometrics NS.XYZ	Interpolation of the three channels K, U and Th with Geosofts Bigrid, gridcell size 8 m. Normalisation of all three channels $K_{norm} = K/(K+U+Th)$ , $U_{norm} = U/(K+U+Th)$ , $Th_{norm} = Th/(K+U+Th)$ Colour composite $K_{norm}$ – green, $U_{norm}$ – blue, $Th_{norm}$ – red	smp_spec_composite_ratios (MapInfo-tif) smp_spec_composite_ratios (ArcView-tif)

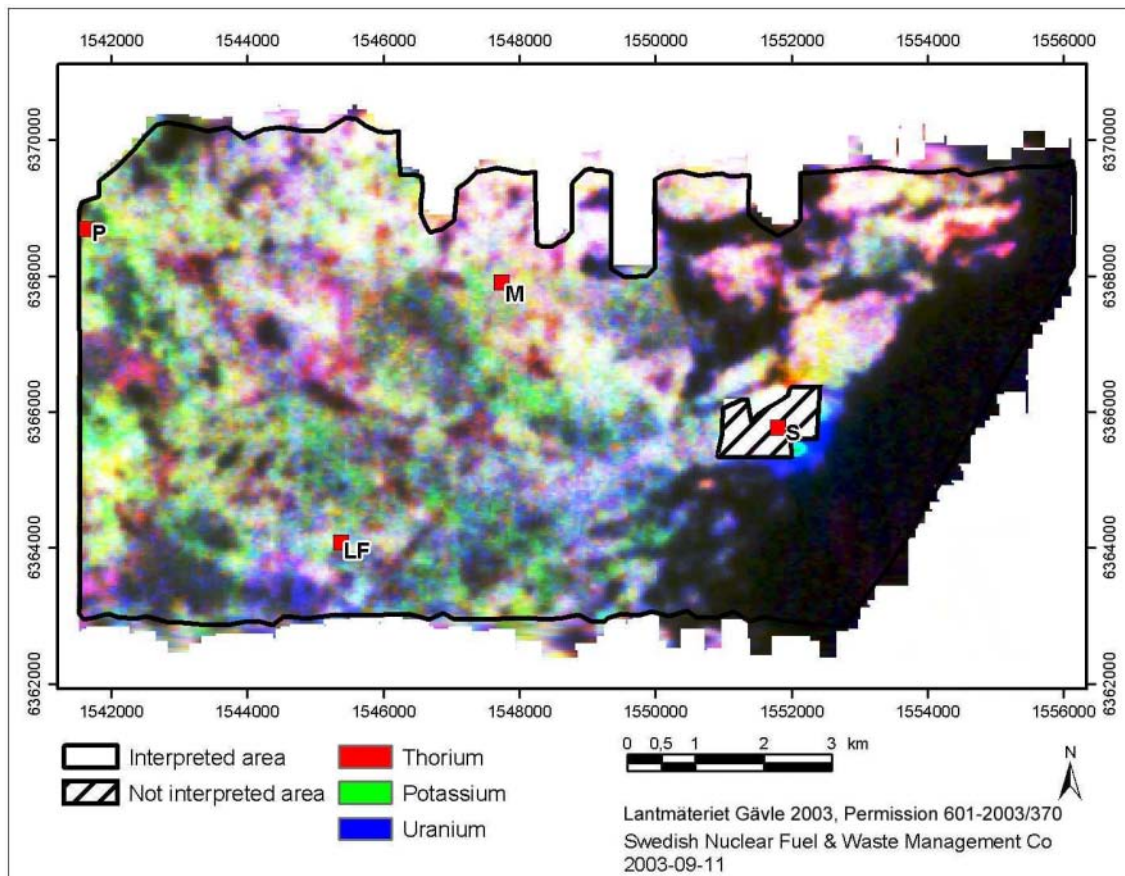


**Figure 4-1.** The grid “smp\_spec\_composite\_lp\_005” shows a composite of the three channels potassium in green, thorium in red and uranium in blue. Low radiation gives a dark colour, high radiation a light colour. As an example a dark bluish colour could mean that the ground surface contains low levels of radiating geological material however with uranium as the dominant element of the three. The area near the nuclear power plants at Simpevarp is masked out. S=Simpevarp power plant, M=Mederhult, LF=Lilla Fjälltorpet and P=Plittorp.

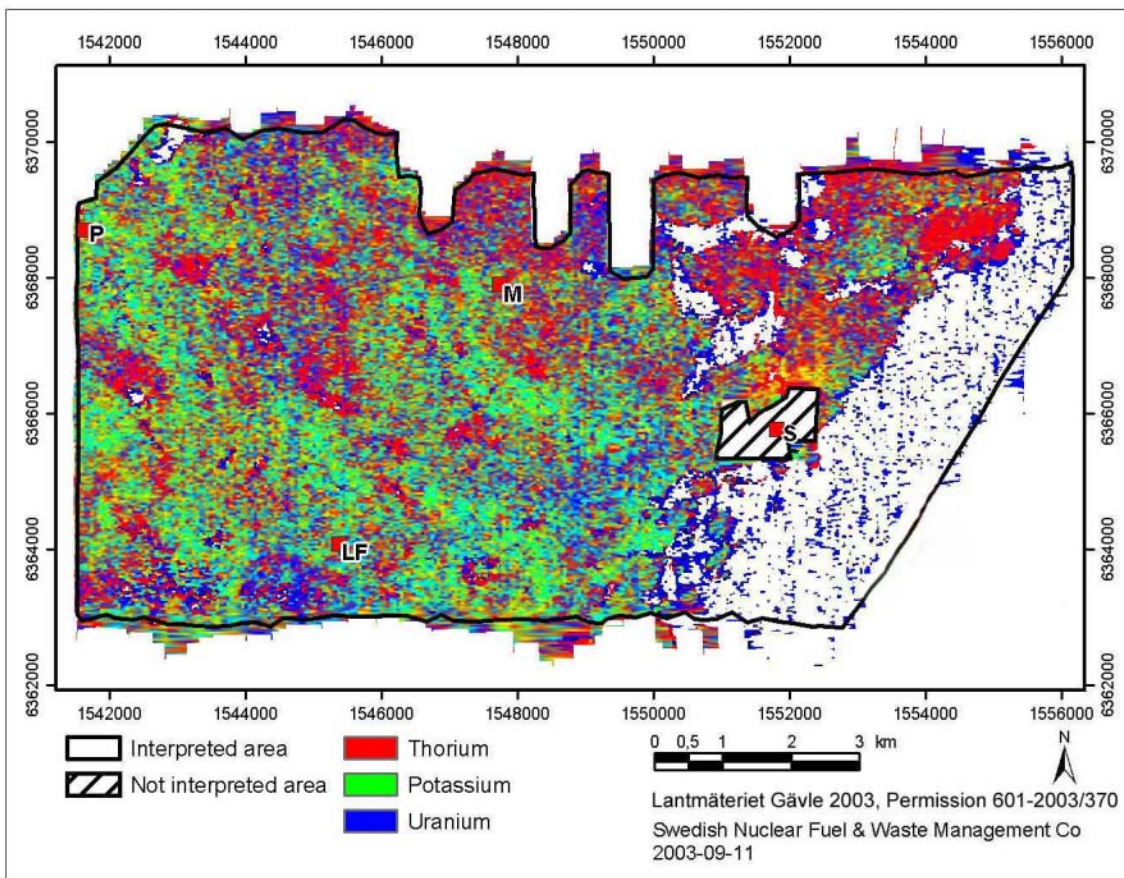


**Figure 4-2.** The grid “*smp\_spec\_composite\_ratios*” shows a composite of the three normalised channels of potassium in green, thorium in red and uranium in blue according to  $K_{norm} = K/(K+U+Th)$ ,  $U_{norm} = U/(K+U+Th)$ ,  $Th_{norm} = Th/(K+U+Th)$ . The area near the nuclear power plants at Simpevarp is masked out. S=Simpevarp power plant, M=Mederhult, LF=Lilla Fjälltorpet and P=Plittorp.

#### 4.1.2 Magnetic total field from the helicopter borne survey 2002

The data from the helicopter borne measurements of the magnetic total field were delivered as a Geosoft XYZ-file “Simpevarp Mag NS”. Data are described in /2/.

Geosoft grid-files were created from the xyz-files which were then processed according to Table 4-2. The resulting grids were exported into MapInfo and ArcView. The processed grids which were used in the interpretation are shown in Figures 4-3 to 4-4.

**Table 4-2. Post-processing of helicopter borne survey data of the magnetic total field.**

Processed primary data	Post-processing	Resulting GIS image
Simpevarp Mag NS.XYZ	Interpolation with Geosofts Bigrid, gridcell size 5 m.	SmpMFL_RTP_MI.tab (MapInfo-tif)
	Reduction to the pole ( $I=71$ degrees, $D=2$ degrees).	SmpMFL_RTP_AV.tfw (ArcView-tif)
	Colour table and vertical illumination is applied.	
Simpevarp Mag NS.XYZ	Interpolation with Geosofts Bigrid, gridcell size 5 m.	SmpMFLRTP_residual_250_MI.tab (MapInfo-tif)
	Reduction to the pole ( $I=71$ degrees, $D=2$ degrees).	SmpMFLRTP_residual_250.tfw (ArcView-tif)
	Upward continuation to 250 m.	
	Subtraction with the upward continued field.	
	Colour table and vertical illumination is applied.	

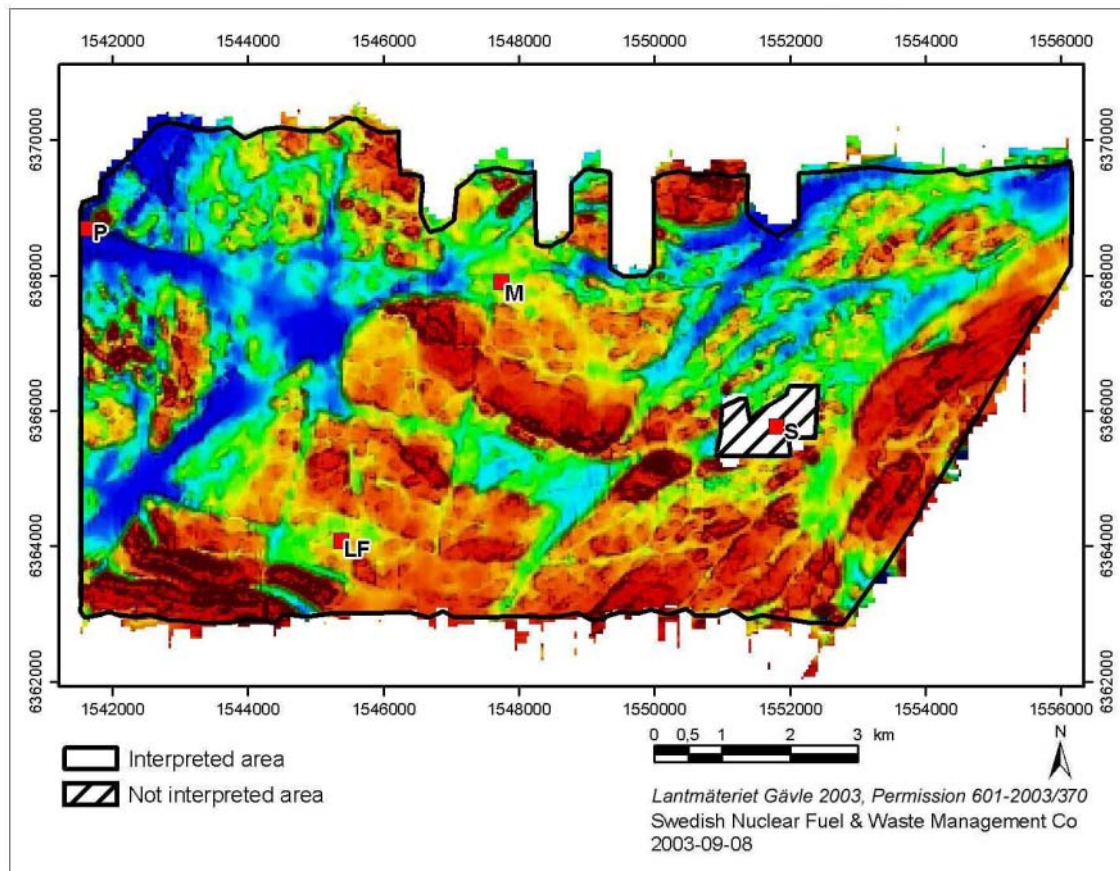


**Figure 4-3.** The grid “SmpMFL\_RTP” in colour shows the magnetic total field reduced to the pole. Low relative levels in the magnetic total field are shown in bluish-greenish colours and high levels in reddish-brownish colours. Shading with vertical inclination of in-coming light enhances gradients. The area near the nuclear power plants at Simpevarp is masked out. S=Simpevarp power plant, M=Mederhult, LF=Lilla Fjälltorpet and P=Plittorp.

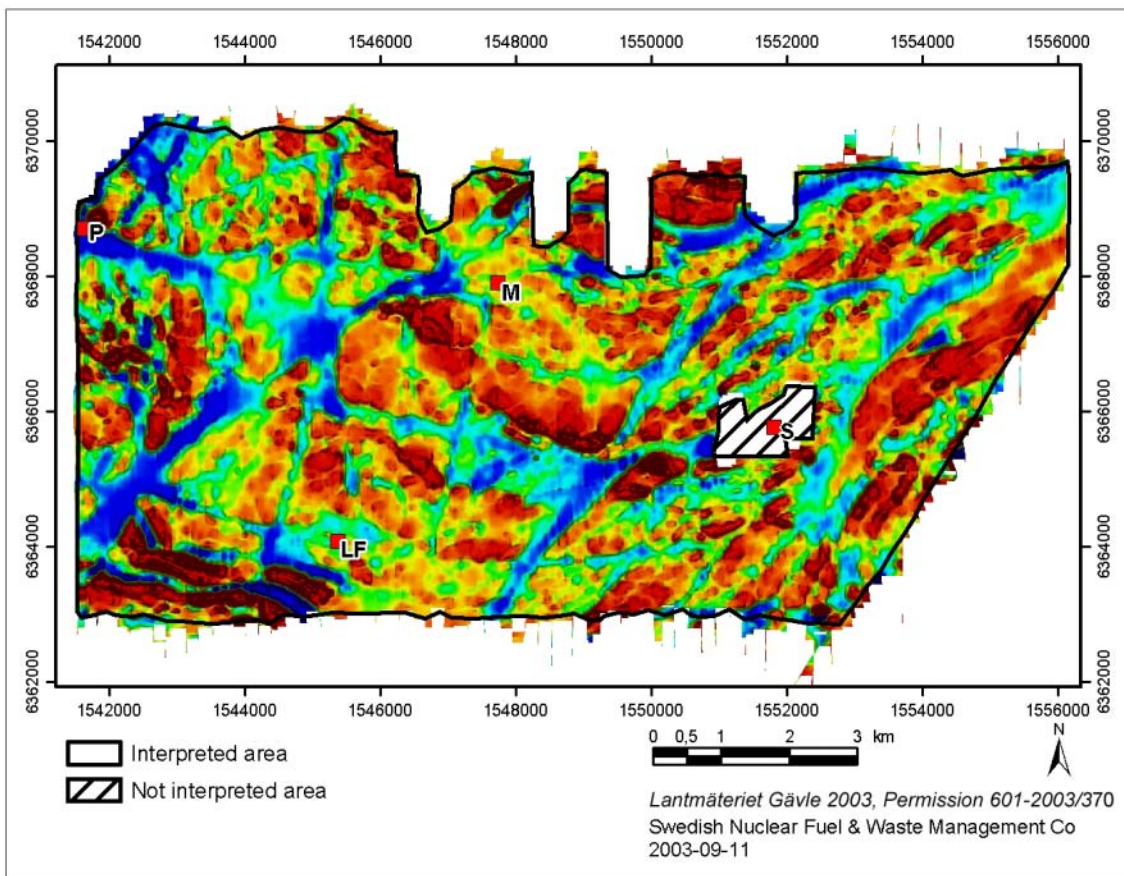


**Figure 4-4.** The grid “SmpMFLRTP\_residual\_250” in colour shows the magnetic total field after reduction to the pole and subtraction of the field from an upward continuation of 250 m. This enhances anomalies from near-surface objects. Low relative levels in the magnetic total field are shown in bluish-greenish colours and high levels in reddish-brownish colours. Shading with vertical inclination of in-coming light enhances gradients. The area near the nuclear power plants at Simpevarp is masked out. S=Simpevarp power plant, M=Mederhult, LF=Lilla Fjälltorpet and P=Plittorp.

Modelling of the response from source bodies in an algorithm allowing 2.5D-models was carried out along three profiles according to Table 4-3. The results are however shown in section 5.2.3.

**Table 4-3. Specification of modelled profiles from the helicopter borne magnetics 2002.**

Profile name	Co-ordinates (RT90 2.5 gon W)
SMP_MAG_MOD_1	Y1,X1 = 6363154/1547362 m, Y2,X2 = 6367764/1549964 m
SMP_MAG_MOD_2	Y1,X1 = 6365471/1554476 m, Y2,X2 = 6368958/1550441 m
SMP_MAG_MOD_3	Y1,X1 = 6363918/1547146 m, Y2,X2 = 6368218/1549248 m

### 4.1.3 Euler deconvolution of the magnetic total field data from the helicopter borne survey of 2002

The data from the helicopter borne measurements of the magnetic total field were delivered as a Geosoft XYZ-file “Simpevarp Mag NS”. Data are described in /2/.

Geosoft grid-files were created from the xyz-files and processed to suit the Euler deconvolution according to a detailed description in Appendix A (in Swedish with English summary) and according to the brief description in Table 4-4. In Appendix A is also given a reference list to the theoretical aspects of Euler deconvolution.

Examples of results from the Euler deconvolution are shown in Figures 4-5 to 4-7.

**Table 4-4. Examples of post-processing of helicopter borne survey data of the magnetic total field in connection to the Euler deconvolution.**

Processed primary data	Post-processing	Resulting GIS image
Simpevarp Mag NS.XYZ	<p>Interpolation with Geosofts Bigrid, gridcell size 10 m.</p> <p>Reduction to the pole (<math>I=71</math> degrees, <math>D=2</math> degrees).</p> <p>Separation into one grid file with flight direction from north to south (_ns), and one with flight direction from south to north (_sn).</p> <p>Upward continuation to 10 m.</p> <p>Geometrical corrections for measurement geometry.</p> <p>Euler deconvolution with structural index 0 (magnetic contact).</p> <p>Recalculation to refer the resulting source depth to the sea level.</p> <p>Presentation of solutions in colour.</p>	Grid_Mag_Euler_0_3x3_10mgrd_ns.tif (ArcView-tif)
Simpevarp Mag NS.XYZ	<p>Interpolation with Geosofts Bigrid, gridcell size 25 m.</p> <p>Reduction to the pole (<math>I=71</math> degrees, <math>D=2</math> degrees).</p> <p>Upward continuation to 25 m.</p> <p>Geometrical corrections for measurement geometry.</p> <p>Euler deconvolution with structural index 0 (magnetic contact).</p> <p>Recalculation to refer the resulting source depth to the sea level.</p> <p>Presentation of solutions in colour.</p>	Grid_Mag_Euler_0_3x3_25mgrd.tif (ArcView-tif)

Processed primary data	Post-processing	Resulting GIS image
Simpevarp Mag NS.XYZ	<p>Interpolation with Geosofts Bigrid, gridcell size 100 m.</p> <p>Reduction to the pole (<math>I=71</math> degrees, <math>D=2</math> degrees).</p> <p>Upward continuation to 500 m.</p> <p>Geometrical corrections for measurement geometry.</p> <p>Euler deconvolution with structural index 0 (magnetic contact).</p> <p>Recalculation to refer the resulting source depth to the sea level.</p> <p>Presentation of solutions in colour.</p>	Grid_Mag_Euler_0_3x3_100mgrdup500.tfw (ArcView-tif)

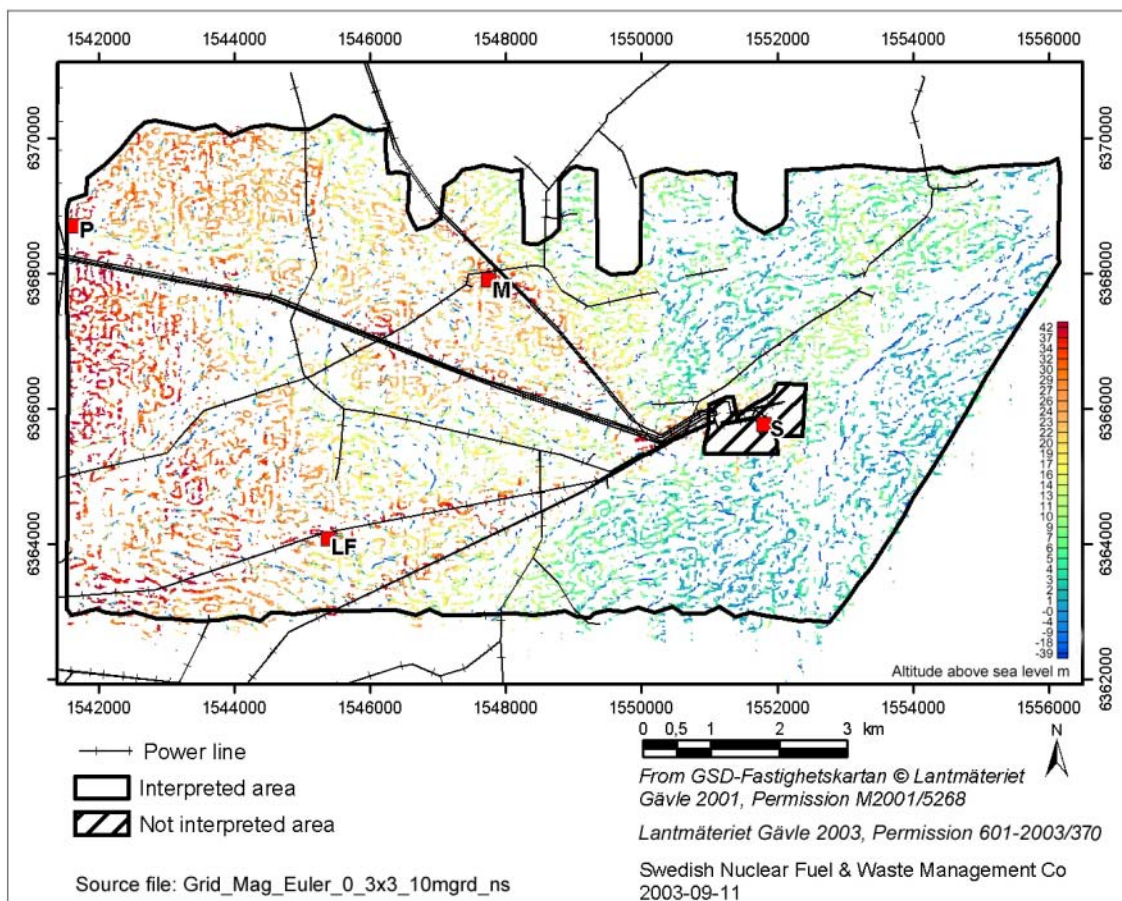


**Figure 4-5.** The result of Euler deconvolution on profiles flown in direction from north towards south using a structural index=0, window=3x3 cells, cell size=10 m. The depths to the detected sources are related to the sea level (=0). The area near the nuclear power plants at Simpevarp is masked out. S=Simpevarp power plant, M=Mederhult, LF=Lilla Fjälltorpet and P=Plittorp.

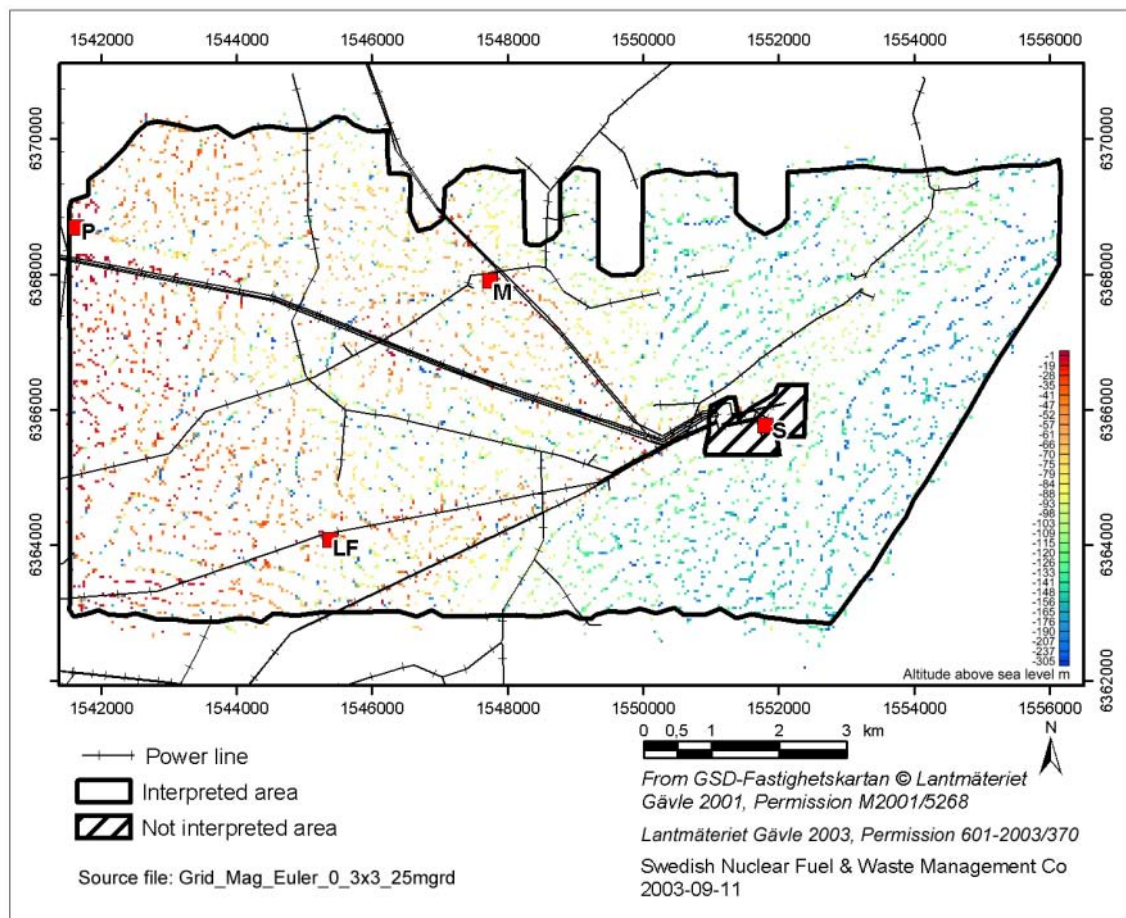


**Figure 4-6.** The result of Euler deconvolution using a structural index=0, window=3x3 cells, cell size=25 m. The depths to the detected sources are related to the sea level (=0). The area near the nuclear power plants at Simpevarp is masked out. S=Simpevarp power plant, M=Mederhult, LF=Lilla Fjälltorpet and P=Plittorp.

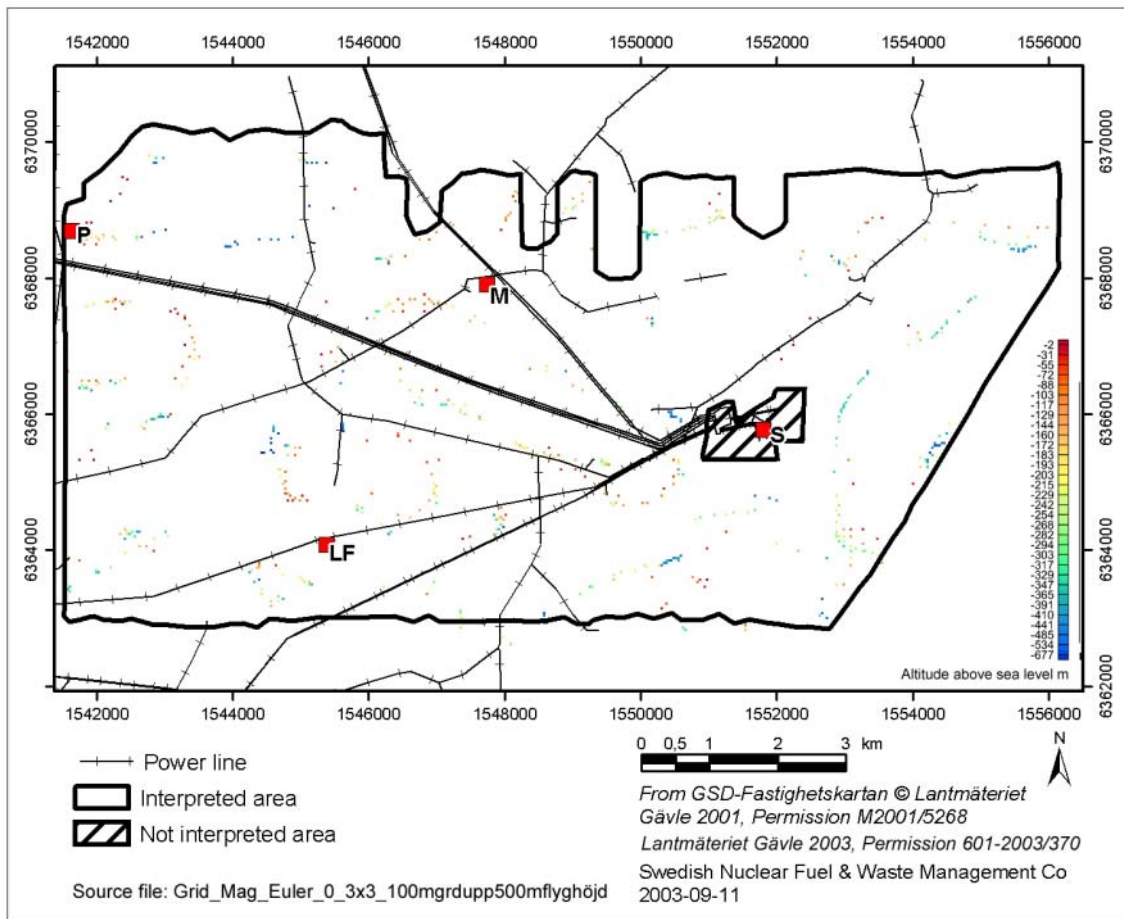


**Figure 4-7.** The result of Euler deconvolution using a structural index=0, window=3x3 cells, cell size=100 m, grid upward continued to 500 m. The depths to the detected sources are related to the sea level (=0). The area near the nuclear power plants at Simpevarp is masked out. S=Simpevarp power plant, M=Mederhult, LF=Lilla Fjälltorpet and P=Plittorp.

#### 4.1.4 Fixed-wing air-borne VLF (1986)

The data from the airborne measurements with VLF were processed in-house at SGU during the previous preliminary interpretation /1/. The same grids have been used in this project, and a brief summary of the processing is given in Table 4-5. The theoretical aspects of the technique are found in /6/, /8/, /10/.

The processed grid mainly used in the interpretation for the identification of lineaments is shown in Figure 4-8.

**Table 4-5. Post-processing of fixed wing borne VLF measurements of 1986.**

Processed primary data	Post-processing	Resulting GIS image
VLF-data measured from two different transmitters, in three orthogonal directions (i.e. Hy, Hx, Hz).	Calculation of the tipper vector (A,B) and the Peaker function which is independent of the geometrical relations between the anomaly source and the two transmitters.	Preal Pimag (MapInfo-tif)
VLF-data measured from two different transmitters, in three orthogonal directions (i.e. Hy, Hx, Hz).	Calculation of the apparent resistivity. Gridding using Geosoft Oasis montaj Bigrid with a cell size of 50x50 m. Colour table with vertical illumination.	App_res (MapInfo-tif)

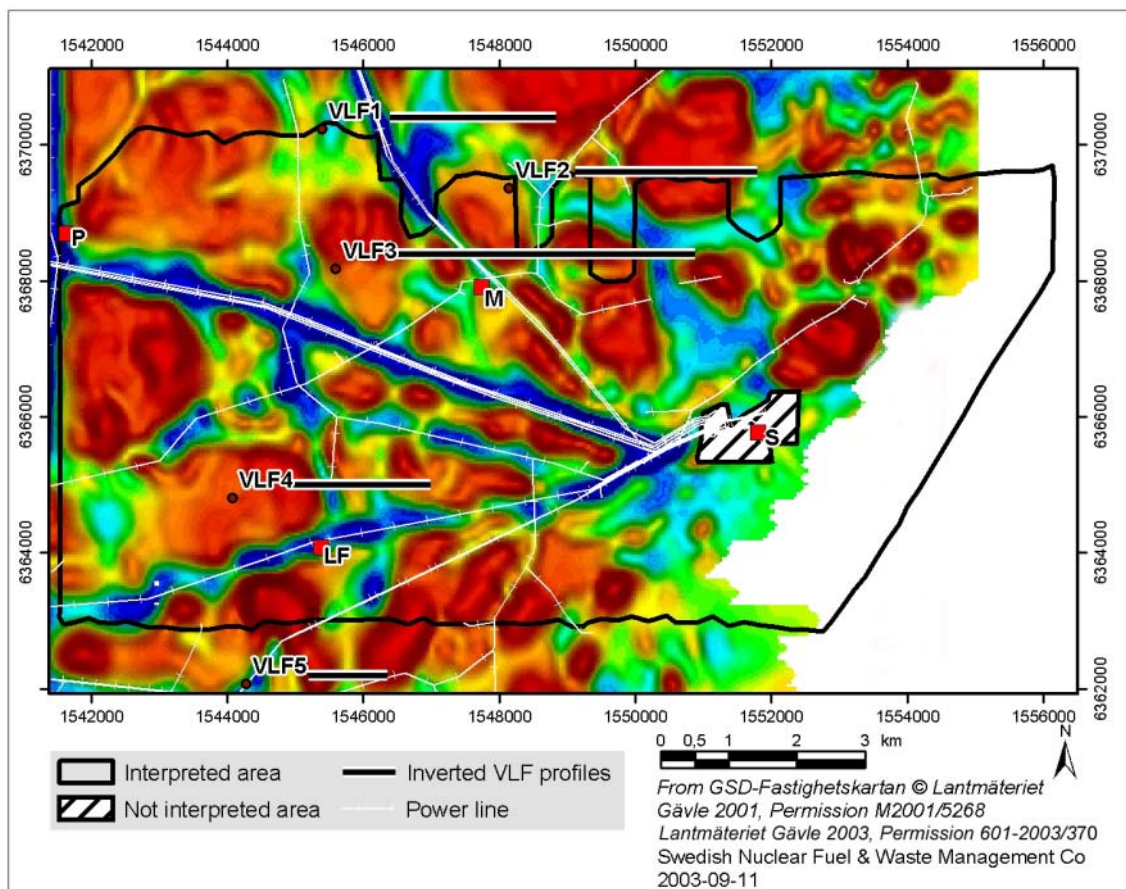


**Figure 4-8.** The grid “App\_res” in colour shows the apparent resistivity as calculated from VLF two transmitter station data. Low relative levels in resistivity are bluish and high are brownish. The power lines are marked as thin white lines and the five profiles inverted with 2D models in black and white (VLF1–VLF5). S=Simpevarp power plant, M=Mederhult, LF=Lilla Fjälltorpet and P=Plittorp.

Furthermore a 2D inversion was carried out along five profiles as marked in Figure 4-8 and with co-ordinates as in Table 4-6. The results of the inversion are presented below in Figures 4-9 to 4-13.

**Table 4-6. Specification of inverted profiles from the fixed wing borne VLF measurements of 1986.**

Profile name	Co-ordinates (RT90 2.5 gon W)	Quantification of the achieved fit between measured and modelled data
VLF1	Y 6370400m, X1=1546400m, X2=1548840m	Model (RMS=1.9)
VLF2	Y 6369600m, X1=1549120m, X2=1551800m	Model (RMS=1.6)
VLF3	Y 6368400m, X1=1546440m, X2=1550880m	Model (RMS=3.1)
VLF4	Y 6365000m, X1=1544880m, X2=1547000m	Model (RMS=1.3)
VLF5	Y 6362200m, X1=1545200m, X2=1546360m	Model (RMS=1.0)

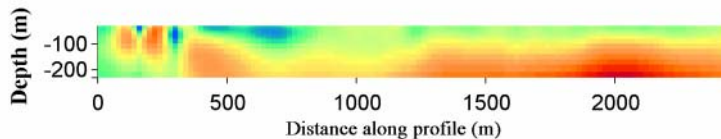


**Figure 4-9.** Result of the inversion of profile VLF1. Bluish colours indicate low relative resistivity and yellowish-brownish high resistivity. The colour scale for resistivities is visible in Figure 4-13 expressed in log10. Location of the profile is given in Figure 4-8 and in Table 4-6.

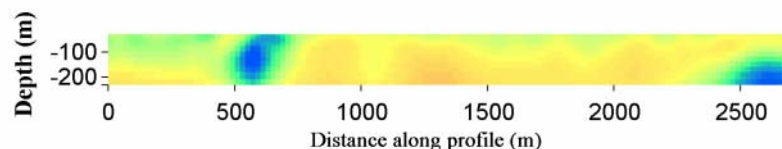


**Figure 4-10.** Result of the inversion of profile VLF2. Bluish colours indicate low relative resistivity and yellowish-brownish high resistivity. The colour scale for resistivities is visible in Figure 4-13 expressed in log10. Location of the profile is given in Figure 4-8 and in Table 4-6.

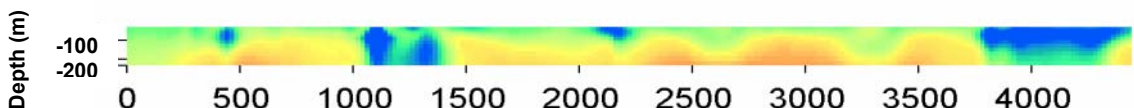


**Figure 4-11.** Result of the inversion of profile VLF3. Bluish colours indicate low relative resistivity and yellowish-brownish high resistivity (depth scale same as for other profiles). The colour scale for resistivities is visible in Figure 4-13 expressed in log10. Location of the profile is given in Figure 4-8 and in Table 4-6.

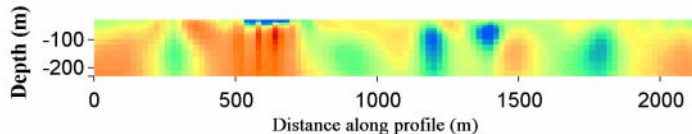


**Figure 4-12.** Result of the inversion of profile VLF4. Bluish colours indicate low relative resistivity and yellowish-brownish high resistivity. The colour scale for resistivities is visible in Figure 4-13 expressed in log10. Location of the profile is given in Figure 4-8 and in Table 4-6.

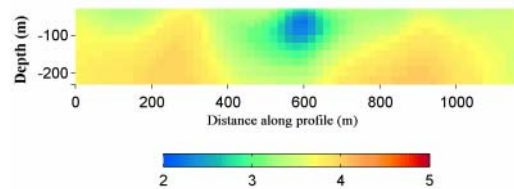


**Figure 4-13.** Result of the inversion of profile VLF5. Bluish colours indicate low relative resistivity and yellowish-brownish high resistivity. The colour scale for resistivities is expressed in log10. Location of the profile is given in Figure 4-8 and in Table 4-6.

#### 4.1.5 Helicopter borne multi-frequency EM (2002)

The data from the helicopter-borne multi-frequency EM-measurements were delivered as a Geosoft XYZ-file “Simpevarp EM NS”. Data are described in /2/. The data have been processed in order to enhance the appearance of lineaments, rock units of anomalous resistivity and electrically conductive soil cover.

Raw data are affected by flight altitude. This effect can be greatly reduced by converting the data to apparent resistivity. Apparent resistivity for the quadrature components were calculated by the contractor and included in the delivery /2/.

Anomalies caused by fractures in the bedrock are often weak in comparison with e.g. long wave-length anomalies caused by variations in soil cover thickness. The secondary field data were therefore AGC-filtered (AGC = automatic gain control) in order to enhance local anomalies.

The secondary field and hence the apparent resistivity contains information about the electrical properties of both the bedrock and the soil cover. It is very difficult to separate the effects of these units by qualitative interpretation. The data were therefore inverted to a two-layer model where the upper layer represents the soil cover and the second layer represents the bedrock. This will create different 1D-models in a grid over the survey area. These are then stitched together to create a pseudo-3D electrical model of the area. The 1D model is not valid at grid nodes where the electrical structure of the subsurface is strongly 2D or 3D. Such problems are however indicated by large residual errors and large confidence limits on the model parameters and can be taken into account during interpretation of the results.

Inversion of EM-data is very sensitive to correct levelling of the data. The secondary field data were therefore first levelled with the support of 1D models obtained from ground geophysics /11/. This information was also used as constraints during the inversion process.

### **Apparent resistivity**

Surfer grid-files of apparent resistivity were created from the XYZ-files according to Table 4-7. An example can be seen in Figure 4-14.

**Table 4-7. Post-processing of helicopter-borne multi-frequency EM-data (ip = in-phase, q = quadrature, freq. 1 = 7001Hz coaxial, freq. 2 = 6606Hz coplanar, freq. 3 = 980Hz coaxial, freq. 4 = 880Hz coplanar, freq. 5 = 34133Hz coplanar).**

Processed primary or intermediate data	Post-processing	Resulting file(s)
Simpevarp EM NS.XYZ Apparent resistivity columns	Interpolation with Surfer "Inverse Distance", grid cell size 10 m, search radius 50 m NS and 150 m EW, 7 search sectors, anisotropy 1.5 EW.  Taking the logarithm (base 10).  Colour table applied.	apprQ1.grd (Surfer grid) apprQ2.grd (Surfer grid) apprQ4.grd (Surfer grid) apprQ5.grd (Surfer grid)  apprQ1.tfw (ArcView-tif) apprQ2.tfw (ArcView-tif) apprQ4.tfw (ArcView-tif) apprQ5.tfw (ArcView-tif)
Simpevarp EM NS.XYZ Secondary field columns	AGC-filtering separately for survey lines and tie lines.	AGCout_60.dat (ASCII) AGCout_60tie.dat (ASCII)
AGCout_60.dat	Interpolation with Surfer "Inverse Distance", grid cell size 10 m, search radius 50 m NS and 150 m EW, 7 search sectors, anisotropy 1.5 EW.  Colour table applied.	ip1agc.grd (Surfer grid) ip2agc.grd (Surfer grid) ip3agc.grd (Surfer grid) ip4agc.grd (Surfer grid) ip5agc.grd (Surfer grid) q1agc.grd (Surfer grid) q2agc.grd (Surfer grid) q3agc.grd (Surfer grid) q4agc.grd (Surfer grid) q5agc.grd (Surfer grid)  ip1agc.tfw (ArcView tif) ip2agc.tfw (ArcView tif) ip3agc.tfw (ArcView tif) ip4agc.tfw (ArcView tif) ip5agc.tfw (ArcView tif) q1agc.tfw (ArcView tif) q2agc.tfw (ArcView tif) q3agc.tfw (ArcView tif) q4agc.tfw (ArcView tif) q5agc.tfw (ArcView tif)
Simpevarp EM NS.XYZ Secondary field columns, quadrature components	Levelling of tie-lines by comparisons with responses from VES-models.  Levelling of survey lines by comparisons with tie lines.  Levelling of survey lines by comparisons with neighbouring lines.	Svarp_EM_lev.dat (ASCII)

<b>Processed primary or intermediate data</b>	<b>Post-processing</b>	<b>Resulting file(s)</b>
Simpevarp EM NS.XYZ Secondary field columns, in-phase components	Subtraction of negative anomalies in 880 Hz coplanar and 980 Hz coaxial data from coplanar and coaxial in-phase components taking coil-separation into account.  Levelling by defining zero-level as secondary field over highly resistive areas.	Svarp_EM_lev.dat (ASCII)
Svarp_EM_lev.dat columns for levelled secondary fields, flight altitude and coordinates	Interpolation with Surfer “Nearest Neighbor”, grid cell size 10 m NS 25 m EW, search radius 100 m.  Blanking of water areas.	ip1_l.grd (Surfer grid) ip2_l.grd (Surfer grid) ip3_l.grd (Surfer grid) ip4_l.grd (Surfer grid) ip5_l.grd (Surfer grid) q1_l.grd (Surfer grid) q2_l.grd (Surfer grid) q3_l.grd (Surfer grid) q4_l.grd (Surfer grid) q5_l.grd (Surfer grid) altitude.grd (Surfer grid) East.grd (Surfer grid) North.grd (Surfer grid)
ip1_l.grd ip2_l.grd ip3_l.grd ip4_l.grd ip5_l.grd q1_l.grd q2_l.grd q3_l.grd q4_l.grd q5_l.grd altitude.grd  rho1apr.grd (see 4.1.7) h1apr.grd       “ rho2apr.grd     “ rho1sapr.grd    “ h1sapr.grd      “ rho2sapr.grd    “	Inversion to two-layer model taking a priori information into account.  Output includes layer parameters ( $\rho_1$ , $h_1$ , $\rho_2$ ), parameter confidence limits ( $\rho_{1s}$ , $h_{1s}$ , $\rho_{2s}$ ), apparent flight altitude (flhout), misfit to EM data (rmsout) and misfit to EM and a priori data (rmsapout).	rho1.grd (Surfer grid) h1.grd (Surfer grid) rho2.grd (Surfer grid) rho1s.grd (Surfer grid) h1s.grd (Surfer grid) rho2s.grd (Surfer grid) flhout.grd (Surfer grid) rmsout.grd (Surfer grid) rmsapout.grd (Surfer)
rho1.grd h1.grd rho2.grd rmsout.grd East.grd North.grd  invoutput.dat	Blanking of grid nodes with large RMS-values.  Conversion of inversion output to column format with original coordinates.  Interpolation with Surfer “Inverse Distance”, grid cell size 10 m, search radius 50 m NS and 150 m EW, 7 search sectors, anisotropy 1.5 EW.  Output includes layer parameters ( $\rho_{1\_inv}$ , $h_{1\_inv}$ , $\rho_{2\_inv}$ ).	invoutput.dat (ASCII)  rho1_inv.grd (Surfer grid) h1_inv.grd (Surfer grid) rho2_inv.grd (Surfer grid)  rho1_i.tif (ArcView tif) h1_i.tif (ArcView tif) rho2_i.tif (ArcView tif)

<b>Processed primary or intermediate data</b>	<b>Post-processing</b>	<b>Resulting file(s)</b>
Svarp_EM_lev.dat columns for levelled secondary fields, flight altitude and coordinates	Interpolation with Surfer “Nearest Neighbor”, grid cell size 10 m NS 25 m EW, search radius 100 m.  Blanking of land areas.	ip1_w.grd (Surfer grid) ip2_w.grd (Surfer grid) ip3_w.grd (Surfer grid) ip4_w.grd (Surfer grid) ip5_w.grd (Surfer grid) q1_w.grd (Surfer grid) q2_w.grd (Surfer grid) q3_w.grd (Surfer grid) q4_w.grd (Surfer grid) q5_w.grd (Surfer grid) altitudew.grd (Surfer grid) Eastw.grd (Surfer grid) Northw.grd (Surfer grid)
ip1_w.grd ip2_w.grd ip3_w.grd ip4_w.grd ip5_w.grd q1_w.grd q2_w.grd q3_w.grd q4_w.grd q5_w.grd altitudew.grd	Inversion to two-layer model taking a priori about water depth and water resistivity information into account.  Output includes water depth and resistivity ( $h_{1w}$ , $\rho_{1w}$ ), parameter confidence limits ( $\rho_{1sw}$ , $h_{1sw}$ ), apparent flight altitude ( $fhoutw$ ), misfit to EM data ( $rmsoutw$ ) and misfit to EM and a priori data ( $rmsapoutw$ ).  Colour table applied.	$\rho_{1w}$ .grd (Surfer grid) $h_{1w}$ .grd (Surfer grid) $\rho_{1sw}$ .grd (Surfer grid) $h_{1sw}$ .grd (Surfer grid) $fhoutw$ .grd (Surfer grid) $rmsoutw$ .grd (Surfer grid) $rmsapoutw$ .grd (Surfer)
$\rho_{1aprw}$ .grd (see 4.1.7) $h_{1aprw}$ .grd      “ $\rho_{1saprw}$ .grd    “ $h_{1saprw}$ .grd    “		
$\rho_{1w}$ .grd $h_{1w}$ .grd $rmsoutw$ .grd Eastw.grd Northw.grd	Conversion of inversion output to column format with original coordinates.	invoutputw.dat (ASCII)
Invoutputw.dat	Interpolation with Surfer “Inverse Distance”, grid cell size 10 m, search radius 50 m NS and 150 m EW, 7 search sectors, anisotropy 1.5 EW.  Output includes apparent water depth ( $h_{1w\_inv}$ ).  Smoothing. Colour table and shading applied.	$h_{1w\_inv}$ .grd (Surfer grid)  $h_{1w\_i}$ .tfw (ArcView tif)

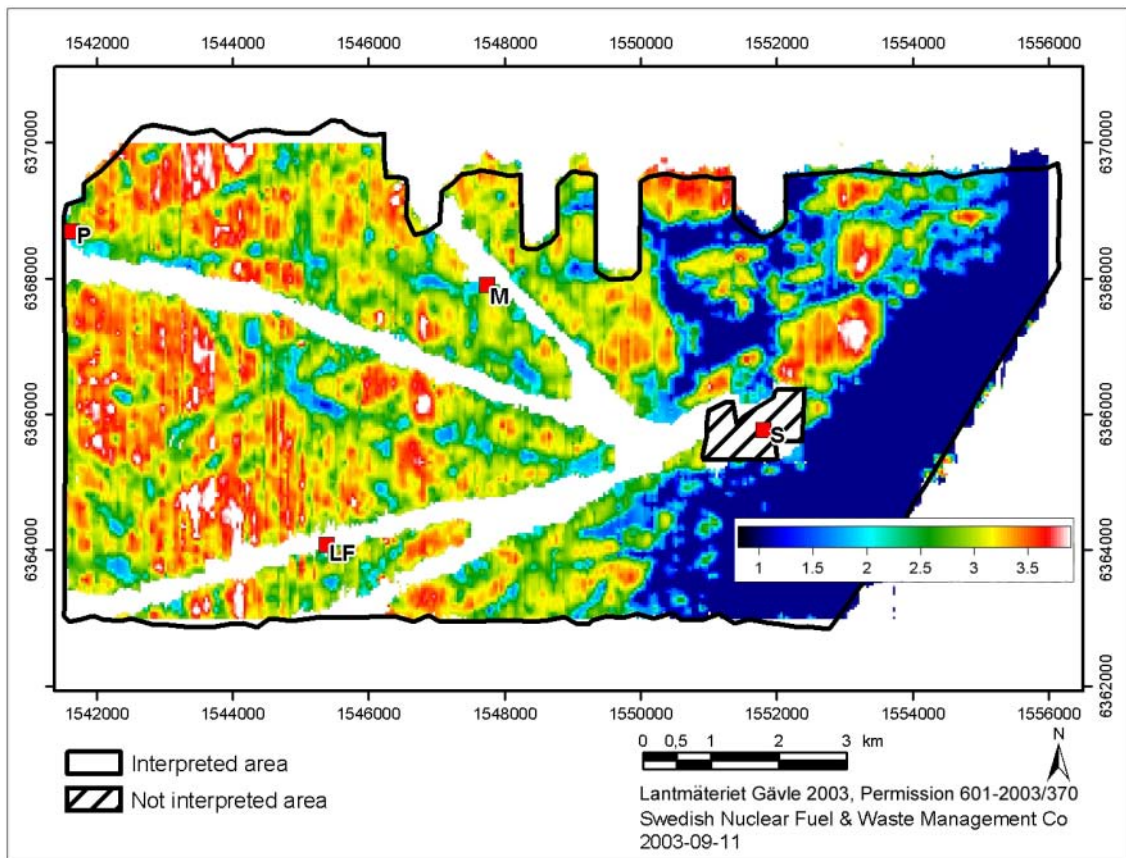


**Figure 4-14.** The grid apprQ5 shows the apparent resistivity calculated from helicopter-borne multi-frequency EM-data, 34133 Hz quadrature component, coplanar coils. Blue and green colours indicate low apparent resistivity. No data are available where the sensor altitude has exceeded 80 metres above power lines and the Simpevarp power plant. S=Simpevarp power plant, M=Mederhult, LF=Lilla Fjälltorpet and P=Plittorp.

### AGC-filtering

Local anomalies were enhanced in the secondary field data by AGC-filtering:

$$AGC = \frac{in - ave(in)}{\left( \frac{1}{N} \cdot \sqrt{SS} \right)^{0.75}}$$

where

$AGC$  = AGC filtered output

$in$  = input data

$ave(in)$  = average of input data in AGC window

$N$  = number of samples in AGC window

and

$$SS = \sum_{i=1}^N (in_i - ave(in))^2$$

Different lengths of the AGC-window were tested. A length of 61 recordings corresponding to around 180 to 200 metres of profile was found to be a good choice. AGC-filtered data were stored in ASCII-format. Surfer grid files were created of the AGC-filtered data. Examples of AGC-filtered data can be seen in Figures 4-15 and 4-16 respectively.

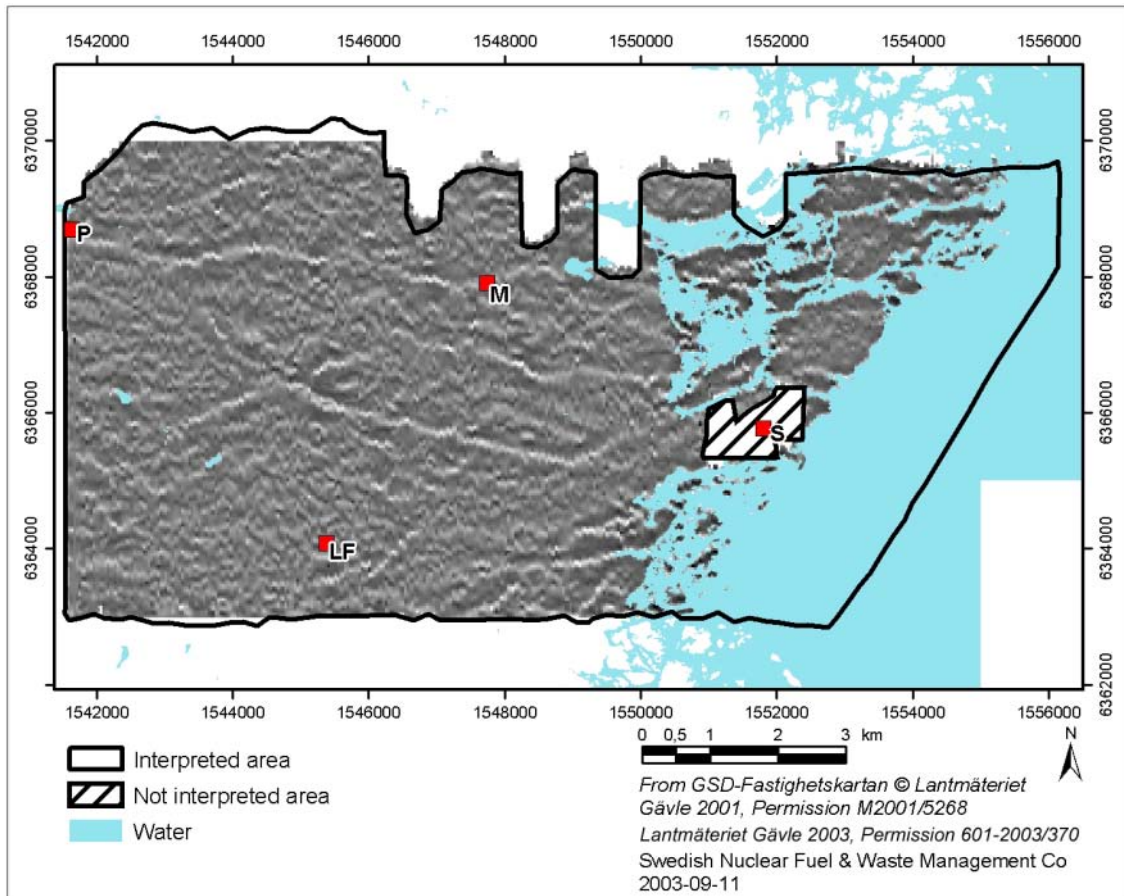


**Figure 4-15.** The grid q5agc shows the AGC-filtered helicopter borne multi-frequency EM-data, 34133 Hz quadrature component, and coplanar coils. Local on-shore anomalies are enhanced and indicated with bright shades. No data are available close to the Simpevarp power plant.

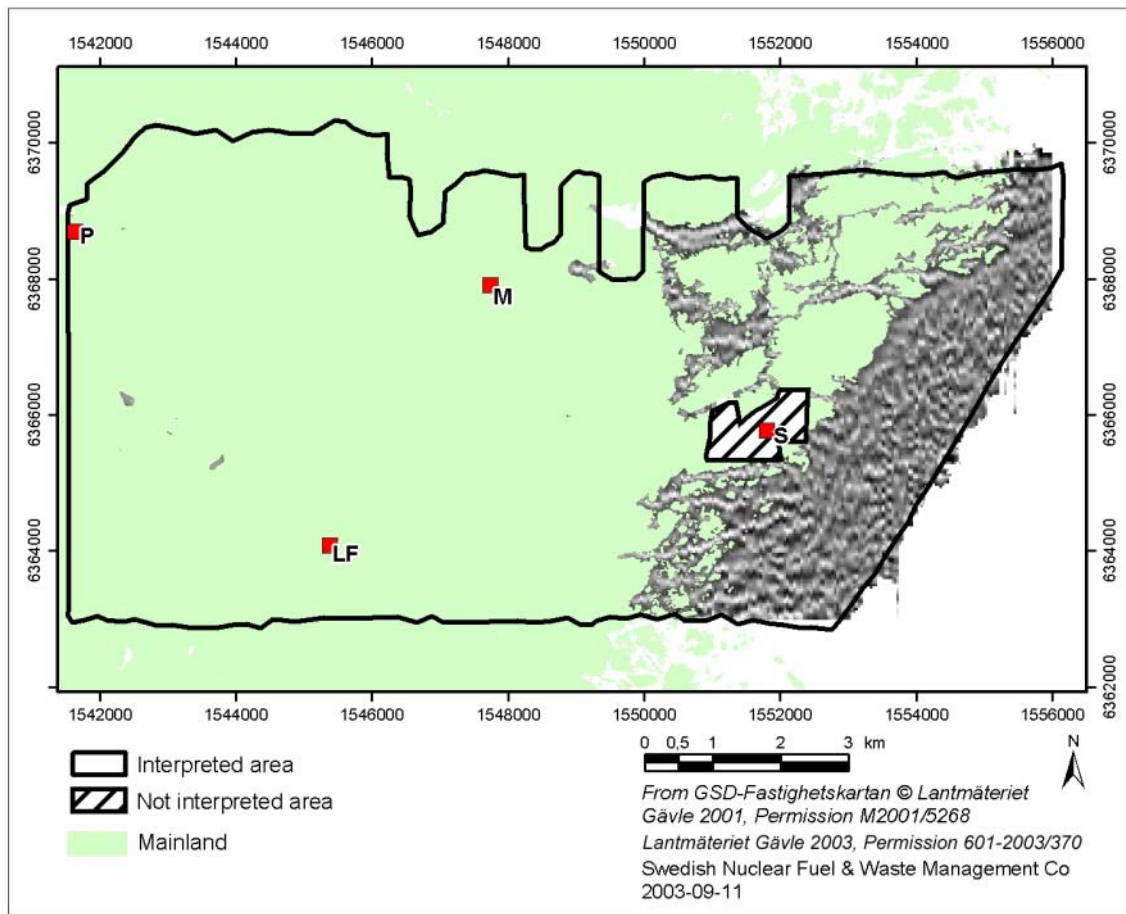


**Figure 4-16.** The grid ip4agc shows the AGC-filtered helicopter borne multi-frequency EM-data, 880 Hz in-phase component, coplanar coils. Local off-shore anomalies are enhanced and indicated with bright shades. S=Simpevarp power plant, M=Mederhult, LF=Lilla Fjälltorpet and P=Plittorp.

### Levelling

Secondary field data along the tie-lines were compared with theoretical anomalies from layered earth models resulting from interpretation of DC electrical soundings (VES) on the ground /11/. Some systematic differences were apparent (Figure 4-17) and the quadrature components were levelled to fit the theoretical anomalies according to procedures described in Appendix B (in swedish). Such levelling could not be performed for the in-phase components since they are affected by magnetic effects. The values subtracted from the quadrature components of the tie-lines are given in Table 4-8. Electric resistivity is to some extent frequency dependent, but measurements on samples from the most common rocks in the area indicate that this effect can be neglected.

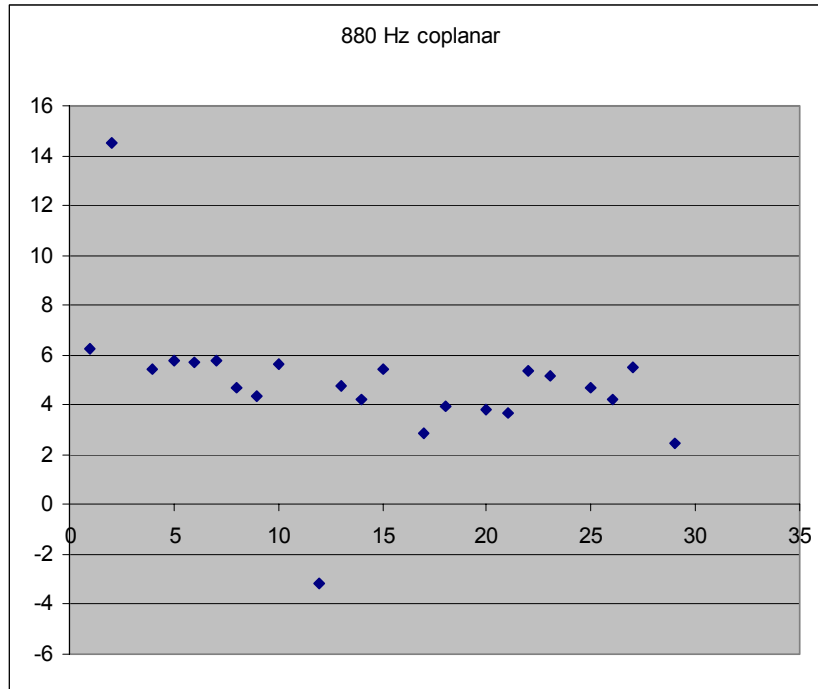


**Figure 4-17.** Difference in secondary field (in ppm) from tie lines of the helicopter borne multi-frequency EM data and synthetic responses calculated for corresponding VES control points on the ground. The first five points are from flight 1 and the remaining from flight 2. The example shown is for 880 Hz coplanar coils, quadrature component.

**Table 4-8. Corrections, in ppm, of tie-line data (quadrature components) based on comparisons with synthetic data from VES-models.**

Flight #	7001 Hz coaxial	6606 Hz coplanar	980 Hz coaxial	880 Hz coplanar	34133 Hz coaxial
1	0.0375	4.89	-0.63	5.8	9.47
2	-0.66	-0.39	-0.92	4.36	3.24

Quadrature components of the secondary field data along the north-south survey lines were levelled by comparing values at cross-over points with the levelled tie-lines. The difference in flight altitude was corrected for by applying an approximate formula valid for moderate altitude differences:

$$tie_{ht\_corr} = tie \cdot \left( \frac{alt_{line}}{alt_{tie}} \right)^a$$

where

$tie_{ht\_corr}$  = secondary field from tie line corrected for altitude difference

$tie$  = uncorrected secondary field from tie line

$alt_{line}$  = flight altitude value from survey line

$alt_{tie}$  = flight altitude value from tie line

$a$  = power coefficient according to Table 4-9.

**Table 4-9. Altitude correction power coefficients for quadrature components.**

7001 Hz coaxial	6606 Hz coplanar	980 Hz coaxial	880 Hz coplanar	34133 Hz coaxial
-1.5	-1.5	-1.42	-1.42	-1.65

Cross-over points in fairly homogeneous high-resistivity areas were considered most reliable for levelling. The secondary fields along survey lines were corrected for by applying a linear trend (Figure 4-18).

Survey lines that could not be reliably levelled with the help of tie-line data were levelled by comparisons with neighbouring lines.

The effect of magnetic susceptibility was estimated from the in-phase components of the 880 Hz and 980 Hz data. The in-phase component of the secondary field due to induction is very close to zero for such low frequencies in the high resistivity environment that is typical for Swedish on-shore areas. The negative anomalies that appear in these data can therefore be regarded as caused by purely magnetic effects. The magnetic effect is more or less frequency independent in high resistivity areas so the negative values mentioned above were subtracted for all frequencies after taking coil-separation into account. The in-phase data were then levelled by assuming that the secondary field should be close to zero over homogeneous, high-resistivity areas. Levelled secondary field data were stored in ASCII-format and Surfer grid files were created.

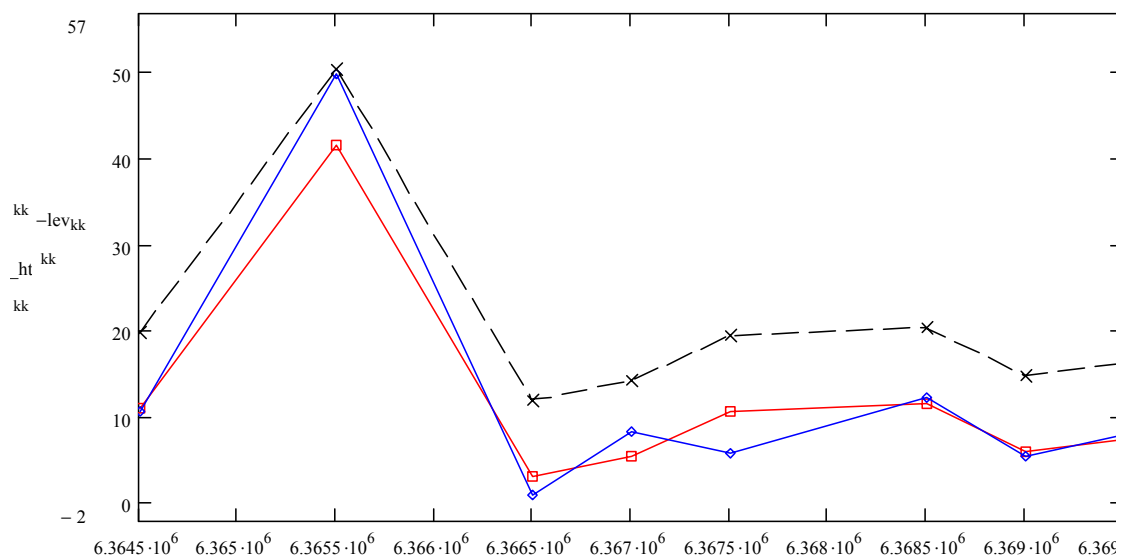


**Figure 4-18.** Example of levelling of a survey line with the help of altitude-corrected tie-line data. The black dashed line shows uncorrected survey line values from crossovers with tie-lines, the blue line shows corresponding tie-line data and the red line shows the survey line data after applying a linear trend reduction (34133 Hz quadrature component, line 1020, 1546100Y).

## Inversion

The levelled EM-data were converted into grid format and inverted to a two-layered model using the a priori data described in section 4.1.7 as regularisation. Interpolation to grids was made with the “Nearest neighbour”-method to avoid mixing of data from different survey lines. Grid files were also created for flight altitude and coordinates. Water covered areas were not included in the inversion. The inversion was performed in accordance with the procedure described in Appendix B (in swedish). Surfer grid files were created of the inversion output (soil cover resistivity and thickness, bedrock resistivity), the estimated parameter errors and the misfit between model response and input data.

Finally, grid nodes in the inversion output where the RMS-error was greater than 6.0 were blanked and the remaining data parameter values were converted to ASCII-format making use of the coordinate grids to restore the original positions. Grid files were then created using “Inverse distance”-interpolation. An example is seen in Figure 4-19.

The EM data from offshore areas were also inverted in the same way as described above. The uppermost layer represents the sea water in this case whereas the second layer represents the sediments and bedrock jointly. Due to the very high resistivity

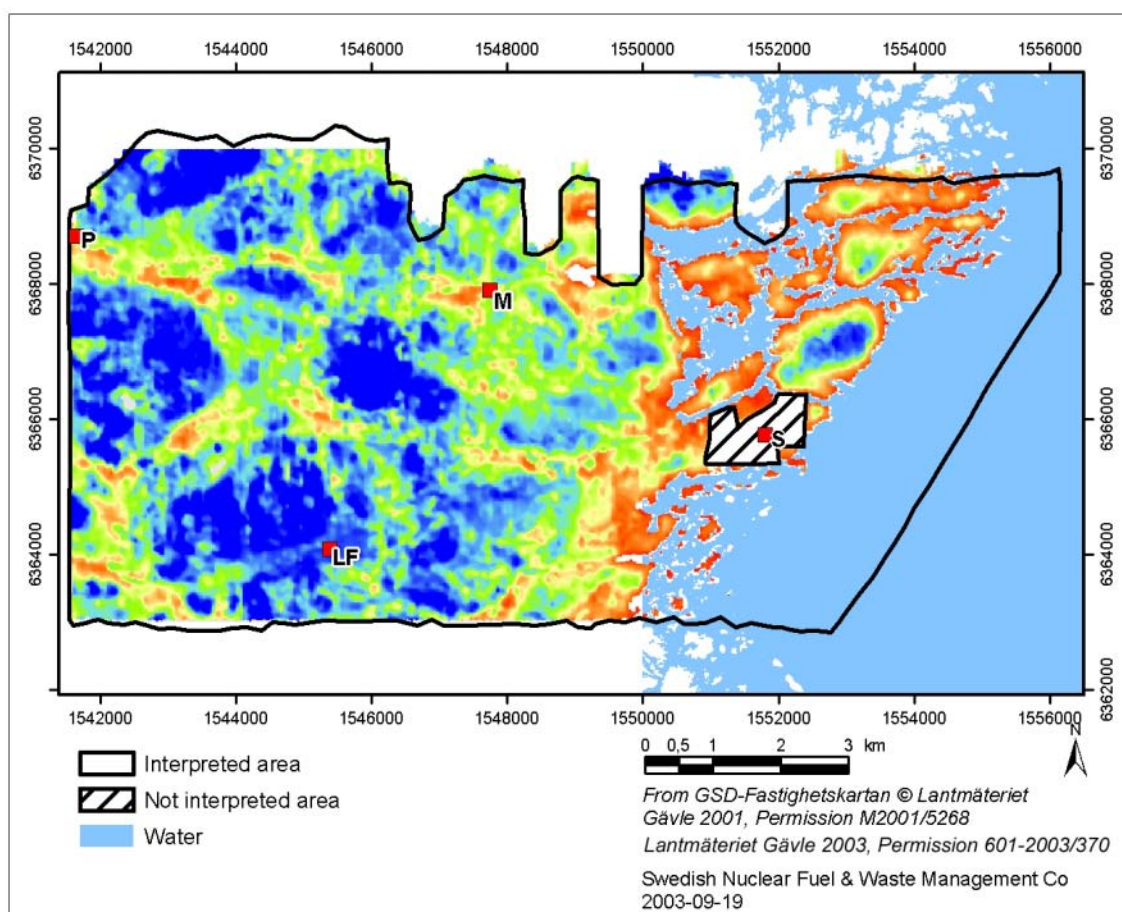


**Figure 4-19.** The grid rho2\_inv shows the estimated resistivity of the bedrock in on-shore areas. S=Simpevarp power plant, M=Mederhult, LF=Lilla Fjälltorpet and P=Plittorp.

contrast between the layers it is not possible to resolve any resistivity variations in the lower layer below the sea. A priori information about water depth was available from bathymetric measurements and the water resistivity was measured during the helicopter borne survey. The water resistivity was more or less the same at the three measuring points and at different depths. A constant value was therefore used as a priori information.

The resistivity of the sea water in the inversion output varied slightly between e.g. different flight lines. The conductance of the water layer can be considered as the best resolved parameter and the inverted water depth was therefore corrected to be in accordance with the a priori information about water resistivity ( $0.87 \Omega\text{m}$ ). The corrected water depths were plotted versus the original bathymetric data. A very good linear relation was found. The inversion output was however 25% lower than the bathymetric data. The reason for this systematic difference has not been investigated but might be due to systematic errors in the helicopter altimeter or in the gain and/or phase of the EM system. The difference was corrected for by multiplying the inversion output with the appropriate constant. The results can be seen in Figure 4-20.

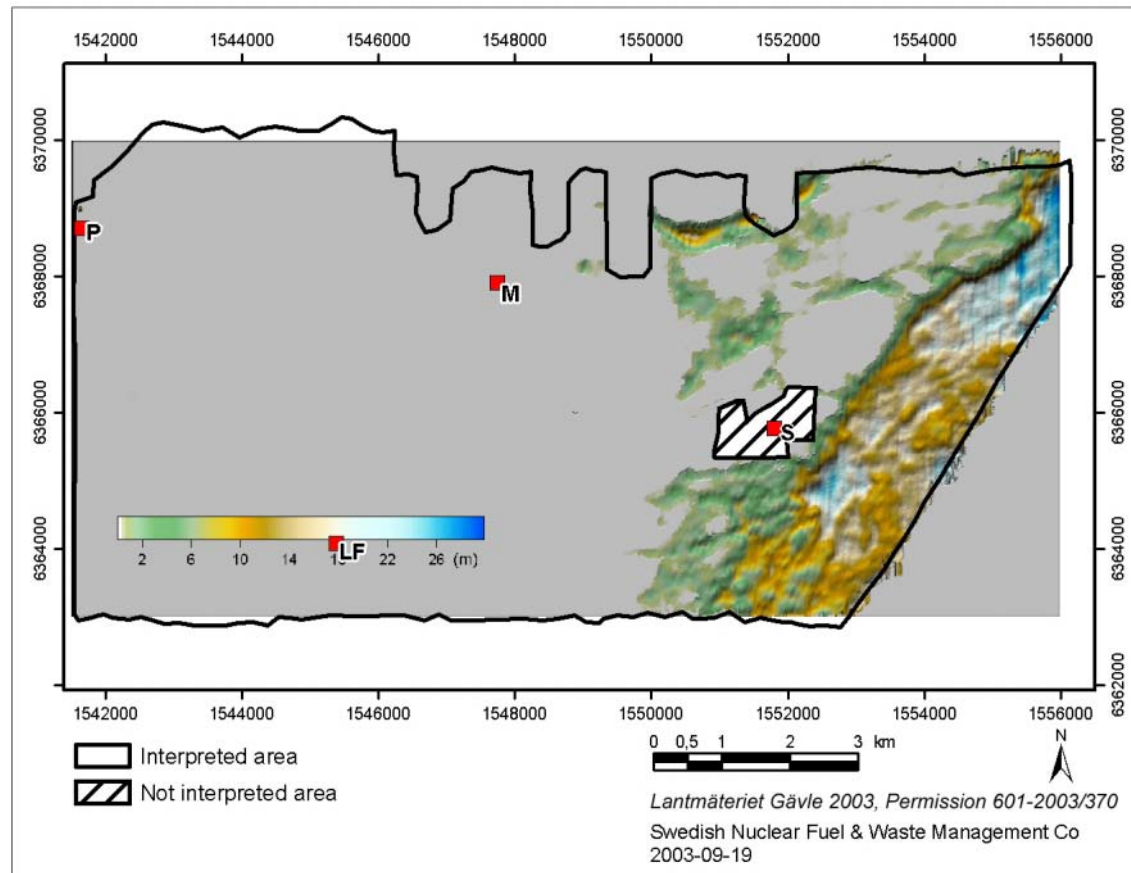


**Figure 4-20.** The grid *h1w\_inv* shows the water depth estimated from multi-frequency EM-measurements through inversion. Interpreted water depth data can however not be used as a basis for navigation of boats. S=Simpevarp power plant, M=Mederhult, LF=Lilla Fjälltorpet and P=Plittorp.

#### 4.1.6 Helicopter borne VLF (2002)

The data from the helicopter-borne VLF-measurements were delivered as part of a Geosoft XYZ-file “Simpevarp EM NS”. Data are described in /2/.

The only post processing that was performed on the helicopter-borne VLF-data was creation of new grid files as specified in Table 4-10. Two grid files are shown in Figures 4-21 and 4-22. The reason behind the disturbed appearance is the change of transmitters during the flying sessions.

**Table 4-10. Post-processing of helicopter-borne VLF-data.**

Processed primary or intermediate data	Post-processing	Resulting file(s)
Simpevarp EM NS.XYZ VLF total field resistivity columns	Interpolation with Surfer “Inverse Distance”, grid cell size 10 m NS and 25 m EW, search radius 50 m NS and 150 m EW, 7 search sectors, anisotropy 1.5 EW.  Colour table applied.	VLT_s.grd (Surfer grid) VOT_s.grd (Surfer grid)  VLT_s.tfw (ArcView-tif) VOT_s (ArcView-tif)

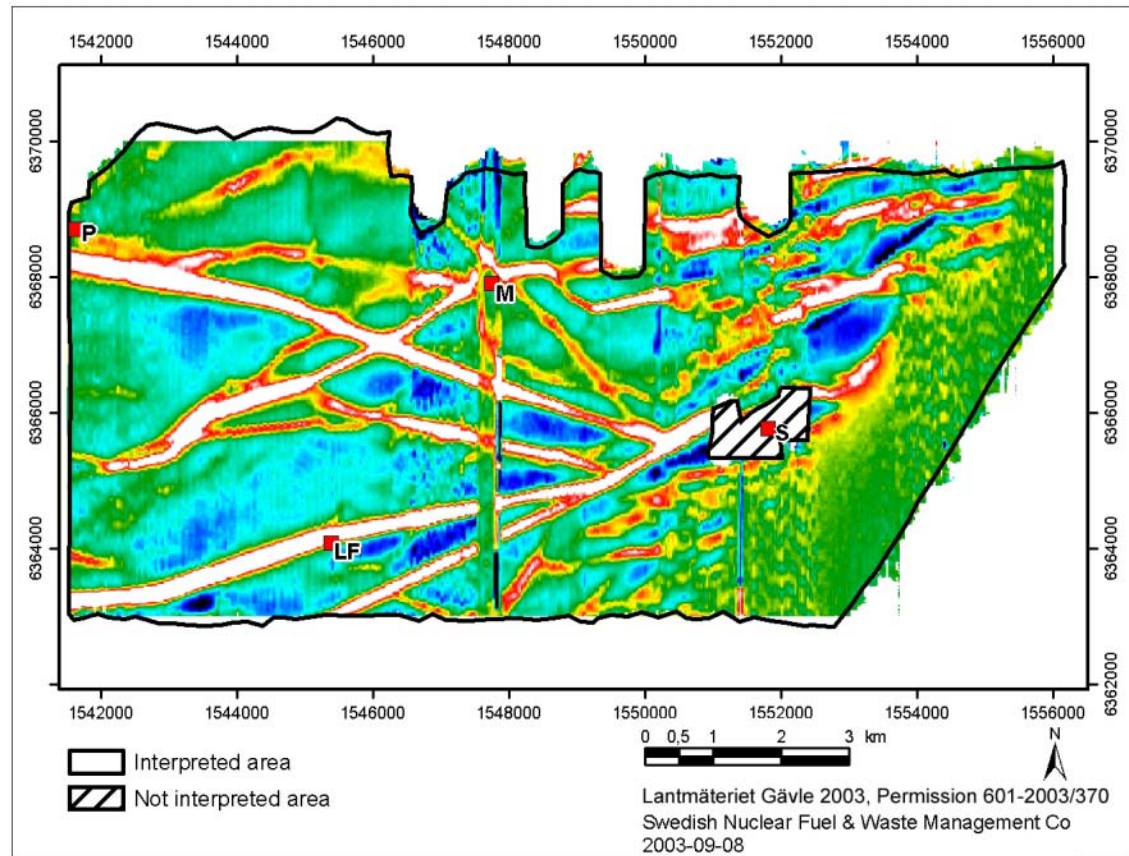


**Figure 4-21.** The grid VLT\_s shows the helicopter-borne VLF-total field anomaly, inline sensor. Positive anomalies are shown with white and red colours. Power lines produce strong anomalies. The shifts of level visible are due to changed transmitters during flying sessions. No data are available close to the Simpevarp power plant. S=Simpevarp power plant, M=Mederhult, LF=Lilla Fjälltorpet and P=Plittorp.

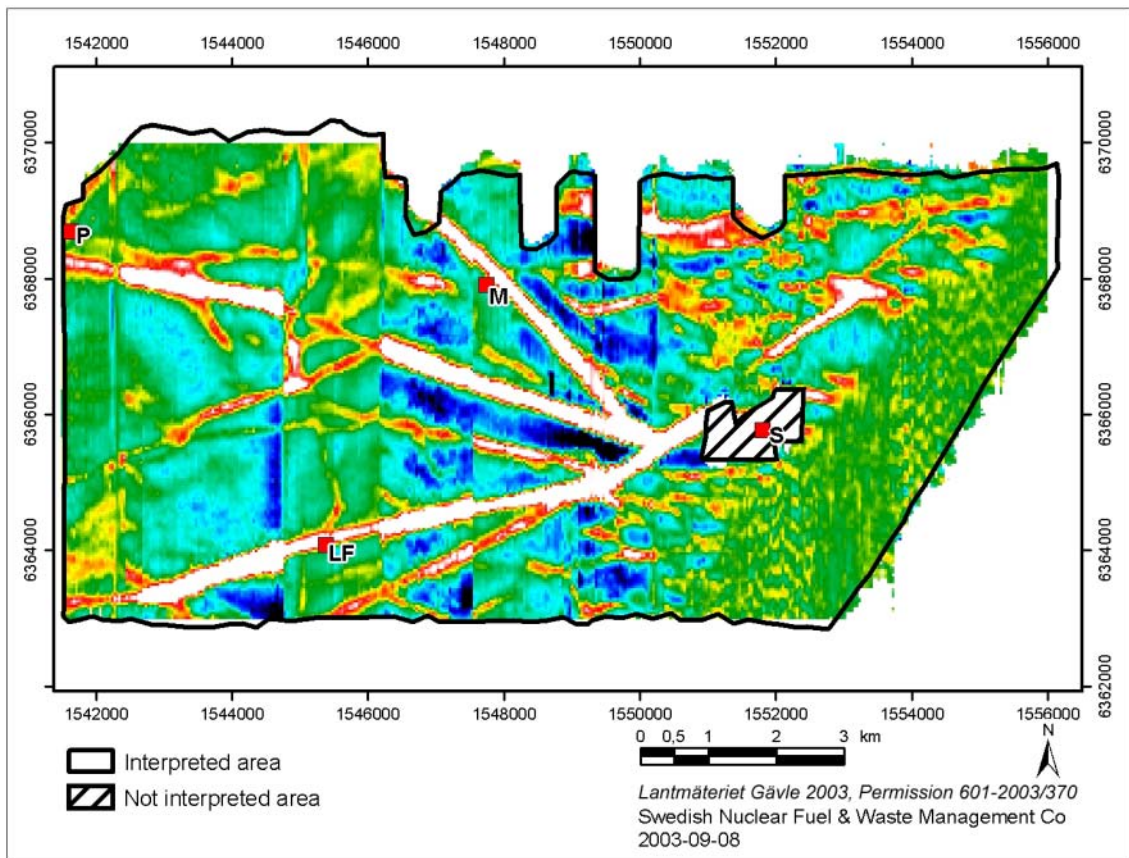


**Figure 4-22.** The grid VOT\_s shows the helicopter-borne VLF-total field anomaly, orthogonal sensor. Positive anomalies are shown with white and red colours. Power lines produce strong anomalies. The shifts of levels visible are due to changed transmitters during flying sessions. No data are available close to the Simpevarp power plant. S=Simpevarp power plant, M=Mederhult, LF=Lilla Fjälltorpet and P=Plittorp.

#### 4.1.7 Miscellaneous

##### **Mask of outcrops**

The preparatory work for the interpretation included the transformation of interpreted probable outcrops to GIS layers which could be used directly in the interpretation. Two masks, one with transparent outcrops and one with opaque outcrops (Figure 4-23), were produced. The masks do however not cover the entire area needed. The reason is that the original interpretation of outcrops carried out by SGU covered the candidate area which is not entirely coinciding with the area surveyed with helicopter.

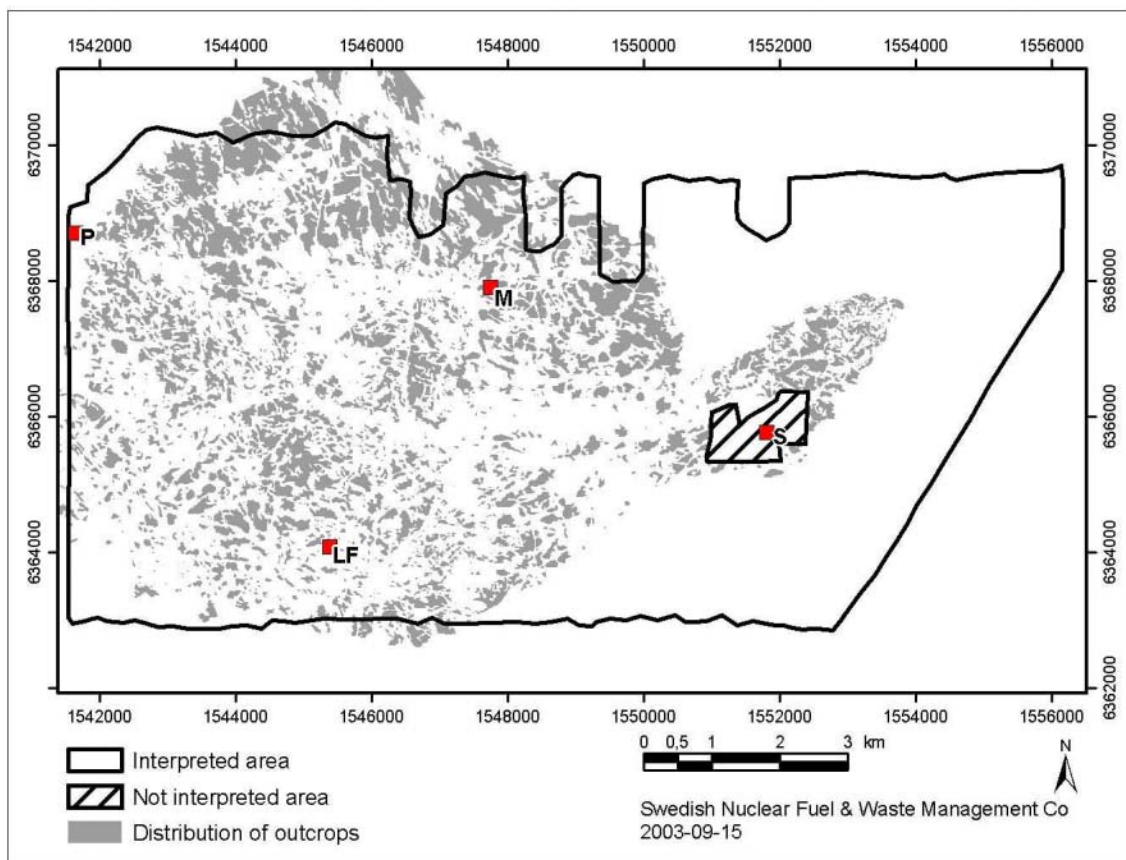


**Figure 4-23.** Distribution of outcrops (in grey) according to an interpretation made by SGU in 2002/2003 over the candidate area. Observe that some areas within the helicopter surveyed area have yet not been interpreted regarding outcrops. S=Simpevarp power plant, M=Mederhult, LF=Lilla Fjälltorpet and P=Plittorp.

### **Lineaments, depressions and topographical data**

The identified lineaments and depressions from topographical data /1/, /4/, as well as altitude data /3/, have been used to support the interpretation of airborne geophysics.

### **Petrophysics**

A petrophysical study as a complement to earlier studies has been available and implemented into a GIS to assist in the interpretation of the airborne survey /12/, /13/.

### **Land cover information**

Information about the land cover was extracted from “Terrängkartan” of the National Land Survey. Data were available as GIS-layers.

## **Vertical electrical soundings**

Information about the electrical structure of the ground is used as a priori information in inversion of helicopter-borne multi-frequency EM-data.

Surfer grid files were created by inverse distance weighting of a priori information of soil cover thickness, soil cover resistivity and bedrock resistivity from VES measurements /11/ as specified in Table 4-11. Corresponding grid files were created showing the estimated standard deviation of the interpolated values. Areas at large distance from any VES station will get a very high standard deviation. Such areas were treated separately:

- The soil cover resistivity was set to  $60 \Omega\text{m}$  for agricultural fields (presumed clayey soil),  $100 \Omega\text{m}$  for bogs/wetlands and  $1200 \Omega\text{m}$  for other areas. The standard deviation for this a priori information was set to fairly high values so that it will not affect inversion in a too significant way.
- The soil cover thickness was set to zero in those areas defined as rock outcrops by SGU (see above).
- The resistivity of the bedrock was estimated from regression analysis of apparent resistivity helicopter EM data versus interpreted bedrock resistivity from VES measurements (Figure 4-24). The standard deviation for this a priori information was set to fairly high values so that it will not affect inversion in a too significant way.

**Table 4-11. Post-processing of VES-data.**

Processed primary or intermediate data	Post-processing	Resulting file(s)
VES_apps40002014.shp	Interpolation with inverse distance weighting, grid cell size 25 m EW 10 m NS, from positions with VES models.	rho1apr.grd (Surfer grid)
X_apps40002014.shp		h1apr.grd (Surfer grid)
My_06hsv.shp		rho2apr.grd (Surfer grid)
My_06gso.shp	Default values from auxiliary data at large distance from VES stations.	rho1sapr.grd (Surfer grid)
oskarshamn_hall_yta.shp		h1sapr.grd (Surfer grid)
apprQ1.grd	Output includes a priori information about layer parameters with estimated standard deviation.	rho2sapr.grd (Surfer grid)

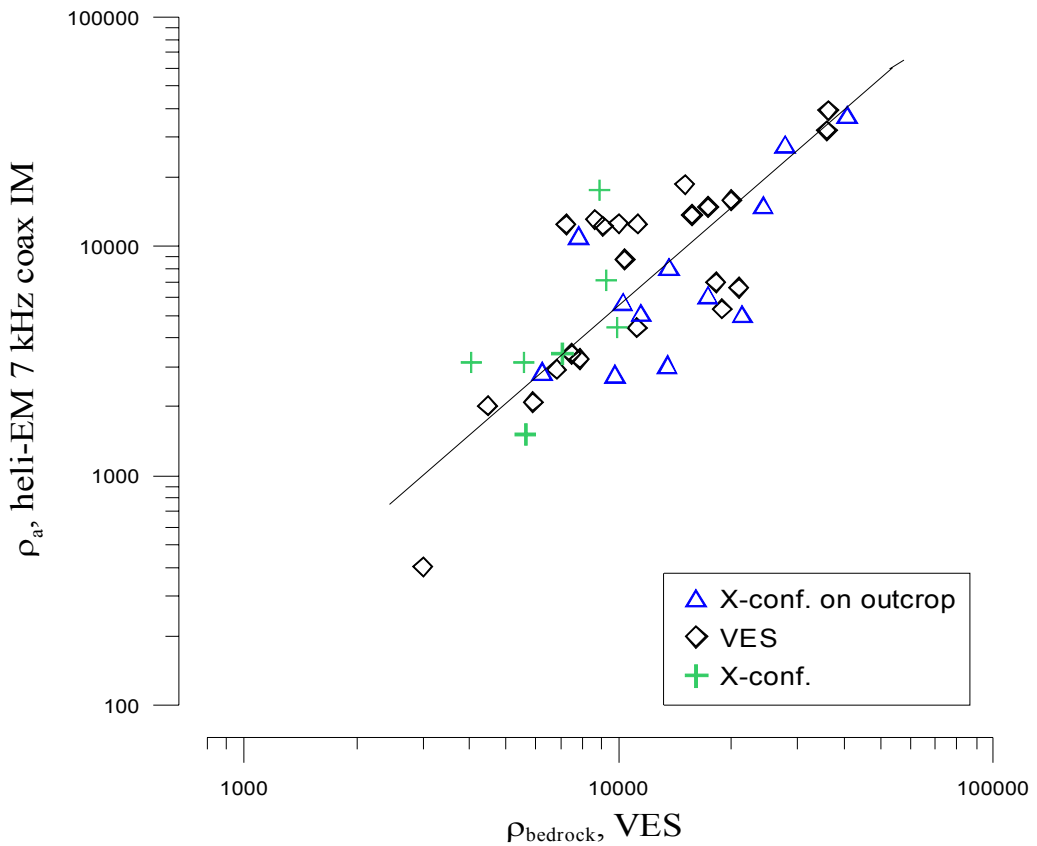


**Figure 4-24.** Relationship between bedrock resistivity estimated from electrical soundings /1/, /11/ and apparent resistivity from helicopter-borne EM-measurements.

### Water depth

Information about the water depth was based on nautical charts of the Hydrographic Office of the Swedish Administration of Shipping and Navigation (Sjöfartsverket). The data are however not public. Data were available as ASCII-files. This information was used as constraints during inversion EM data over water covered areas. A Surfer grid file (h1aprw.grd) was created with inverse distance interpolation, see also Table 4-12 below. Interpreted water depth data can however not be used as a basis for navigation of boats.

### Water resistivity

The resistivity of the sea water was measured by Jenette Carmström 2002-10-10 at three locations concurrently with the helicopter borne survey. This information was used as constraints during inversion of EM data over water covered areas. A Surfer grid file (rho1aprw.grd) was created with constant values corresponding to the average measured water resistivity, see also Table 4-12 below.

**Table 4-12. Post-processing of a priori data regarding water depth and water resistivity.**

Processed primary or intermediate data	Post-processing	Resulting file(s)
omr1a.dat	Interpolation with inverse distance weighting, grid cell size 25 m EW 10 m NS.	rho1aprw.grd (Surfer grid) h1aprw.grd (Surfer grid)
omr1b.dat		
omr2.dat		
omr3.dat		
flyggeofysikkonduktivitet.xls	Output includes a priori information about water layer parameters with estimated standard deviation.	rho1saprw.grd (Surfer grid) h1saprw.grd (Surfer grid)

## 4.2 Interpretation

The interpretation technique used is briefly described below in connection to the results presented. For detailed descriptions the reader is referred to the method descriptions MD 211.003 and 120.001 (SKB internal controlling documents).

### 4.2.1 Gamma ray spectrometry from the helicopter borne survey of 2002

The interpretation technique used is based on visual inspections in a GIS of the different products from the post-processing of the helicopter borne gamma ray spectrometry. The products are presented in section 4.1.1.

The visual inspection has to a high degree been based on the use of a colour composite map showing the normalisation of all three channels according to

$$K_{\text{norm}} = K/(K+U+Th),$$

$$U_{\text{norm}} = U/(K+U+Th),$$

$$Th_{\text{norm}} = Th/(K+U+Th)$$

On the colour composite map the three different channels have been presented according to  $K_{\text{norm}}$  – green,  $U_{\text{norm}}$  – blue,  $Th_{\text{norm}}$  – red. As an example an area where the blue colour is dominating indicates that the radiation in the channel showing the uranium content at the ground surface is high relative to its normal value and relative to the total radiation in the area. It is however important to note that it does not implicate that the absolute uranium content needs to be higher than the thorium content.

Absolute radiation levels have also been considered in the interpretation.

Gamma ray spectrometry on ground has been carried out only at few locations so far, but is planned to continue in connection to the geological mapping of the area. The limited amount of ground spectrometry data available limits the motivation for profound comparisons of ground and helicopter borne data. Only some general conclusions are so far possible to draw and have been commented in chapter 5. In connection to the geological mapping however, the correlation between the homogeneity areas identified from spectrometry and the geology will be elaborated.

#### **4.2.2 Magnetic total field from the helicopter borne survey 2002**

In the interpretation of the magnetic total field data the first step aims to identify lineaments and to delineate homogeneity volumes, i.e. volumes which are homogeneous in respect to others regarding the amount and distribution of magnetic minerals. This step is based on visual inspections in a GIS of the different products from the post-processing of the helicopter borne measurements of the total magnetic field. The products are presented in section 4.1.2.

An important input in the delineation process is the results from the Euler deconvolution which among other presents probable positions of contacts between different homogeneity volumes. The Euler processing could be regarded as an interpretation, but is here described in section 4.1.3 as a sub-section in the description of the post-processing of air borne geophysical survey data. Another source of input in the delineation work is the petrophysical properties of rocks available.

The second step in the interpretation is the quantitative modelling which has been applied on a few sources to anomalies in the total magnetic field. A 2.5D modelling algorithm has been used. Also here both results from the Euler deconvolution and petrophysics bring possible constraints to models which are important to respect.

#### **4.2.3 Electromagnetic data**

Lineaments were identified independently for helicopter borne multi-frequency EM-data, helicopter borne VLF-data and fixed-wing airborne VLF-data respectively. The work was carried out by visual interpretation of post-processed data in a desk-top GIS environment. Images or GIS-layers representing different measurement parameters were overlaid on each other. The level of uncertainty for different lineaments was set depending on the magnitude of the corresponding EM-anomaly, the length of the lineament, the number of measurement components indicating the lineament and the presence of possible noise sources. Inverted water depth was used to identify topographic lineaments on the sea-floor.

Areas of low bedrock resistivity were identified by setting threshold values of 6500, 4000 and 2000  $\Omega\text{m}$  respectively on the output from the two-layer inversion of multi-frequency data. The areas were slightly smoothed. The areas corresponding to the above thresholds were labelled moderate, low and very low resistivity respectively. Areas close to the major power lines and the power plants were removed from the interpretation. Areas with thick soil cover were identified by setting thresholds of 2.5 and 5 metres on the inversion output. Areas with electrically conductive, presumably clayey, soil were identified by setting thresholds on the ratio of soil thickness to soil resistivity in the inversion output. These thresholds were 0.005 and 0.02 Siemens.

## **5 Results**

The results from the processing and interpretation of the airborne geophysical data reported data has been inserted in the database (SICADA) of SKB. The SICADA reference to the present activity is field note no 140.

### **5.1 Identification of homogeneity areas at the ground surface from helicopter borne gamma ray spectrometry**

#### **5.1.1 Background**

Helicopter borne gamma ray spectrometry is a remote sensing, geophysical technique which provides information about the distribution of K, U and Th that is directly interpretable in terms of surface geology /14/. It is however a surface technique as only gamma rays from the top few tens of cm from below the surface of the ground is detected. This implies that the full interpretation requires an understanding of the nature of the relationship between the bedrock geology and the overburden.

For the Simpevarp area the overburden is in general rather thin and the grade of bedrock exposure high. According to /5/ about 71% of the onshore regional model area is covered by thin till or exposures. The thickest deposits onshore are probably found in the valleys and in the south-western part of the helicopter surveyed area where outcrops are less common and sandy to silty till occur together with glacial clay and post-glacial sediments. Thus quite a large proportion of the surveyed area is covered by a thin layer of till or exposed bedrock. The composition in a thin layer of till is in general regarded to highly reflect the composition of the underlying bedrock.

The interpretation of outcrops made aside from this interpretation activity pinpoints the position of outcrops. The radiation from these outcrops, provided their size is enough and if they are not covered by thick layers of organic matter, will estimate the content of K, U, Th in the bedrock.

In summary the gamma ray spectrometry over the major part of the surveyed area is considered to reflect the bedrock geology. The exceptions are primarily found in the vast topographical depressions or valleys and in areas where eskers or thicker layers of Quaternary deposits occur.

#### **5.1.2 Identified areas with homogeneous distribution pattern and content of K, U and Th in helicopter borne gamma ray spectrometry**

The post-processed products as described in section 4.1.1 above, visualising the distribution of K, U and Th over the helicopter surveyed area, were used in the interpretation together with other data and information described in section 4.1.7 above.

The identification of homogeneity areas i.e. areas with a homogeneous pattern of distribution and content of K, U and Th, has to a high degree been based on colour composite maps built up on three normalised channels where the green channel represents the normalised potassium content, the red channel the thorium content and the blue channel the uranium content (see also section 4.2.1). Absolute radiation levels have however also been considered in the interpretation as they may contribute to the possibility of classifying the sources. As an example mafic rocks are often characterised by low radiation.

The identification of homogeneity areas have resulted in seven groups representing different characteristics according to the relative content of the three elements. The names of the groups should be understood as representing the relative contribution to the total radiation from each channel (or element). They are thus misleading, if they are interpreted to reflect absolute contents of the different elements.

The seven groups are:

- Potassium-dominant
- Thorium-dominant
- Uranium-dominant
- Potassium-Thorium-Uranium
- Potassium-Thorium-dominant
- Potassium-Uranium-dominant
- Thorium-Uranium-dominant

The combinations are presented in detail below and summarized in Figure 5-8. All homogeneity units have been assigned attributes according to the Table 5-1.

**Table 5-1. List of attributes for identified homogeneity areas in helicopter borne gamma ray spectrometry (example from the group “Potassium dominant”).**

Name of attribute	Values in this activity (not used is marked by n.a.)	Comment
ID_T	n.a.	
ORIGIN_T	helicopter borne spectr.	
METHOD_T	gamma ray spectrometry	
CHAR_1_T	potassium dominant	The character of the identified homogeneity area.
CHAR_2_T	partly high uranium-thorium	The character of the identified homogeneity area.
CHAR_3_T	low radiation	The character of the identified homogeneity area.
UNCERT_T	medium	Medium is default
COMMENT_T	n.a.	
PROCESS_T	image analysis	
DATE_D	20030721	Date when the last change was made in the individual homogeneity area.
SCALE_T	n.a.	
PLATFORM_T	helicopter borne geophysics	The IR images and Fastighetskartan have been left out since they were used only for control
SIGN_T	CAT/GeoVista	Interpreted by Carl-Axel Triumf, GeoVista AB

## **Potassium-dominant**

The identified potassium dominant areas are displayed in Figure 5-1. Furthermore they have been divided into four sub groups:

1. Potassium-dominant
2. Potassium-dominant, with low general radiation level
3. Potassium-dominant, with locally increased content of thorium and/or uranium
4. Potassium-dominant, with locally increased content of thorium and/or uranium and with low general radiation level

As these potassium-dominant areas are not significantly coupled to the areas on the map showing the Quaternary deposits most of the information is considered to reflect variations in mineralogy in the bedrock. A few exceptions are however the following:

The area “s1” (see Figure 5-1) coincides with a portion of thicker sandy to silty till at the southwestern corner of the surveyed area.

The area “s2” is found in an area with sparse outcrops which could imply a source reflecting variations in the overburden without connection to bedrock geology. This area is however concordant with a magnetic anomaly with a similar bow-formed appearance. It is thus considered to reflect a geological unit or a variation of the bedrock geology.

In the area of “s3” organic matter is found on the map of the Quaternary deposits. Whether this is the source of the relative enrichment of potassium is however unclear. Here the frequency of outcrops is difficult to estimate as this area is outside the area interpreted regarding outcrops.

Relative enrichments of potassium where the source is believed to be in the bedrock are commented below.

The north-western part of the surveyed area “s4” is potassium-dominant, partly with increased content of thorium and uranium. This area coincides with the “medium to coarse grained granite to quartz syenite” within the Småland “granite” rock suite /5/. As outcrops are quite common here, possibly the identified homogeneity areas are partly reflecting the extent of this variety of the Småland granite. Here also a minor potassium-dominant area with lower absolute radiation levels is found. It coincides with a pronounced local magnetic maximum probably indicating rocks of mafic composition.

The areas “s5” and “s6” are probably reflecting geological sub-units not discerned in the map over the bedrock geology.

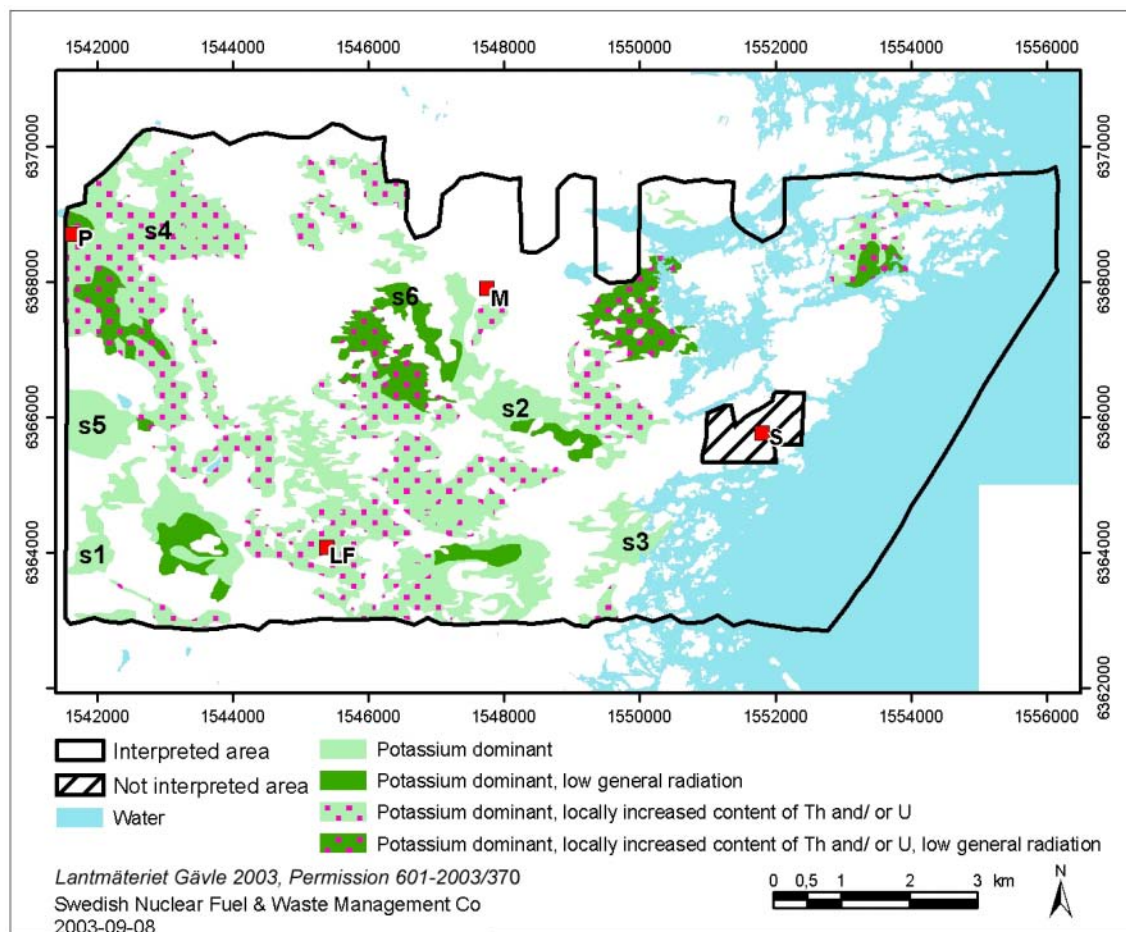


**Figure 5-1.** Potassium-dominant areas identified in the gamma ray spectrometry over the Simpevarp area from helicopter survey data. “s1” to “s6” refer to comments in text regarding potassium-dominant areas. The area around the Simpevarp nuclear power plant has not been interpreted. S=Simpevarp power plant, M=Mederhult, LF=Lilla Fjälltorpet and P=Plittorp.

### Thorium-dominant

The identified thorium-dominant areas are displayed in Figure 5-2. Furthermore they have been divided into two sub groups:

1. Thorium-dominant
2. Thorium-dominant, with low general radiation level

Many of these thorium-dominant areas are significantly coupled to units on the map showing the Quaternary deposits. The areas “s7”–“s12” are all more or less coinciding with glacial clay or post-glacial sand, gravel and clay. The area “s13” is partly coinciding with glacial clay and post-glacial sand, gravel and clay and sandy to silty till.

Thorium is however also found at high relative concentrations in connection to granitic dykes in the bedrock /15/. Some of the thorium-dominant areas at the northern part of the surveyed area may be related to this source type. The areas “s14” and “s15” may belong to this group.

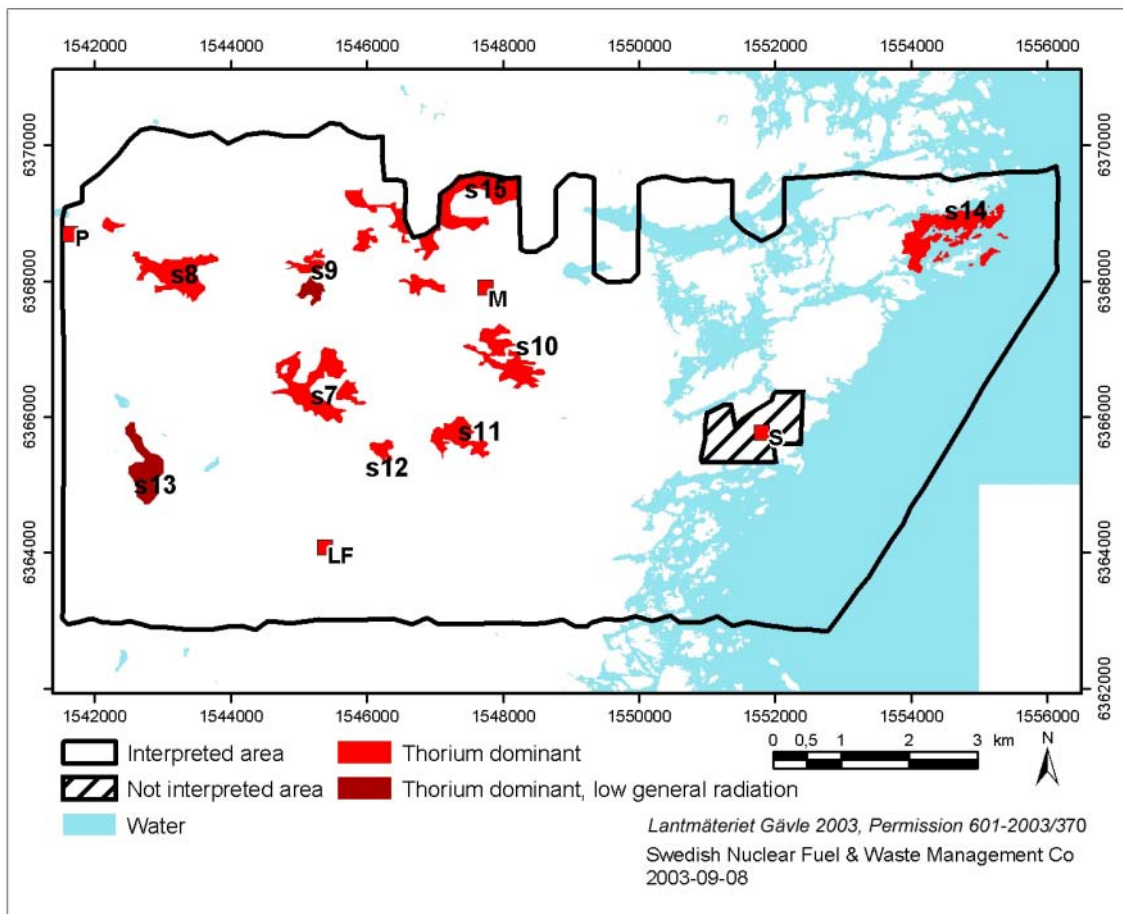


**Figure 5-2.** Thorium-dominant areas identified in the gamma ray spectrometry over the Simpevarp area from helicopter survey data. Areas marked with darker tint may have lower absolute content of thorium or lower radiation levels due to absorbing matter at surface. “s7” to “s15” refer to comments in text regarding thorium-dominant areas. The area around the Simpevarp nuclear power plant has not been interpreted. S=Simpevarp power plant, M=Mederhult, LF=Lilla Fjälltorpet and P=Plittorp.

### Uranium-dominant

The identified uranium dominant areas are displayed in Figure 5-3. Furthermore they have been divided into four sub groups:

1. Uranium-dominant
2. Uranium-dominant, with partly higher potassium and thorium
3. Uranium-dominant, with partly higher potassium and thorium and with low general radiation level
4. Uranium-dominant, with low general radiation level

The areas “s16” and “s17” are found adjacent to “diorite and gabbro” within the Småland “granites”. In both areas granite dykes or minor massifs of “granite to quartz syenite” also occur according to /5/. Furthermore the magnetic total field is high in these both areas indicating rocks with high magnetic susceptibility.

The area “s18” is found at the southern margin of the Småland ”granite” unit of granodioritic to quartz monzodioritic composition. Here the magnetic total field indicates a rock volume with apparently quite low magnetization.

At the north-western corner of the survey area a complex of several sub-areas “s19” are found which are interpreted as uranium dominant. A few of these are apparently correlated to rock units with higher magnetic susceptibility. It can not be ruled out that these sub-areas have the same type of sources as “s16” and “s17”.

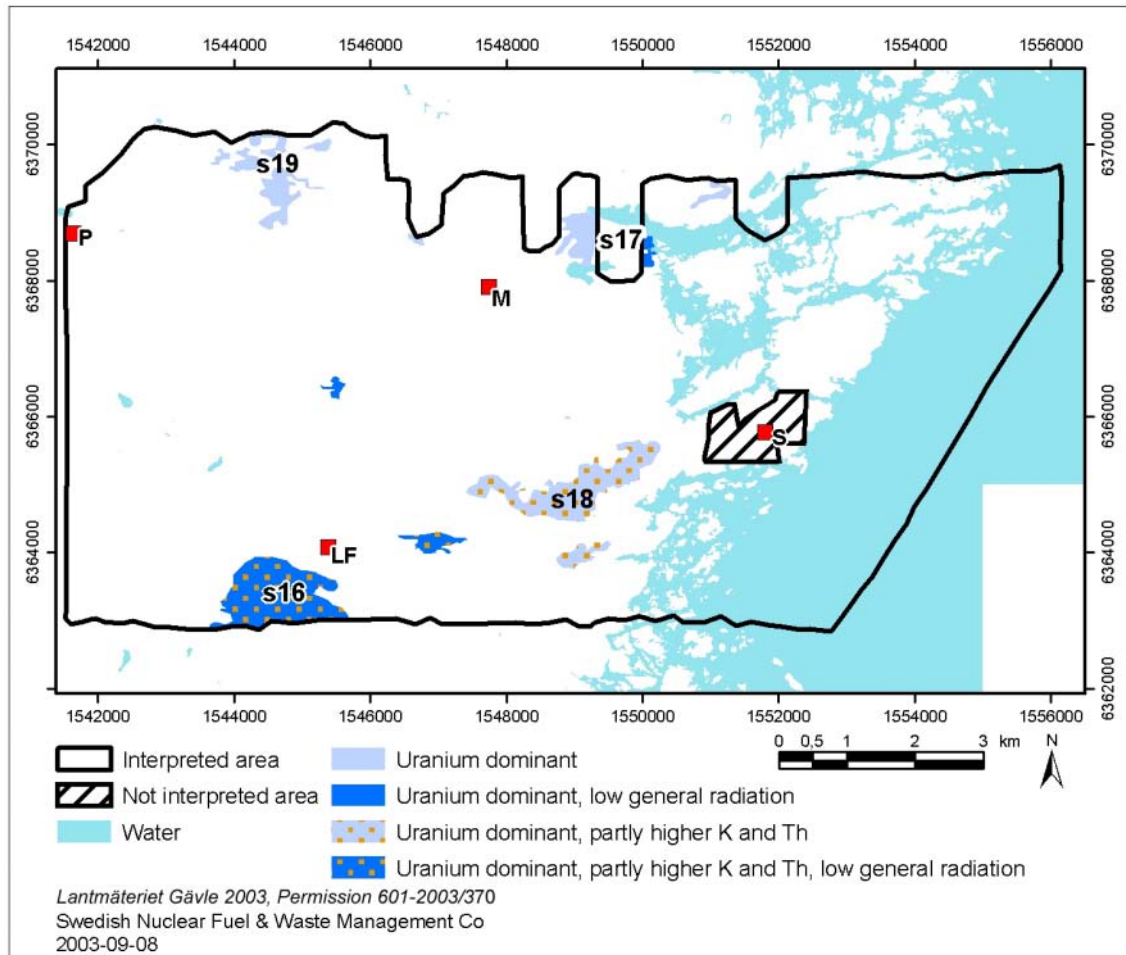


**Figure 5-3.** Uranium-dominant areas identified in the gamma ray spectrometry over the Simpevarp area from helicopter survey data. Lower absolute content of uranium or lower radiation levels due to absorbing matter at surface are indicated by darker blue areas. “s16” to “s19” refer to comments in text regarding uranium-dominant areas. The area around the Simpevarp nuclear power plant has not been interpreted.  
S=Simpevarp power plant, M=Mederhult, LF=Lilla Fjälltorpet and P=Plittorp.

## Potassium-Thorium-Uranium

The identified areas with approximately average relative contributions to the radiation from the three elements are displayed in Figure 5-4. Furthermore they have been divided into two sub groups:

1. approximately equal amounts of potassium, thorium and uranium
2. approximately equal amounts of potassium, thorium and uranium, with low general radiation level

These areas are apparently found in areas where outcrops are quite common indicating that a major source could be the bedrock. There appears to be two major areas where they are found; at the western border of the “granite to granodiorite” of the Småland “granites” and within the same type of Småland “granites” directly east of the Äspö shear zone (ZSM0005A0) /5/.

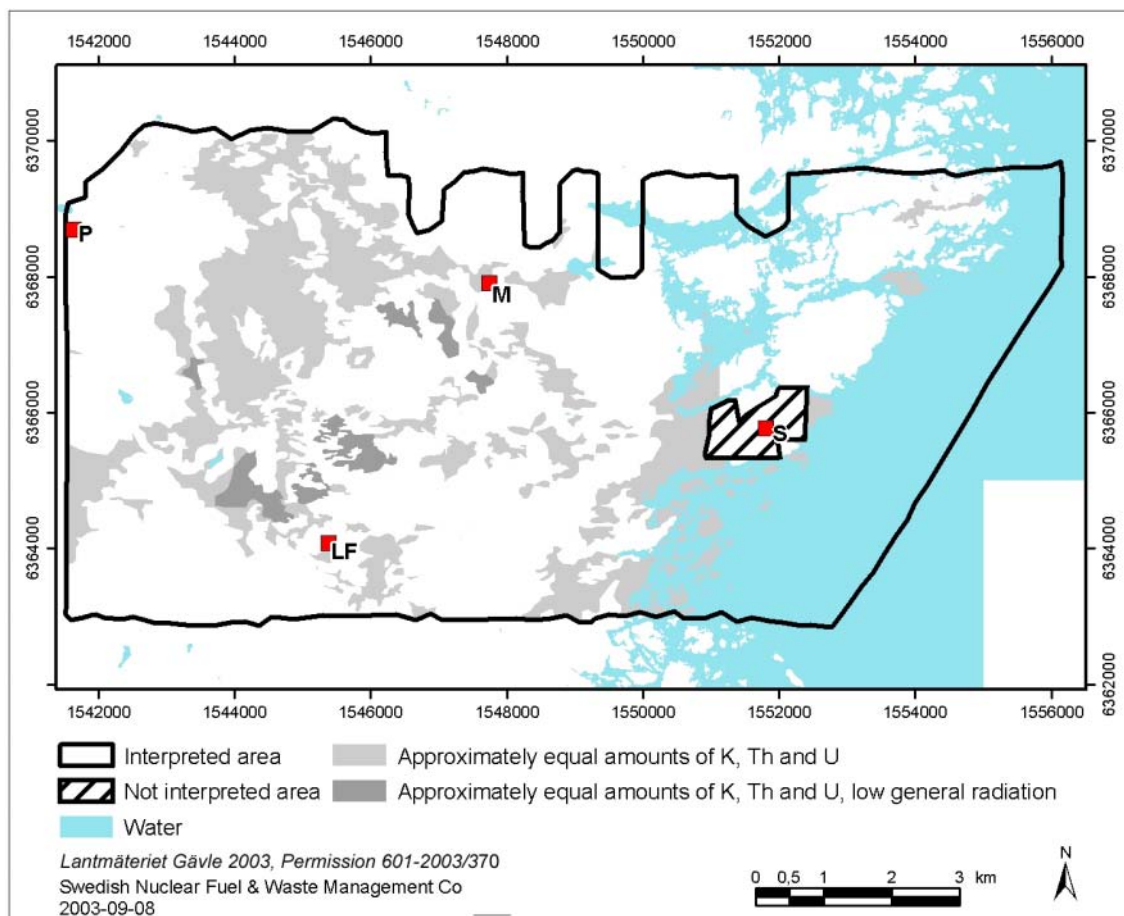


**Figure 5-4.** Areas with approximately average relative contributions to the radiation from the three elements potassium, thorium and uranium identified in the gamma ray spectrometry over the Simpevarp area from helicopter survey data (grey areas). The darker areas have lower general radiation levels. The area around the Simpevarp nuclear power plant has not been interpreted. S=Simpevarp power plant, M=Mederhult, LF=Lilla Fjälltorpet and P=Plittorp.

### Potassium-Thorium-dominant

The identified potassium-thorium dominant areas are displayed in Figure 5-5.

These areas are found around the nuclear power plants of Simpevarp. It is not unlikely that they more reflect a disturbance from the power plant than a significant variation in geology.

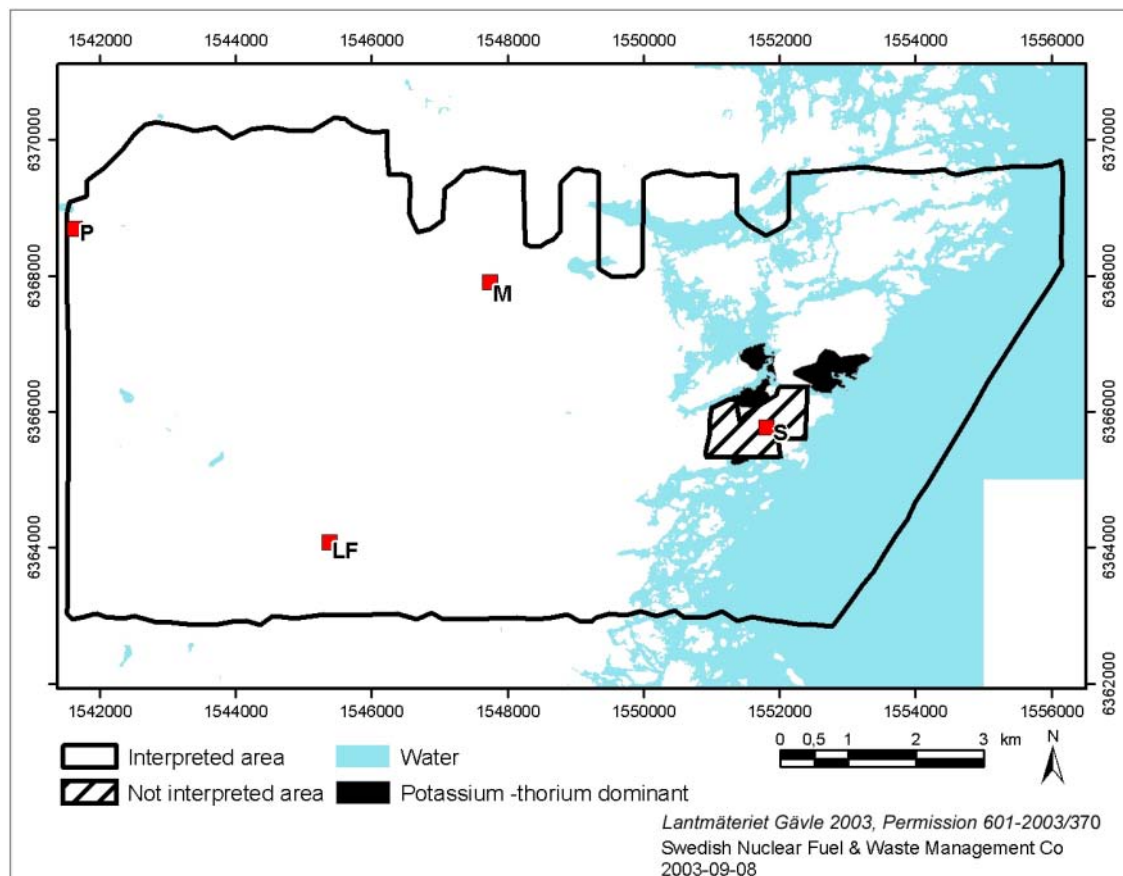


**Figure 5-5.** Potassium-thorium dominant areas are found near the nuclear power plant only (in black). The area around the Simpevarp nuclear power plant has not been interpreted. S=Simpevarp power plant, M=Mederhult, LF=Lilla Fjälltorpet and P=Plittorp.

### Potassium-Uranium-dominant

The identified potassium-uranium dominant areas are displayed in Figure 5-6.

These areas are apparently coupled to relative depressions in the terrain why an influence from Quaternary deposits can not be excluded. One of the areas is found where glacial clay or post-glacial sand, gravel and clay are marked on the map over Quaternary deposits.

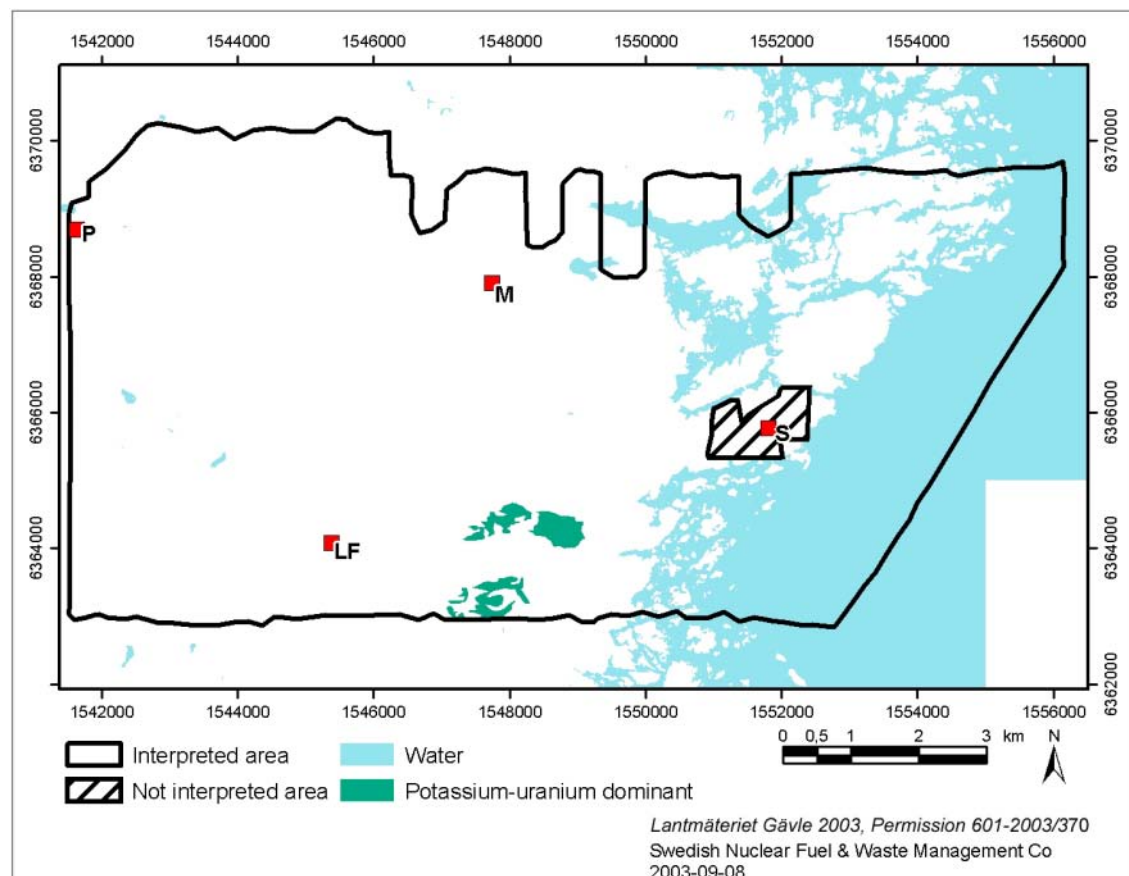


**Figure 5-6.** Potassium-uranium dominant areas are found at the south-eastern part of the survey area (in dark blue green). The area around the Simpevarp nuclear power plant has not been interpreted. S=Simpevarp power plant, M=Mederhult, LF=Lilla Fjälltorpet and P=Plittorp.

### ***Thorium-Uranium dominant***

The identified thorium-uranium dominant areas are shown in Figure 5-7.

Two sub groups are distinguished

1. Thorium-uranium dominant
2. Thorium-uranium dominant, with low general radiation level

In /15/ it was concluded that red to reddish grey equigranular granites of the Småland series and granite dykes very often have high concentrations of thorium in relation to potassium. Higher levels of uranium are also commonly found in pegmatites. It is thus likely that many of the thorium-uranium dominant areas may be associated with reddish equigranular granites, granite dykes or pegmatites. The thorium-uranium dominating areas are covering a large proportion of the north-eastern part of the helicopter surveyed area "s20". From here are known several small massifs and inclusions of red to reddish grey equigranular granites. Granite dykes are also occurring in the area.

As pointed out above, higher relative concentrations of thorium are also found to be well correlated with glacial clay or post-glacial sand, gravel and clay. As a consequence probably also some of the areas which are thorium-uranium dominant should be well correlated with these types of Quaternary deposits. Comparing the map of the Quaternary deposits with thorium-uranium dominant areas shows several examples of good correlation of which a few are commented below:

"s21" is found in a terrain depression where organic deposits, mostly fen peat is reported on the map of the Quaternary deposits /5/. "s22", "s23", "s24" and "s25" are found in terrain depressions where glacial clay and post-glacial sand, gravel and clay, including gyttja clay is reported on the map of the Quaternary deposits /5/.

In a few cases it is more difficult to judge whether the source is from increased content of glacial clay and post-glacial sand, gravel and clay or from a change in the bedrock.

Two examples are commented below:

"s26" and "s27" are found in areas where the concentration of outcrops is less than in the surroundings. In part of the areas organic deposits and glacial clay or post-glacial sand, gravel and clay is reported on the map of the Quaternary deposits /5/. In "s27" also sandy to silty till is found according to /5/. The bedrock geology within these areas is however heterogeneous as indicated both on the geological map of the bedrock /5/ and on the map over the magnetic total field. This indicates bedrock sources in combination with Quaternary sources to be possible producers of the relative thorium-uranium surplus.

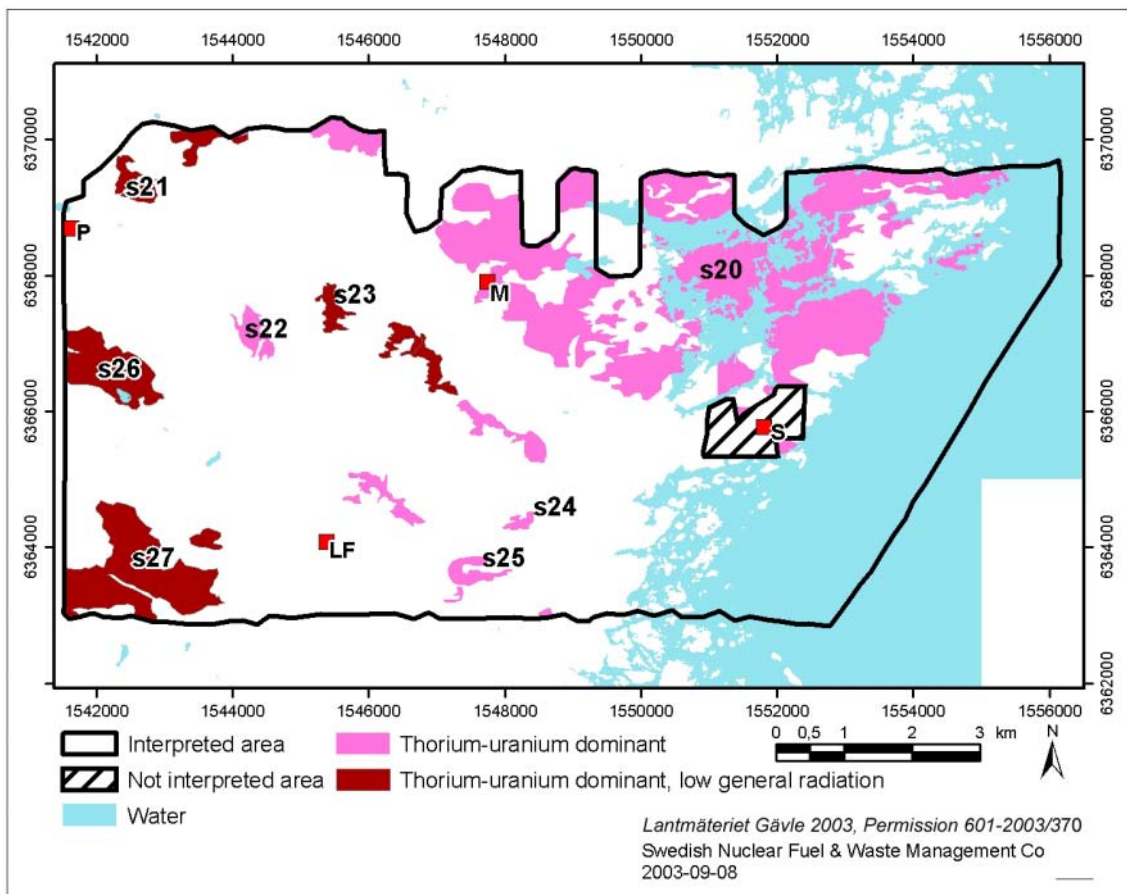


**Figure 5-7.** Thorium-uranium dominant areas are found in pinkish to pinkish-brownish areas marked on the map. Darker background colour indicates lower absolute content of thorium and uranium or lower radiation levels due to absorbing matter at surface. “s20” to “s27” refer to comments in text regarding thorium-uranium dominant areas. The area around the Simpevarp nuclear power plant has not been interpreted. S=Simpevarp power plant, M=Mederhult, LF=Lilla Fjälltorpet and P=Plittorp.

#### **Summary of identified areas with homogeneous distribution pattern and content of K, U and Th in helicopter borne gamma ray spectrometry**

All the identified areas with homogeneous distribution pattern and content of K, U and Th discerned in the data from the helicopter borne gamma ray spectrometry are summarised in Figure 5-8.

At the north-western corner of the helicopter surveyed area there is one minor area which has not been classified. It has very low radiation levels which results in a high degree of unreliability and coincides with organic deposits as marked on the map over Quaternary deposits /5/.

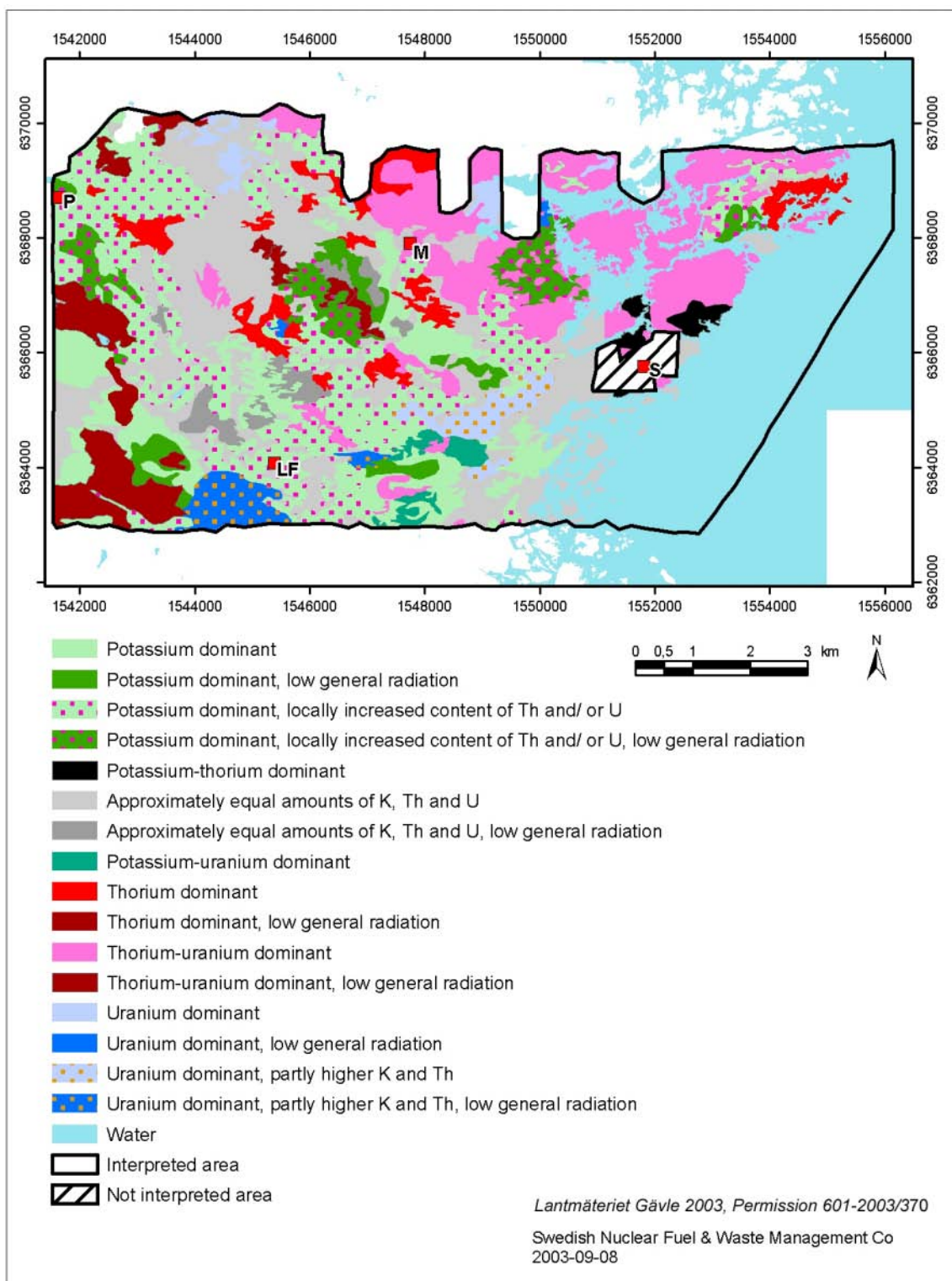


**Figure 5-8.** Summary of identification of homogeneity areas from helicopter borne gamma ray spectrometry. The area around the Simpevarp nuclear power plant has not been interpreted. S=Simpevarp power plant, M=Mederhult, LF=Lilla Fjälltorpet and P=Plittorp.

## **5.2 Identification of homogeneity volumes and lineaments from helicopter borne measurements of the magnetic total field**

### **5.2.1 Background**

Helicopter borne measurements of the magnetic total field is a remote sensing, geophysical technique which provides information about the magnetic properties of the ground. The properties are interpretable in terms of bedrock geology. The technique provides information about the distribution of magnetic minerals in the ground down to substantial depths (several hundreds of metres).

As the rocks in the Simpevarp area in general have rather high but varying magnetic susceptibilities they are well suited for magnetic surveys. Investigations from the Simpevarp area show that the relatively high magnetic susceptibility in fresh rocks stands in sharp contrast to the tectonically affected rock volumes. The effect can be studied directly on the map over the magnetic total field where structures in the bedrock due to different tectonic processes are clearly visible as anomalies indicating low relative magnetic field strength. Thus magnetic surveys in the Simpevarp area are highly diagnostic when the aim is to enlighten the tectonic overprint on rocks. Regarding the classification of rock type the task is more complicated. First several rock types distinguished on the map of the bedrock geology /5/ are probably overlapping each other regarding the level of the magnetic susceptibility. Furthermore the rocks in the Småland “granite” suite are found to intermix with each other at many localities.

A petrophysical survey has partly been carried out and shows some general trends /12/, /13/. The sampling for petrophysical studies will however continue and detailed comparisons between the results from the petrophysics and the interpretation in question will be made in close relation to the planned geological mapping.

The interpretation of data from helicopter borne measurements of the magnetic total field has included the identification of:

- lineaments, which may reflect the tectonics of the Simpevarp area,
- units of approximately equal magnetic susceptibility (low, medium, high, extra high).

Furthermore modelling of a few anomaly sources has been made.

## 5.2.2 Qualitative interpretation of data over the magnetic total field from the helicopter borne survey 2002

### **Lineaments and rock volumes with low relative magnetisation**

Lineaments identified in this interpretation are shown in Figure 5-9. All lineaments have been assigned attributes according to the structure in Table 5-2.

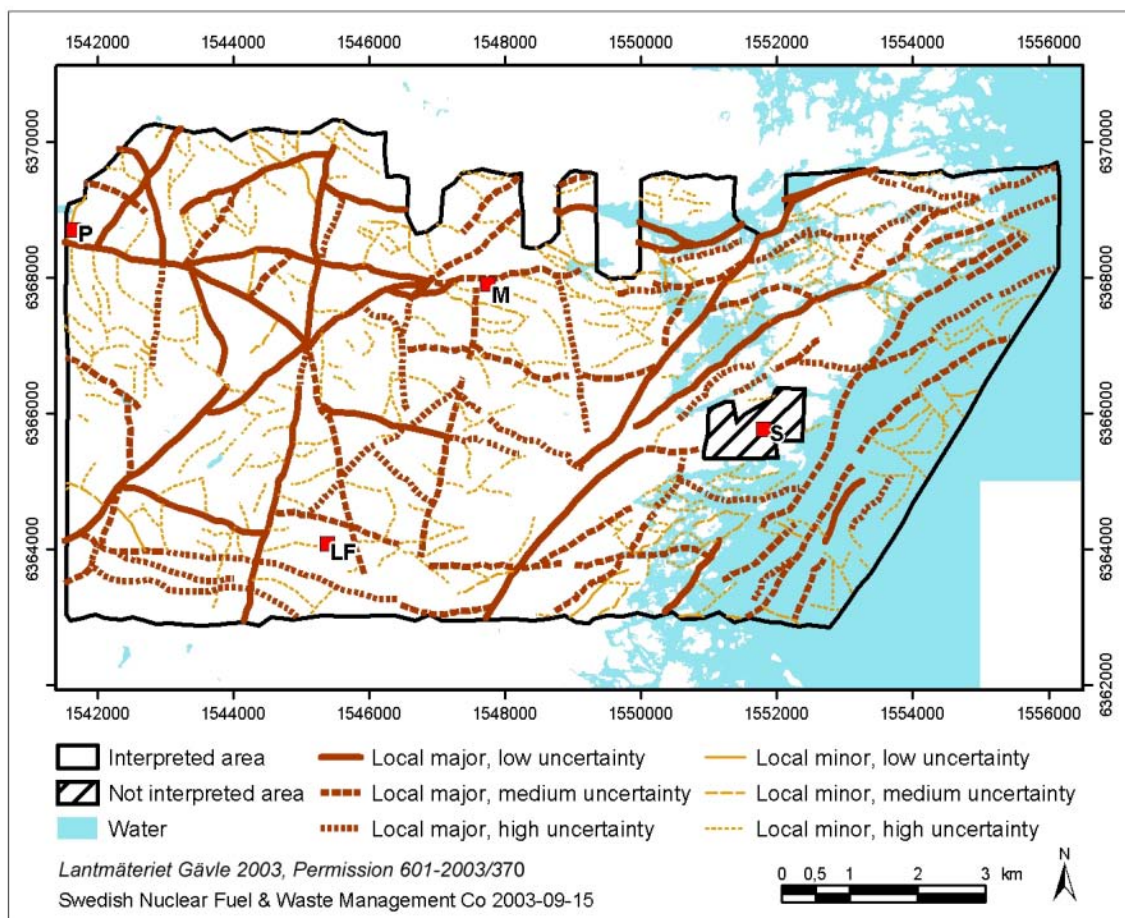


**Figure 5-9.** Lineaments identified in data over the magnetic total field. The lineaments are interpreted to reflect influence from tectonics. The thick lines are ranked as local major, the thin lines as local minor. High degree of dashing of the line indicates high level of uncertainty. The area near the Simpevarp power plants is not interpreted. S=Simpevarp power plant, M=Mederhult, LF=Lilla Fjälltorpet and P=Plittorp.

**Table 5-2. List of attributes for the individual lineaments identified in magnetic data.**

Name of attribute	Values in this activity (not used is marked by n.a.)	Comment
ID_T	n.a.	Identities have not been assigned to the individual lineaments.
ORIGIN_T	helicopter borne magnetics	
METHOD_T	magnetic total field	
CHAR_T	n.a.	The character of the lineaments has not been assigned.
UNCERT_T	low, medium, high	
CLASS_T	local major, local minor	This classification is mainly based on the total length of the sub-sections constituting a possible system of lineaments. A high degree of personal judgement is introduced when such systems are defined. Threshold values for lengths are local major 1–10 km, local minor < 1 km. In a few cases a pronounced visibility of the lineament has implied a higher rank than would be expected if purely based on length.
COMMENT_T		
PROCESS_T	image analysis	
DATE_D	20030701 (default)	Date when the last change was made in the individual lineament.
SCALE_T	n.a.	
PLATFORM_T	helicopter borne geophysics	
WIDTH_N	0	Has not been specified.
PRECIS_N	0	Has not been specified.
SIGN_T	CAT/GeoVista AB	Interpreted by Carl-Axel Triumf, GeoVista AB.

Rock volumes with estimated low relative magnetisation are shown in Figure 5-10. They have been assigned attributes according to Table 5-3.

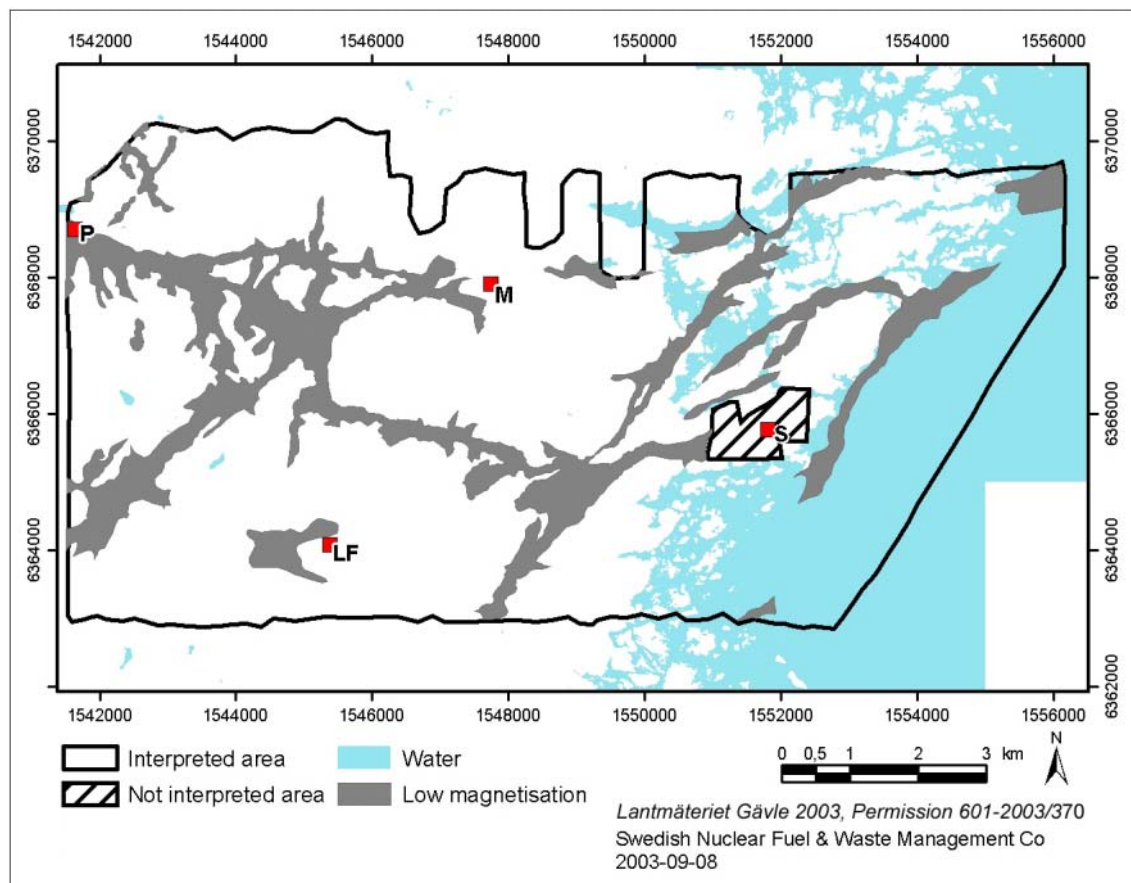


**Figure 5-10.** Areas with estimated low magnetisation. They are interpreted in most cases to reflect the effects of tectonic processes. The area near the Simpevarp power plant is not interpreted. S=Simpevarp power plant, M=Mederhult, LF=Lilla Fjälltorpet and P=Plittorp.

**Table 5-3. List of attributes for the identified rock volumes with low relative magnetisation.**

Name of attribute	Values in this activity (not used is marked by n.a.)	Comment
ID_T	n.a.	Identities have not been assigned.
ORIGIN_T	helicopter borne magnetics	
METHOD_T	magnetic total field	
CHAR_T	magnetic minima	
UNCERT_T	Low	
CLASS_T	n.a.	
COMMENT_T		
PROCESS_T	image analysis	
DATE_D	20030721 (default)	Date when the last change was made in the individual rock volume.
SCALE_T	n.a.	
PLATFORM_T	helicopter borne geophysics	
WIDTH_N	0	Has not been specified.
PRECIS_N	0	Has not been specified.
SIGN_T	CAT/GeoVista AB	Interpreted by Carl-Axel Triumf, GeoVista AB.

### **Rock volumes with high or extra high magnetisation**

Rock volumes which were identified to have high or extra high magnetisation (probably mostly affected by magnetic susceptibility) are shown in Figure 5-11. The rock volumes have been assigned attributes according to the Table 5-4.

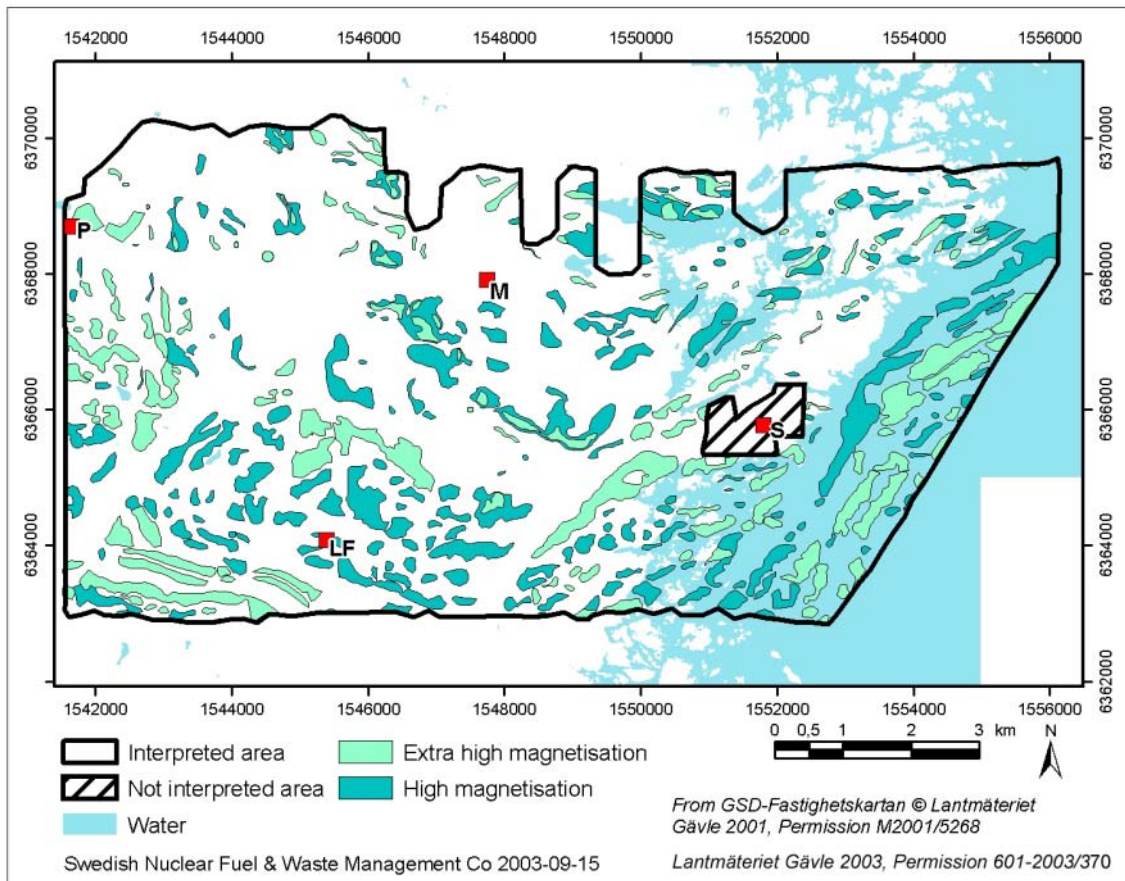


**Figure 5-11.** Units delineated according to their level of magnetisation (magnetic susceptibility). They are interpreted in most cases to reflect variations in bedrock composition due to rock forming processes, and their distribution to some extent to reflect the effect of tectonic processes. The area near the Simpevarp power plant is not interpreted. S=Simpevarp power plant, M=Mederhult, LF=Lilla Fjälltorpet and P=Plittorp.

**Table 5-4. List of attributes for the identified rock volumes with high or extra high relative magnetisation.**

Name of attribute	Values in this activity (not used is marked by n.a.)	Comment
ID_T	n.a.	Identities have not been assigned.
ORIGIN_T	helicopter borne magnetics	
METHOD_T	magnetic total field	
CHAR_T	susc-high, susc-xhigh	Magnetisation has been changed to magnetic susceptibility here as the Q-factor is normally below 0.2
UNCERT_T	medium	
CLASS_T	n.a.	
COMMENT_T		
PROCESS_T	image analysis	
DATE_D	20030721 (default)	Date when the last change was made in the individual volume.
SCALE_T	n.a.	
PLATFORM_T	helicopter borne geophysics	
WIDTH_N	0	Has not been specified.
PRECIS_N	0	Has not been specified.
SIGN_T	CAT/GeoVista AB	Interpreted by Carl-Axel Triumf, GeoVista AB.

## **Summary of the qualitative interpretation of data of the magnetic total field from the helicopter borne survey 2002**

Figure 5-12 shows the summary of the interpretation of data of the magnetic total field from the helicopter borne survey 2002.

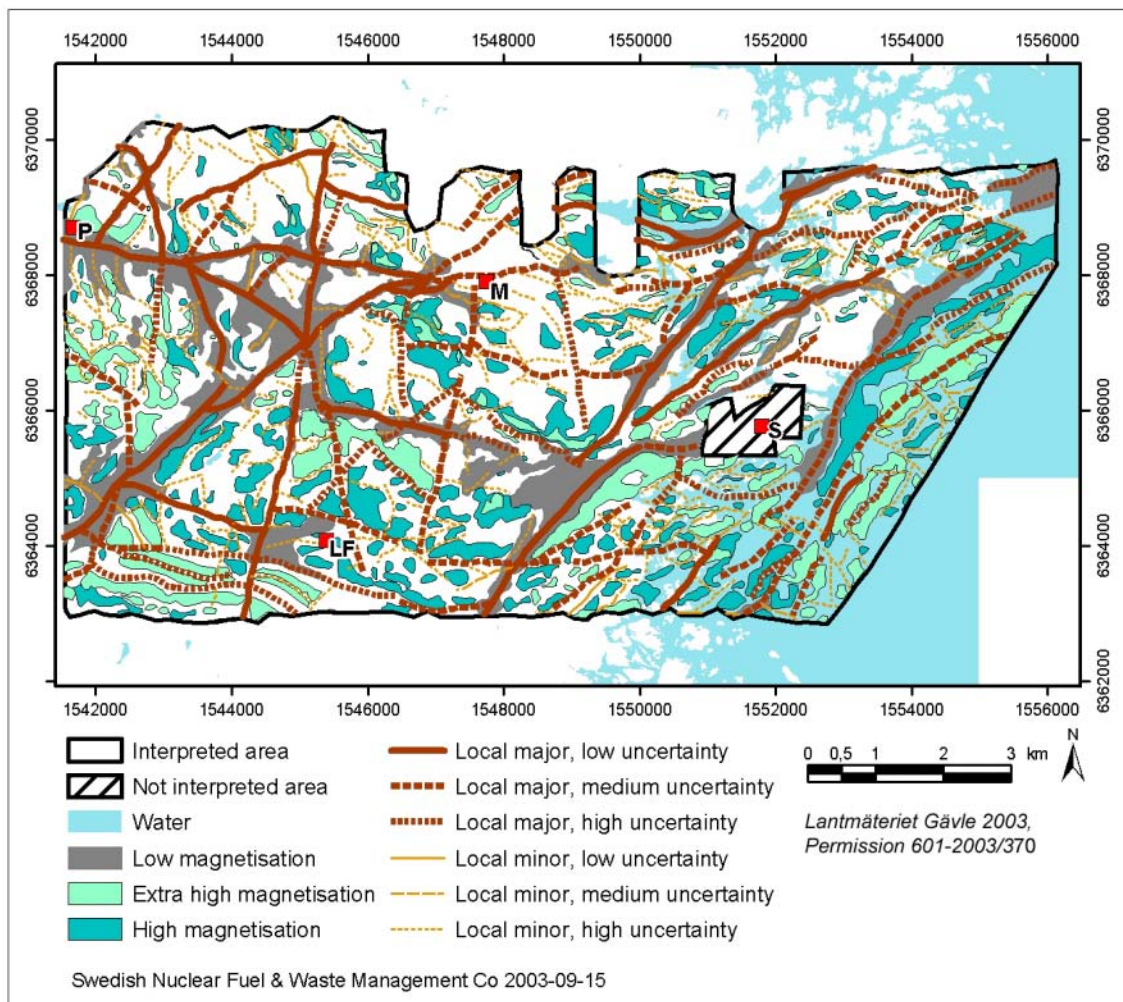


**Figure 5-12.** The results of the qualitative interpretation of data over the magnetic total field from the helicopter borne survey 2002. The area near the Simpevarp power plant is not interpreted. S=Simpevarp power plant, M=Mederhult, LF=Lilla Fjälltorpet and P=Plittorp.

### 5.2.3 Quantitative interpretation of data over the magnetic total field from the helicopter borne survey 2002

#### **Modelling using a 2.5D model**

Quantitative modelling has been carried out using data from three sampled profiles from the grid over the magnetic total field from the helicopter borne survey. The location of the three profiles is shown in Figure 5-13.

The aim of the modelling has varied depending on profile. In the modelling the focus has been on depths less than 500 m. This means that the geometries at greater depths than a few hundred of metres should be paid less attention.

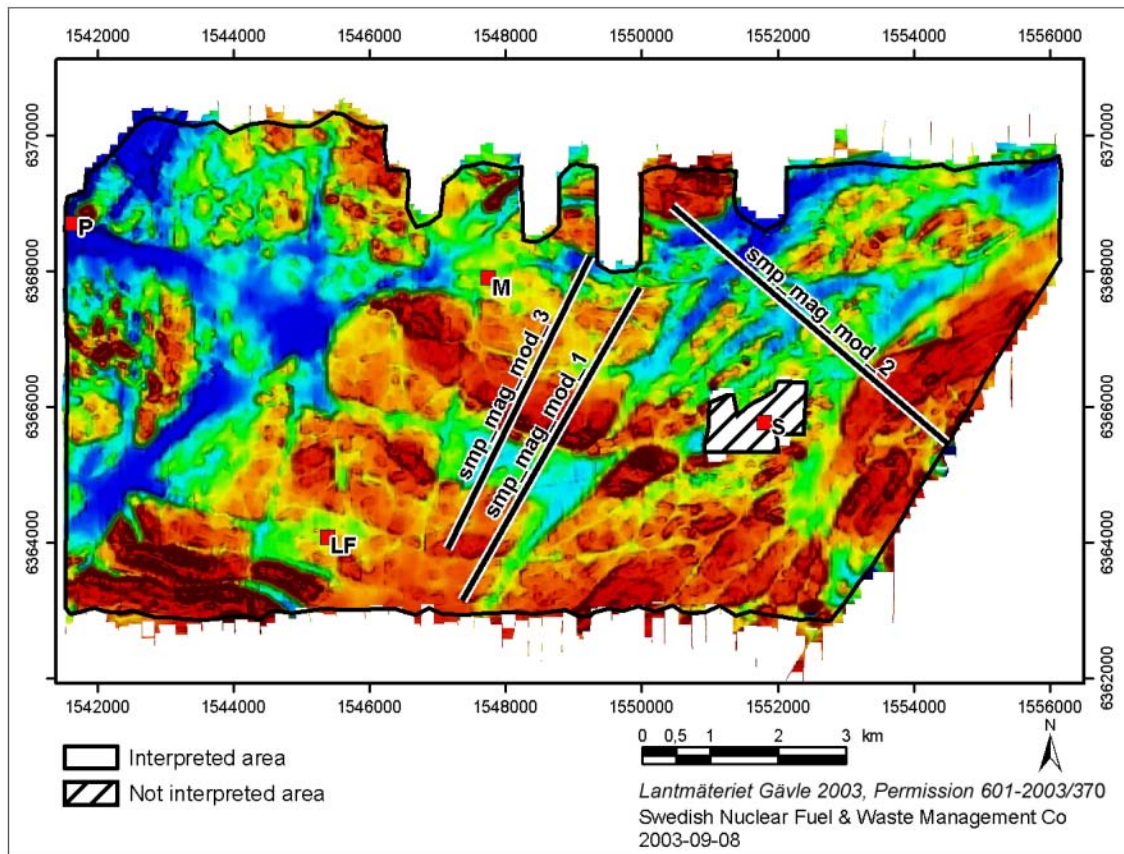


**Figure 5-13.** Three profiles sampled from a grid over the magnetic total field from the helicopter borne survey have been modelled using a 2.5D modelling algorithm. The location and naming of the three profiles is shown in the figure together with the magnetic total field in the background. S=Simpevarp power plant, M=Mederhult, LF=Lilla Fjälltorpet and P=Plittorp.

### **Profile “smp\_mag\_mod\_1”**

The task of the modelling of magnetic total field data from profile “smp\_mag\_mod\_1” is to indicate a probable dip of the highly magnetised rock at the centre of the helicopter survey area. The magnetic positive anomaly is very pronounced and high susceptibilities have been measured on outcrops in the area. Values between  $5000 \times 10^{-5}$ – $10000 \times 10^{-5}$  SI-units are commonly encountered on mafic rocks, but also the granodiorite to quartz monzodiorite of the “Småland granite” suite is reported to have susceptibilities up to around  $5000 \times 10^{-5}$  [SI].

The modelling indicates the dip of the entire body to be around 45 to 60 degrees towards north (Figure 5-14). The surface near part at the southern contact appears to have another dip – steeper or vertical. The cause to the anomaly shape of the southern flank could however also be attributed to lateral effects from minor adjacent source bodies.

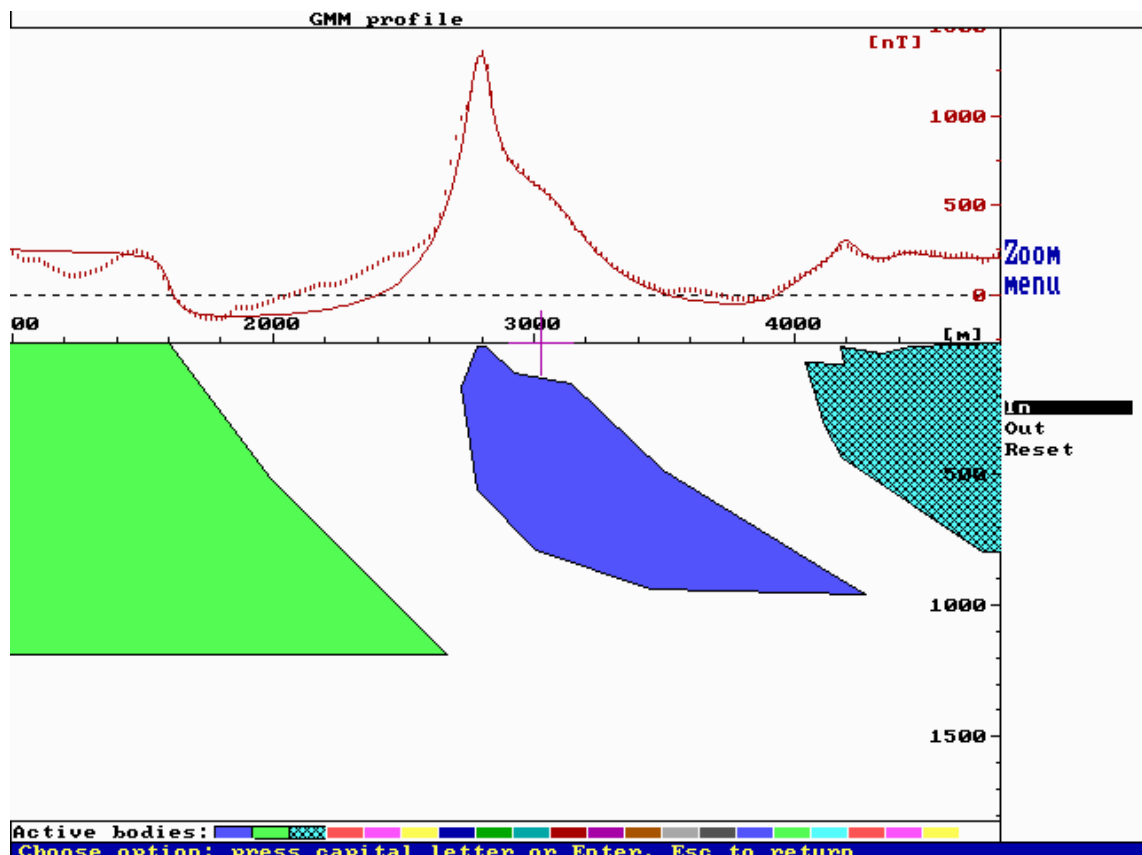


**Figure 5-14.** Result of the modelling of profile “smp\_mag\_mod\_1” with a fairly simple 2.5D model. The primary task of the modelling was to get an indication of the dip of the central (blue) source body. It shows a probable dip of around 45–60 degrees towards north-north-east (north-north-east to the right in the figure).

### **Profile “smp\_mag\_mod\_3”**

The profile is sub-parallel to profile “smp\_mag\_mod\_1” described above.

The magnetic positive anomaly is very pronounced and high susceptibilities have been measured on outcrops in the area (se above).

The modelling indicates the dip of the entire body to be around 45 to 70 degrees towards north (Figure 5-15). Near the surface at the southern contact a tendency to almost vertical dips is recognised. Lateral effects and a super-posing of the anomaly from a minor source body situated immediately at south of the body of interest is however giving a bit uncertain results.

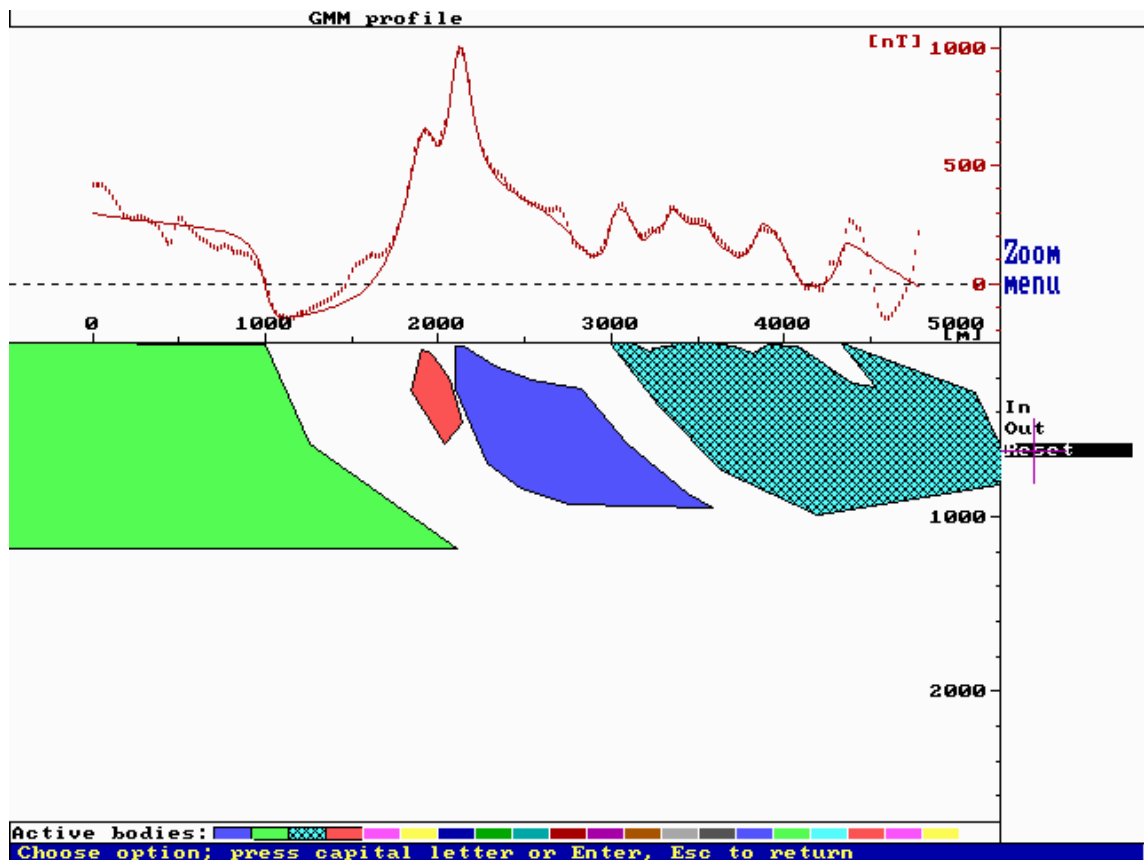


**Figure 5-15.** Result of the modelling of profile “smp\_mag\_mod\_3” with a fairly simple 2.5D model. The primary task of the modelling was to get an indication of the dip of the central (blue) source body. It shows a probable dip of around 30–70 degrees towards north-north-east (north-north-east to the right in the figure).

It is however important to illustrate the equivalence problem which should always be remembered in potential field modelling. It states that one anomaly in principle has an infinite number of source solutions. The way of constraining the modelling process towards the “true” solution is to apply knowledge from other sources. These could be direct observations of geology, but also data from other investigations techniques which are complementary regarding the petrophysical parameters investigated.

In Figure 5-16 the primary target source body has been replaced by two source bodies, giving essentially the same fit, but another geological model. The source body of primary interest in Figure 5-15 has diminished through the introduction of a new source body with typical magnetic susceptibilities for granites in the Simpevarp area (around  $2000 \times 10^{-5}$  SI). The principle dips are however not affected very much but this model gives a larger volume, which is not affected by the high susceptibility rocks (probably a mixture of granodiorite-quartz monzodiorite to gabbro and other mafic rocks).

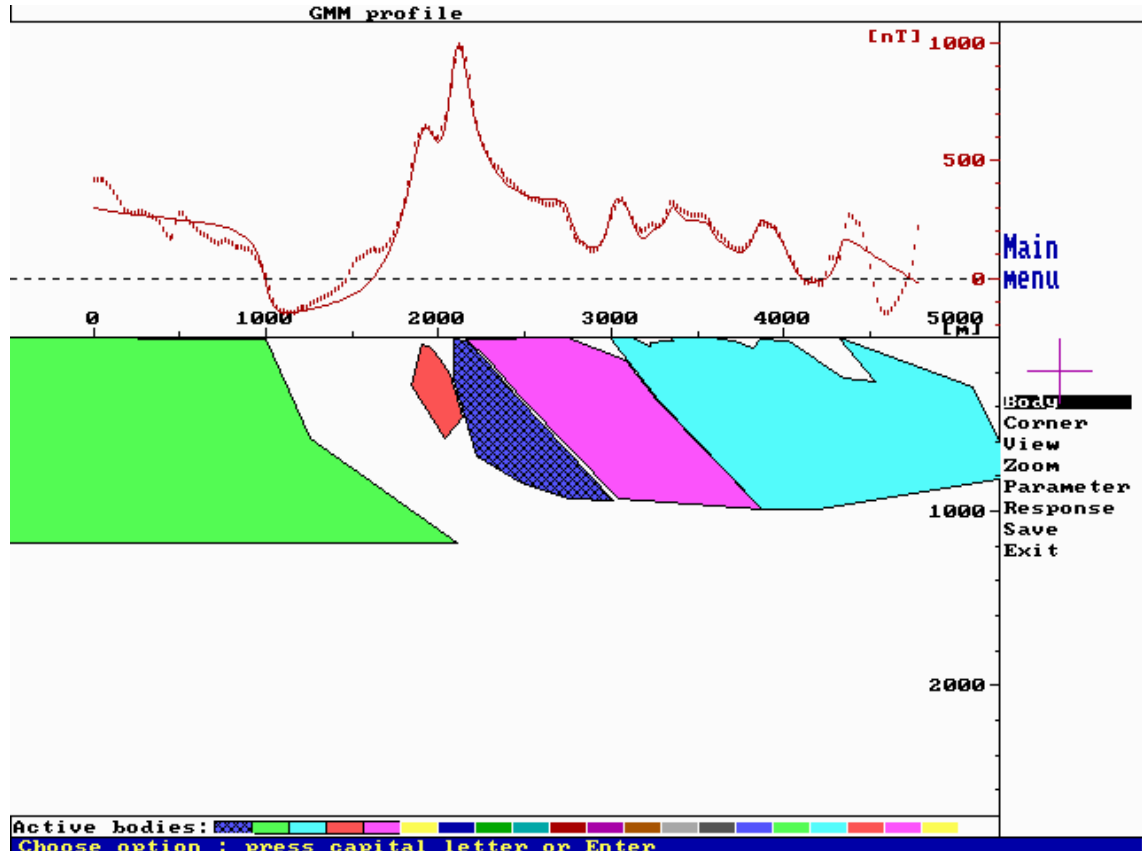


**Figure 5-16.** Result of the modelling of profile “smp\_mag\_mod\_3” with a slightly more complex 2.5D model as compared to the one presented in Figure 5-15. The primary task of the modelling was to get an indication of the dip of the central (blue) source body. It shows a probable dip of around 50–70 degrees towards north-north-east (north-north-east to the right in the figure). The volume without high susceptibility rocks is larger in this model as compared to the model presented in Figure 5-15.

### ***Profile “smp\_mag\_mod\_2”***

The primary task of the modelling of magnetic total field data from profile “smp\_mag\_mod\_2” was to indicate a probable dip of the source to the lineament identified in the sea just outside of the Ävrö island and the Simpevarp peninsula. The lineament is striking approximately NNE and east of it a package of rocks with high relative magnetic susceptibility are prognosticated.

The magnetic profile modelled is quite complicated. As usual in potential field modelling several solutions are possible to find, here are presented two alternatives.

The first alternative is shown in Figure 5-17. The modelling indicates an almost vertical or slight dip towards north-west, of the low magnetic susceptibility zone which should be the source to the lineament in question.

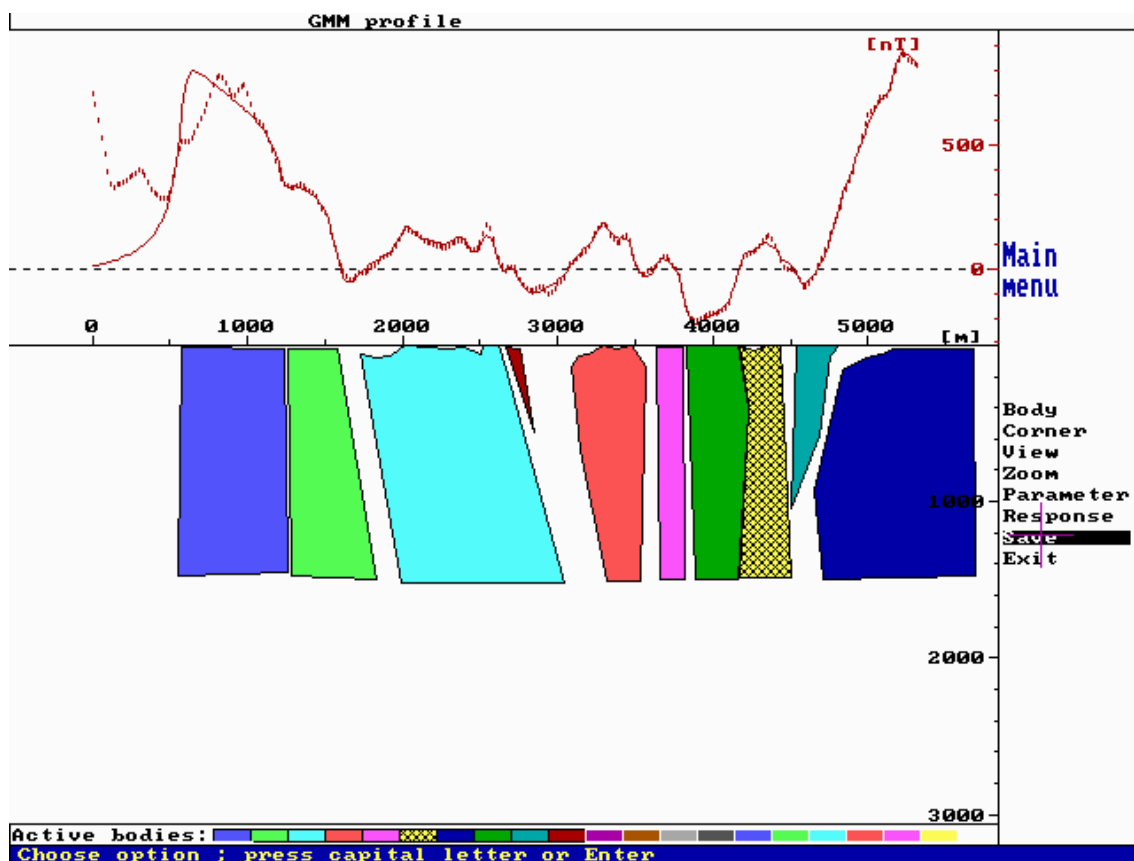


**Figure 5-17.** Result of the modelling of profile “smp\_mag\_mod\_2” with a slightly more simple model as compared to the one presented in Figure 5-18. The primary task of the modelling was to get an indication of the dip of the low magnetization zone between the light greenish and light bluish source bodies at the left part of the profile above. It shows a slight dip towards right in the figure (corresponds to geographic north-west).

The second alternative is shown in Figure 5-18. Here the modelling indicates a south-east dipping low magnetized zone to be the source to the lineament in question. This shows the inherent problem in potential field modelling. A common remedy to these problems associated with the “principle of equivalence” is to invoke constraints in the interpretation. Direct observations of the geology and petrophysical properties will often disqualify some of the apparently acceptable solutions. In this case the zone would be outcropping at the shore line of Ävrö. As such a zone is not easily recognised in the outcrops the solution presented in Figure 5-18 is less probable than the model presented in Figure 5-17.

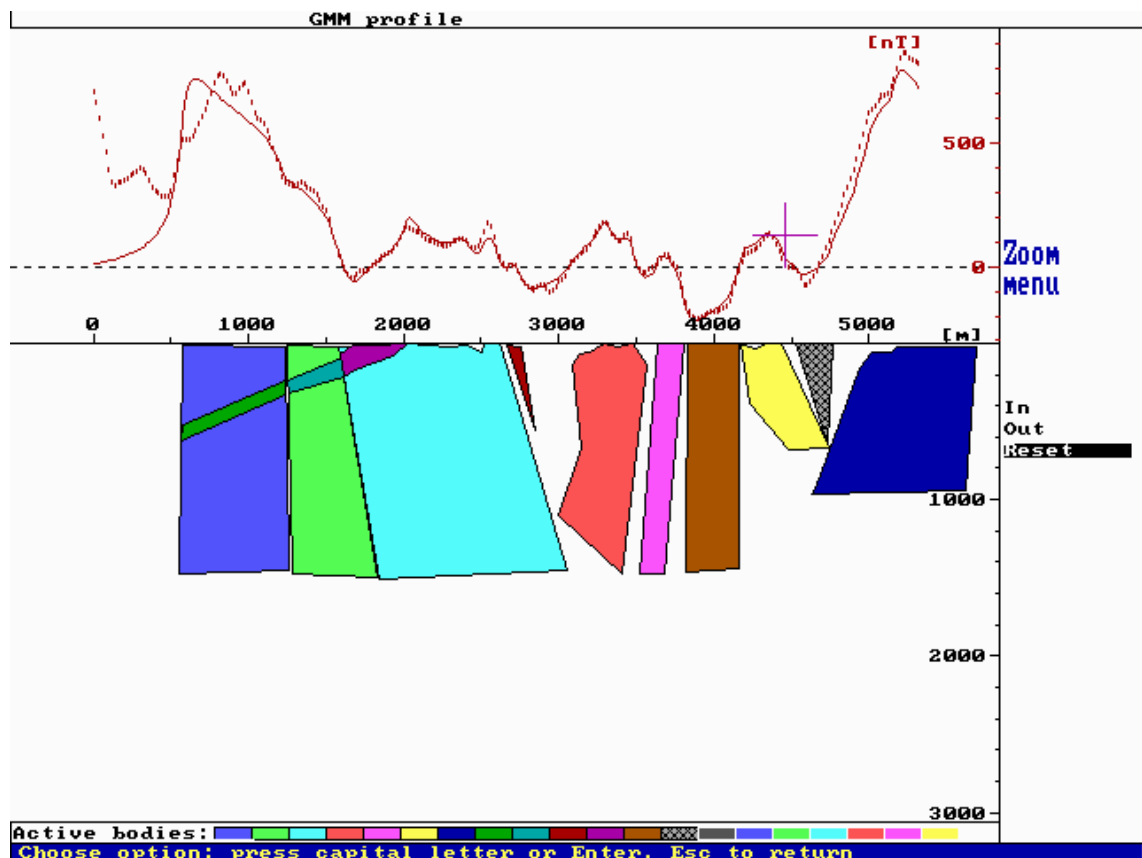


**Figure 5-18.** Result of the modelling of profile “smp\_mag\_mod\_3” with a slightly more complex 2.5D model as compared to the one presented in Figure 5-17 above. The primary task of the modelling was to get an indication of the dip of the low magnetization zone at the left part of the profile above. It shows a fairly flat dip towards left in the figure (corresponds to geographic south-east) of the zone (the source in three different colours).

## **5.3 Identification of homogeneity volumes and lineaments from airborne EM-measurements**

### **5.3.1 Background**

Helicopter-borne EM-measurements is a geophysical technique which provides information about the electric properties of the soil cover and the bedrock. The technique provides information about conductive minerals, the amount of water contained in soil and rock pore-space and rock fractures and the salinity of this water. The depth of investigation is dependent upon the electrical structure of the ground and the type of measuring system but is usually moderate (ca 30 to 200 metres) under normal Swedish conditions.

As the rocks in the Simpevarp in general have rather high electric resistivity they will give weak responses to the EM system. However, EM-anomalies are expected for clayey and/or thick soil cover and for water-bearing and/or clay-altered fractures in the bedrock.

The interpretation of EM-data from airborne measurements has included the identification or determination of:

- Lineaments from helicopter borne multi-frequency EM-data, which may reflect the presence of bedrock fractures and/or depressions in the bedrock surface covered by soil.
- Units of lower than normal (for the area) resistivity in the bedrock.
- Units of conductive overburden.
- Units of thicker than normal (for the area) soil cover.
- Water depth.
- Lineaments from helicopter borne VLF-data.
- Lineaments from fixed wing air-borne VLF-data.

### **5.3.2 Interpretation of multi-frequency EM-data from the helicopter-borne survey 2002**

#### ***Lineaments caused by low-resistivity structures***

Lineaments identified in this interpretation are shown in Figure 5-19. Weak EM-anomalies might be difficult to recognize in maps based on grids of secondary fields or apparent resistivity. However, they are easier to recognize in maps of AGC-filtered data or in profile plots. This has the consequence that lineaments that strike in directions close to the NS line direction of the survey will be difficult to identify and hence probably are under-represented in the interpretation. Also, the power lines will influence the measurements. The noise level is high close to the major power lines and the flight altitude is higher than the nominal value. Except for a few exceptions, no lineaments have been identified close to major power lines. Minor power lines do not degrade data quality in a serious way but they will in many cases cause EM anomalies. EM anomalies that coincide with known power-lines have not been included in the

interpreted lineaments unless there is some doubt about the cause of the anomaly. In a few cases EM anomalies close to minor power lines have been classified as “low uncertainty” or “medium uncertainty” if the anomaly nature is typical for an anomaly caused by e.g. a bedrock fracture. Such closeness to any power line has however been noted in the comment field of the attribute table. All lineaments have been assigned attributes according to the structure in Table 5-5.

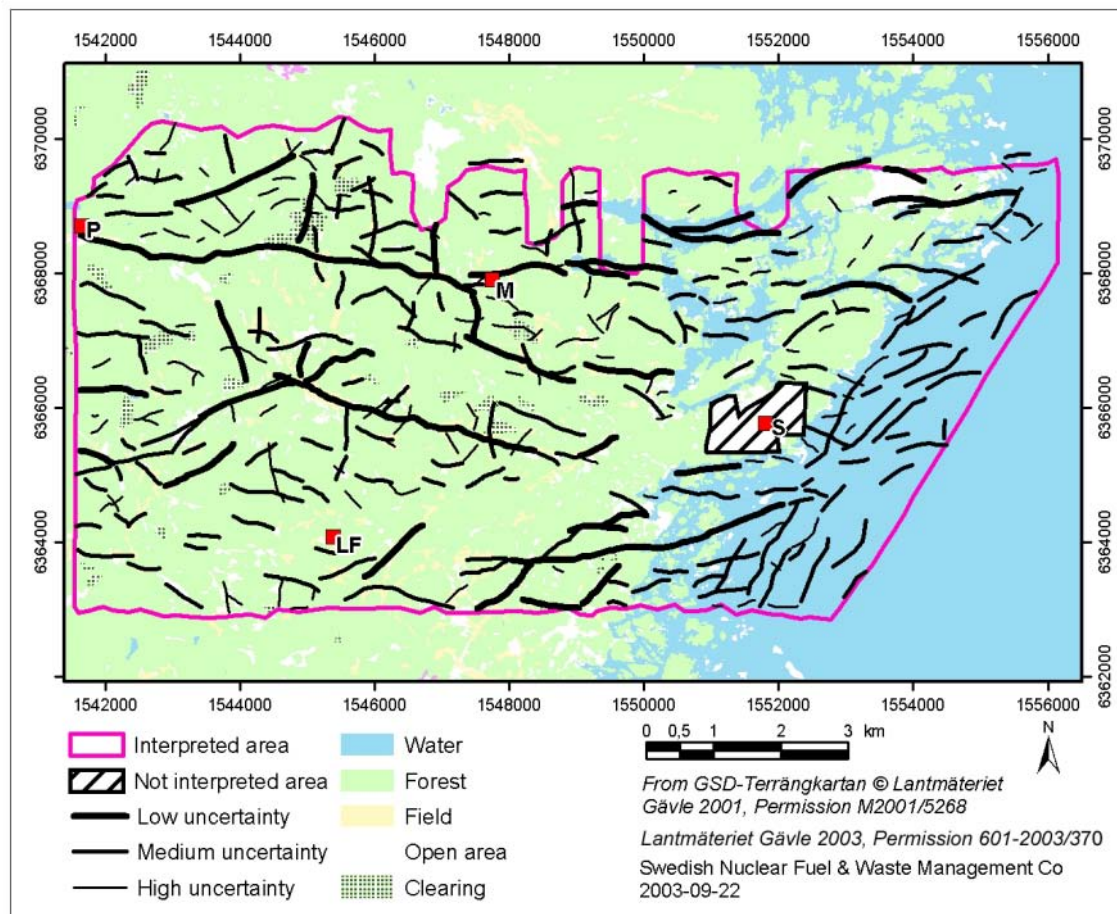


**Figure 5-19.** Lineaments identified in helicopter-borne multi-frequency EM-data. The lineaments are interpreted to reflect presence of bedrock fractures and/or soil covered depressions in bedrock topography. The areas near the Simpevarp power plants and the major power lines are not interpreted. S=Simpevarp power plant, M=Mederhult, LF=Lilla Fjälltorpet and P=Plittorp.

**Table 5-5. List of attributes for the individual lineaments identified in helicopter borne multi-frequency EM data.**

Name of attribute	Values in this activity (not used is marked by n.a.)	Comment
ID_T	n.a.	Identities have not been assigned to the individual lineaments.
ORIGIN_T	electromagnetic	
CLASS_T	n.a.	No classification of the individual lineaments have been made.
METHOD_T	helicopter slingram	
CHAR_T	conductor, sea-floor topography	Some lineaments in water-covered areas are identified as sea-floor topographic features.
UNCERT_T	low, medium, high	Level of uncertainty.
COMMENT_T		Comments mostly inform about possible power line effects.
PROCESS_T	AGC filtered/Apparent resistivity Two-layer inversion	Inverted water depth has been used over water covered areas.
DATE_D	20030806	Date when the last change was made in the individual lineament.
SCALE_T	n.a.	
PLATFORM_T	helicopter bird nom	
WIDTH_N	0	Has not been specified.
PRECIS_N	0	Has not been specified.
SIGN_T	HT/GeoVista AB	Interpreted by Hans Thunehed, GeoVista AB.

### **Rock volumes with moderate or low electric resistivity**

Rock volumes which were identified to have moderate, low or very low electric resistivity are shown in Figure 5-20. The results are based on the inversion of the EM-data to a two-layered model. Low bedrock resistivity can be caused by a higher than normal fracture frequency and/or pore-water salinity. Conductive soil cover of significant thickness might mask the effect of low resistivity bedrock to the inversion algorithm. The rock volumes have been assigned attributes according to the Table 5-6.

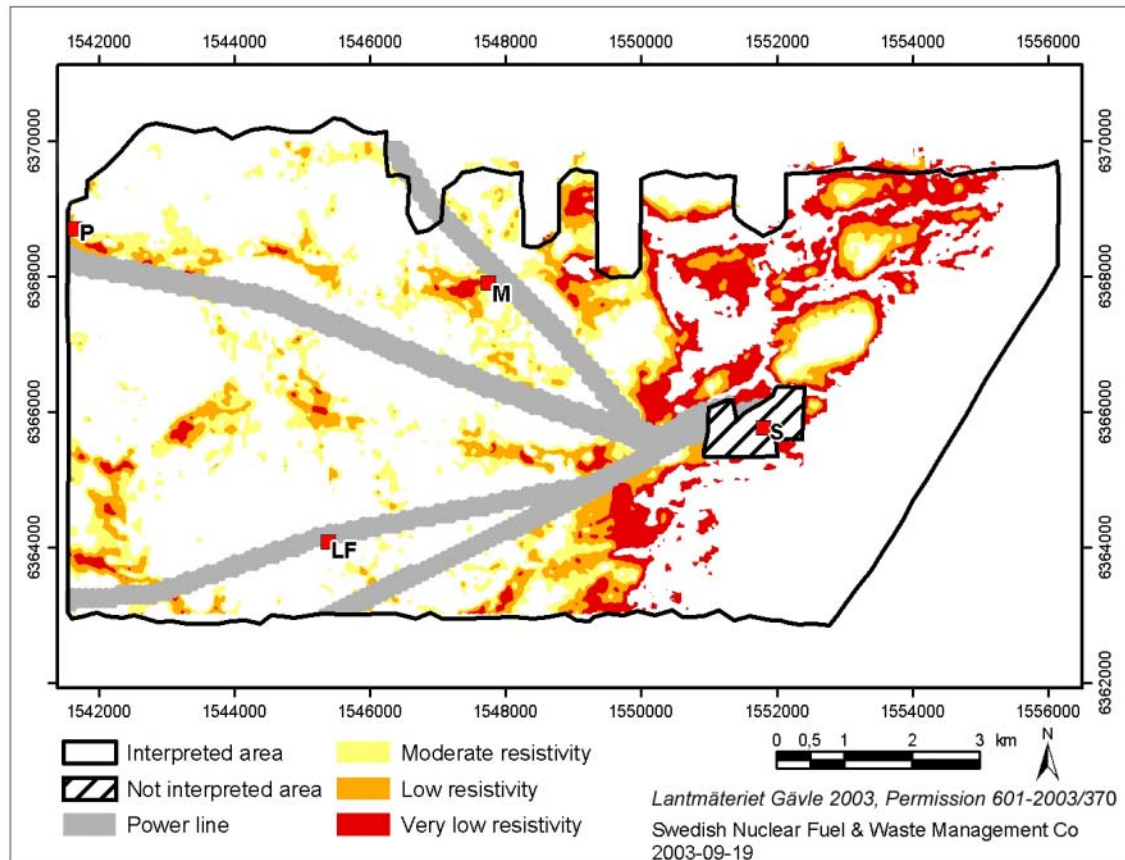


**Figure 5-20.** Areas with moderate or low bedrock resistivity as identified from helicopter-borne multi-frequency EM-measurements. The areas near the Simpevarp power plants and the major power lines are not interpreted. S=Simpevarp power plant, M=Mederhult, LF=Lilla Fjälltorpet and P=Plittorp.

**Table 5-6. List of attributes for the identified rock volumes with moderate or low electric resistivity.**

Name of attribute	Values in this activity (not used is marked by n.a.)	Comment
ID_T	n.a.	Identities have not been assigned to the individual volumes.
ORIGIN_T	electromagnetic	
CLASS_T	n.a.	No classification of the individual volumes have been made.
METHOD_T	helicopter slingram	
CHAR_T	moderate resistivity, low resistivity, very low resistivity	
UNCERT_T	medium	Level of uncertainty.
COMMENT_T	n.a.	
PROCESS_T	two-layer inversion, smoothing	
DATE_D	20030821	Date when the last change was made in the individual volume.
SCALE_T	n.a.	
PLATFORM_T	helicopter bird	
WIDTH_N	0	Has not been specified.
PRECIS_N	0	Has not been specified.
SIGN_T	HT/GeoVista AB	Interpreted by Hans Thunehed, GeoVista AB.

### **Areas with electrically conductive soil cover**

Areas which were identified to have electrically conductive soil cover are shown in Figure 5-21. The results are based on the inversion of the EM-data to a two-layered model. Soil cover with high electric conductance can correspond to clayey soil or bogs with significant thickness. The conductance is the ratio between soil cover thickness and resistivity. These two parameters can generally not be determined individually. The areas have been assigned attributes according to the Table 5-7.

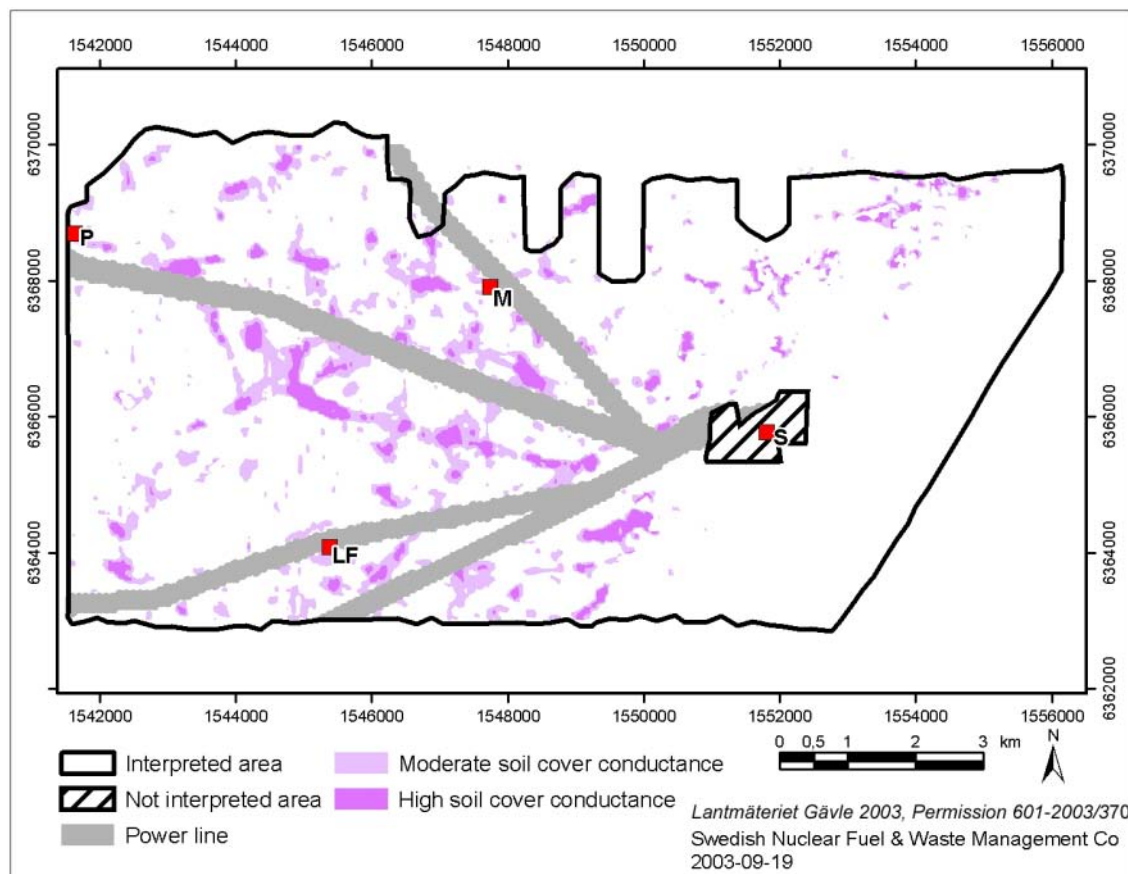


**Figure 5-21.** Areas with moderate or high soil cover conductance identified from helicopter-borne multi-frequency EM-measurements. The areas near the Simpevarp power plants and the major power lines are not interpreted. S=Simpevarp power plant, M=Mederhult, LF=Lilla Fjälltorpet and P=Plittorp.

**Table 5-7. List of attributes for the areas with electrically conductive soil cover.**

Name of attribute	Values in this activity (not used is marked by n.a.)	Comment
ID_T	n.a.	Identities have not been assigned to the individual areas.
ORIGIN_T	electromagnetic	
CLASS_T	n.a.	No classification of the individual areas have been made.
METHOD_T	helicopter slingram	
CHAR_T	moderate conductance, high conductance	
UNCERT_T	medium	Level of uncertainty.
COMMENT_T	n.a.	
PROCESS_T	two-layer inversion, smoothing	
DATE_D	20030821	Date when the last change was made in the individual area.
SCALE_T	n.a.	
PLATFORM_T	helicopter bird	
WIDTH_N	0	Has not been specified.
PRECIS_N	0	Has not been specified.
SIGN_T	HT/GeoVista AB	Interpreted by Hans Thunehed, GeoVista AB.

### **Areas with thick soil cover**

Areas which were identified to have thick soil cover are shown in Figure 5-22. The results are based on the inversion of the EM-data to a two-layered model. The soil cover thickness is however rather poorly determined by the inversion. The soil cover conductance is a better determined parameter (see above). Large parts of the area have outcropping bedrock or very thin moraine cover. The limit for thick soil cover has therefore been set to a rather low value of 2.5 metres. The areas have been assigned attributes according to the Table 5-8.

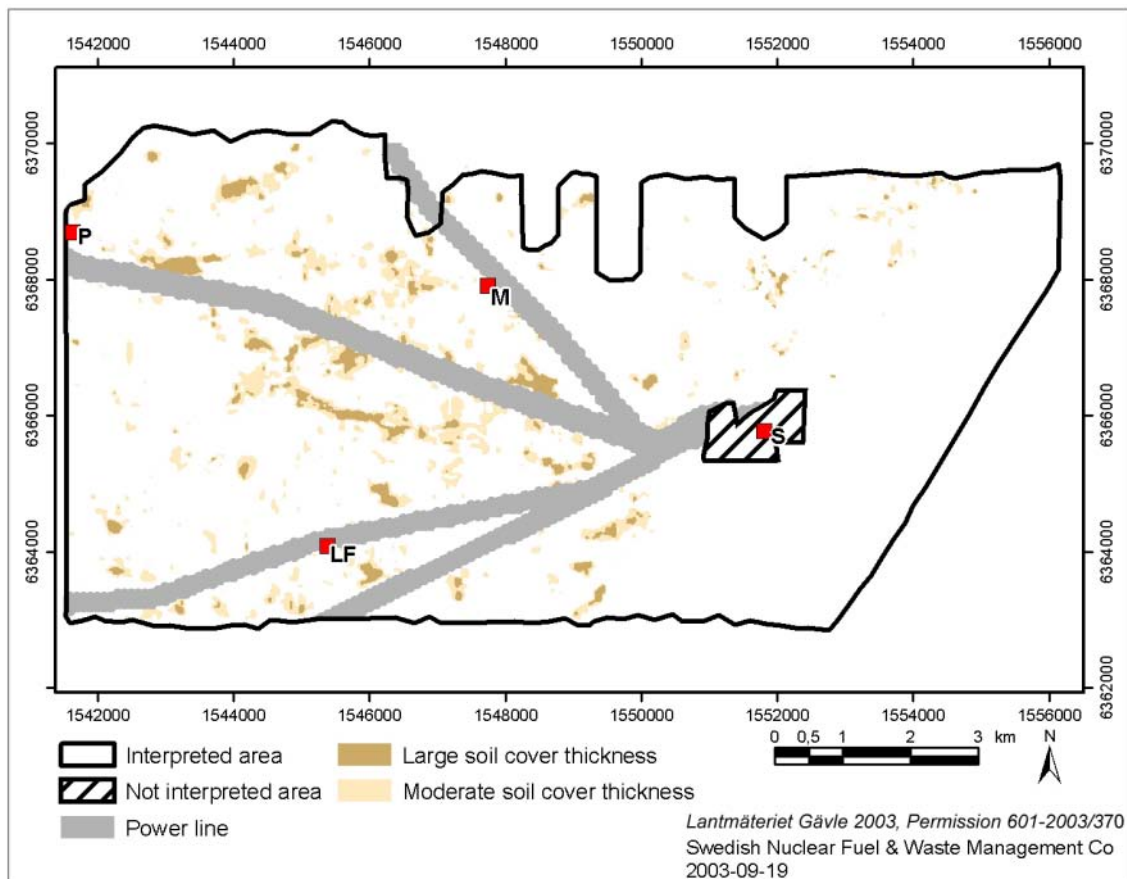


**Figure 5-22.** Areas with moderate or large soil cover thickness as identified from helicopter-borne multi-frequency EM-measurements. The areas near the Simpevarp power plants and the major power lines are not interpreted. S=Simpevarp power plant, M=Mederhult, LF=Lilla Fjälltorpet and P=Plittorp.

**Table 5-8. List of attributes for the areas with thick soil cover.**

Name of attribute	Values in this activity (not used is marked by n.a.)	Comment
ID_T	n.a.	Identities have not been assigned to the individual areas.
ORIGIN_T	electromagnetic	
CLASS_T	n.a.	No classification of the individual areas have been made.
METHOD_T	helicopter slingram	
CHAR_T	moderate thickness, large thickness	
UNCERT_T	high	Level of uncertainty.
COMMENT_T	n.a.	
PROCESS_T	two-layer inversion, smoothing	
DATE_D	20030821	Date when the last change was made in the individual area.
SCALE_T	n.a.	
PLATFORM_T	helicopter bird	
WIDTH_N	0	Has not been specified.
PRECIS_N	0	Has not been specified.
SIGN_T	HT/GeoVista AB	Interpreted by Hans Thunehed, GeoVista AB.

## **Summary of the interpretation of multi-frequency EM-data from the helicopter borne survey 2002**

Figure 5-23 shows the summary of the results with focus on information regarding linaments and areas with low resistivity in the bedrock.

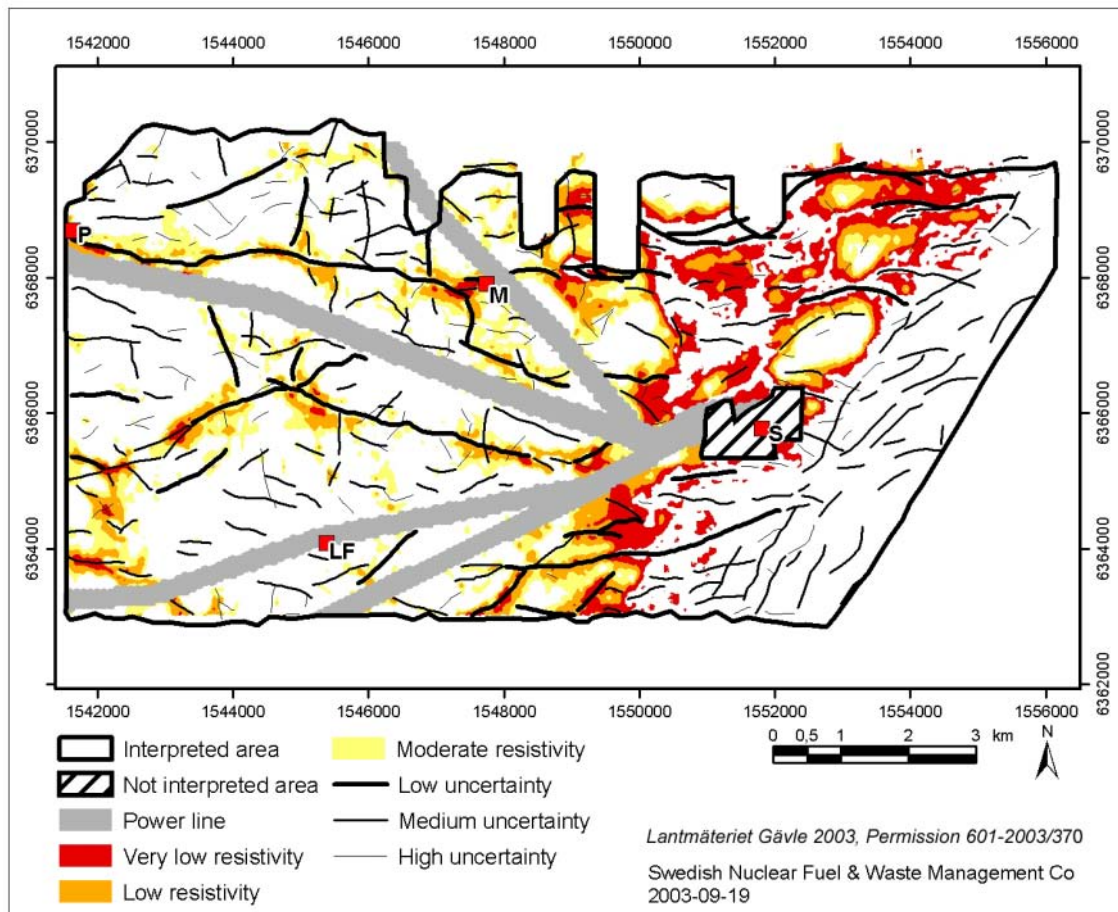


**Figure 5-23.** The results of the interpretation of multi-frequency EM-data from the helicopter borne survey 2002. Areas with low resistivity in bedrock are shown. The areas near the Simpevarp power plant and the major power lines are not interpreted. S=Simpevarp power plant, M=Mederhult, LF=Lilla Fjälltorpet and P=Plittorp.

### 5.3.3 Interpretation of VLF-data from the helicopter-borne survey 2002

#### **Lineaments caused by low-resistivity structures**

Lineaments identified in this interpretation are shown in Figure 5-24. The VLF-measurements were performed as an option during the survey. However, the data coverage was complete although different VLF-transmitters were utilized for different flights. The direction of the primary fields of the transmitters varied slightly which has the consequence that some lineaments have been interrupted. Also, the transmitters for the orthogonal receiver had primary fields that were not perpendicular to the survey lines. Therefore, lineaments that strike in directions close to the NS line direction of the survey will probably be under-represented in the interpretation. The power lines will influence the measurements. The noise level is high close to the major power lines and the flight altitude is higher than the nominal value. Except for a few exceptions, no lineaments have been identified close to major power lines. Minor power lines do not degrade data quality in a serious way but they will in many cases cause EM anomalies.

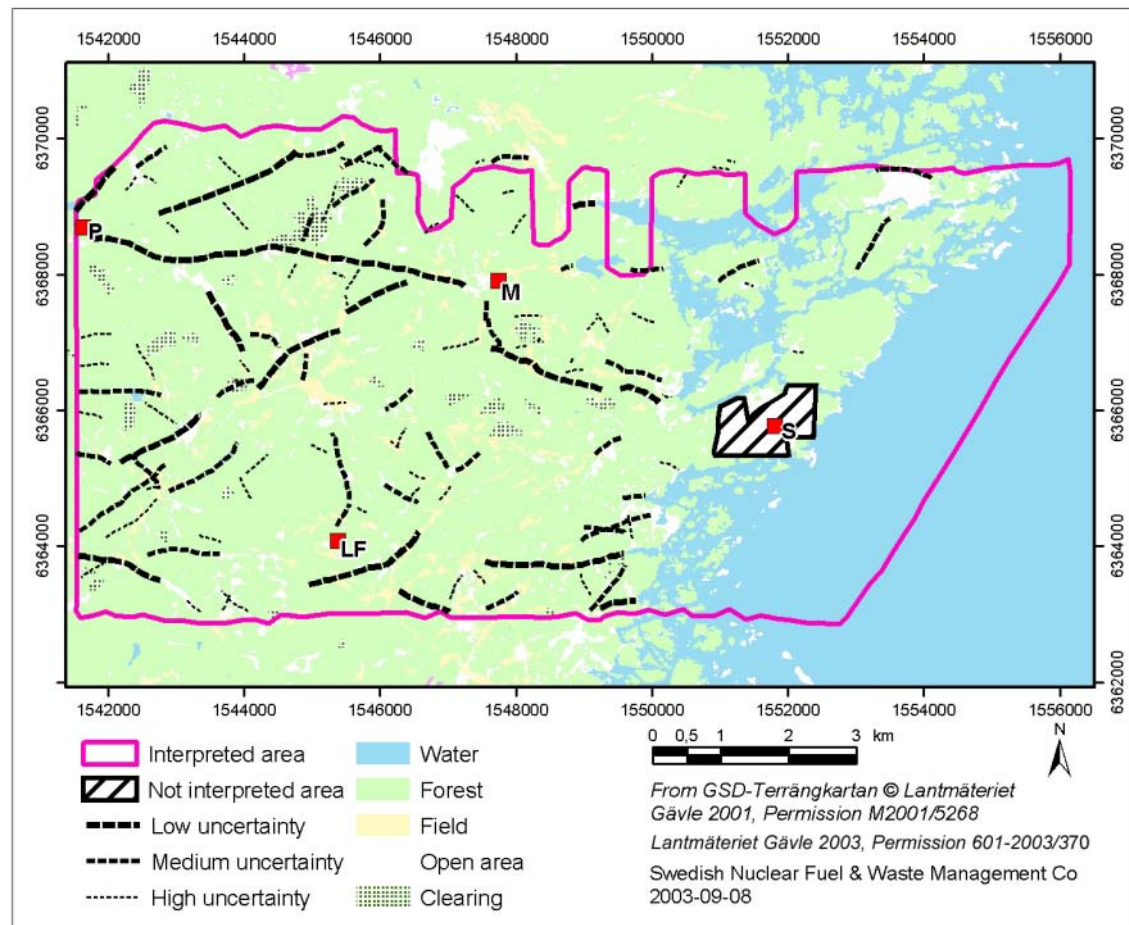


**Figure 5-24.** Lineaments identified in helicopter-borne VLF-data. The lineaments are interpreted to reflect presence of bedrock fractures or possibly soil covered depressions in bedrock topography. The thick lines are ranked as low uncertainty, the thin lines as high uncertainty. The areas near the Simpevarp power plants and the major power lines are not interpreted. S=Simpevarp power plant, M=Mederhult, LF=Lilla Fjälltorpet and P=Plittorp.

EM anomalies that coincide with known power-lines have not been included in the interpreted lineaments unless there is some doubt about the cause of the anomaly. All lineaments have been assigned attributes according to the structure in Table 5-9.

**Table 5-9. List of attributes for the individual lineaments identified in helicopter borne VLF-data.**

Name of attribute	Values in this activity (not used is marked by n.a.)	Comment
ID_T	n.a.	Identities have not been assigned to the individual lineaments.
ORIGIN_T	electromagnetic	
CLASS_T	n.a.	No classification of the individual lineaments have been made.
METHOD_T	helicopter borne VLF	
CHAR_T	conductor	
UNCERT_T	low, medium, high	Level of uncertainty.
COMMENT_T		
PROCESS_T	image analysis	
DATE_D	20030810	Date when the last change was made in the individual lineament.
SCALE_T	n.a.	
PLATFORM_T	helicopter borne VLF	
WIDTH_N	0	Has not been specified.
PRECIS_N	0	Has not been specified.
SIGN_T	HT/GeoVista AB	Interpreted by Hans Thunehed, GeoVista AB.

### 5.3.4 Interpretation of VLF-data from the fixed-wing airborne survey 1986

#### **Lineaments caused by low-resistivity structures**

Lineaments identified in this interpretation are shown in Figure 5-25. The VLF-measurements were made with two transmitter fields in the fixed-wing airborne measurements performed in 1986. The line spacing of 200 metres between the EW lines makes NS trending lineaments easier to detect. Therefore, lineaments that strike in directions close to the EW line direction of the survey will probably be under-represented in the interpretation. The power lines have influenced the measurements. No lineaments have been identified close to major power lines. Minor power lines do not degrade data quality in a serious way but they will in many cases cause EM anomalies. EM anomalies that coincide with known power-lines have not been included in the interpreted lineaments unless there is some doubt about the cause of the anomaly. All lineaments have been assigned attributes according to the structure in Table 5-10.

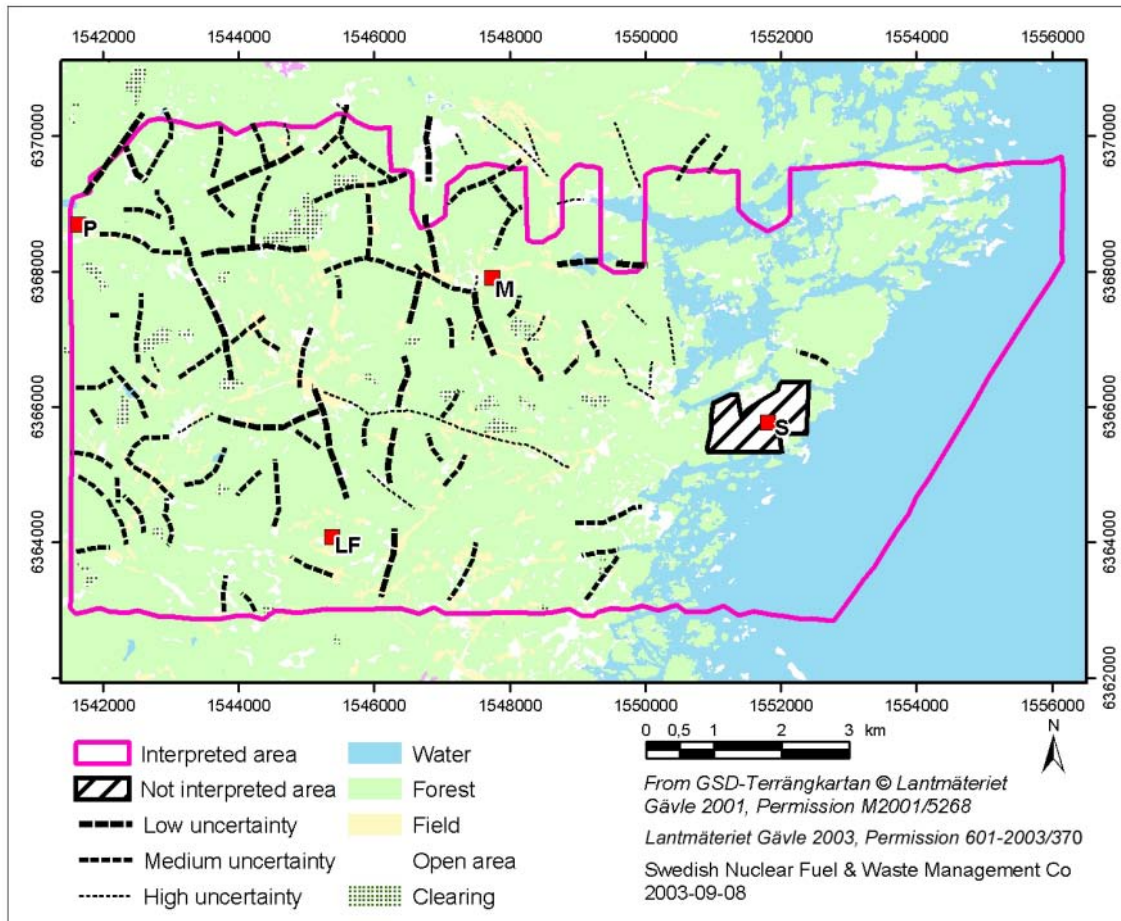


**Figure 5-25.** Lineaments identified in fixed-wing air-borne VLF-data from 1986. The lineaments are interpreted to reflect presence of bedrock fractures or possibly soil covered depressions in bedrock topography. The thick lines are ranked as low uncertainty, the thin lines as high uncertainty. The areas near the Simpevarp power plants and the major power lines are not interpreted. S=Simpevarp power plant, M=Mederhult, LF=Lilla Fjälltorpet and P=Plittorp.

**Table 5-10. List of attributes for the individual lineaments identified in fixed-wing air-borne VLF-data.**

Name of attribute	Values in this activity (not used is marked by n.a.)	Comment
ID_T	n.a.	Identities have not been assigned to the individual lineaments.
ORIGIN_T	electromagnetic	
CLASS_T	n.a.	No classification of the individual lineaments have been made.
METHOD_T	fixed wing VLF 2 station	
CHAR_T	resistivity minima or resistivity gradient	
UNCERT_T	low, medium, high	Level of uncertainty.
COMMENT_T		
PROCESS_T	apparent resistivity calc. from two transmitters	
DATE_D	20030810	Date when the last change was made in the individual lineament.
SCALE_T	n.a.	
PLATFORM_T	fixed wing air plane	
WIDTH_N	0	Has not been specified.
PRECIS_N	0	Has not been specified.
SIGN_T	LP/ SGU and HT/GeoVista AB	Interpreted by Lena Persson, SGU and Hans Thunehed, GeoVista AB.

## 5.4 Discussion

The general philosophy reflected in the instruction and guidelines from SKB for the processing and interpretation of airborne geophysical data is to avoid unnecessary bias between interpretations of different data sets at early stages of the site investigation. This makes future reconstructions and analysis possible of the maturing process where primary data are transformed into useful geological information. Our results reflect these intentions in such a way that several different sets of interpretation results are presented, all of which are more or less independent of each other.

The processing and interpretation of the airborne geophysical data from Oskarshamn has resulted in lineaments, surfaces or volumes with homogeneous characteristics regarding petrophysical parameters, and, geometrical information such as thickness of overburden, depth to anomaly sources, dips of anomaly sources. When studying all the results obtained from airborne geophysical data it is obvious that they contain substantial amounts of useful information for the site descriptive model of the area, both for the regional model and for the local models. This information will successively be implemented into site descriptive models, however it is necessary to relate them to other information in joint interpretation activities. Here we consider the results from the identification of lineaments in digital elevation models, the geological mapping of outcrops and the marine geological survey to be some of the most important information sets to relate to our findings.

## References

- /1/ **Wahlgren C-H, Persson L, Danielsson P, Berglund J, Triumf C-A, Mattsson H, Thunehed H, 2003.** Geologiskt underlag för val av prioriterad plats inom området väster om Simpevarp. Delrapport 1-4. SKB P-03-06. Svensk Kärnbränslehantering AB.
- /2/ **Rønning J H S, Kihle O, Mogaard J O, Walker P, 2003.** Simpevarp site investigation. Helicopter borne geophysics at Simpevarp, Oskarshamn, Sweden. SKB P-03-25. Svensk Kärnbränslehantering AB.
- /3/ **Wiklund S, 2002.** Digitala ortofoton och höjdmodeller. Redovisning av metodik för platsundersökningssområdena Oskarshamn och Forsmark samt förstudieområdet Tierp Norra. SKB P-02-02. Svensk Kärnbränslehantering AB.
- /4/ **Triumf C-A, 2003.** Oskarshamn site investigation. Identification of lineaments in the Simpevarp area by the interpretation of topographical data. SKB P-03-99. Svensk Kärnbränslehantering AB.
- /5/ **SKB, 2002.** Simpevarp – site descriptive model version 0. SKB R-02-35. Svensk Kärnbränslehantering AB.
- /6/ **Pedersen L B, Qian W, Dynesius L, Zhang P, 1994.** An airborne tensor VLF system. From concept to realization. *Geophysical Prospecting*, 42, 863–883.
- /7/ **Becken M, Pedersen L B, 2003.** Transformation of VLF anomaly maps into apparent resistivity and phase. *Geophysics*, 68, 497–505.
- /8/ **Persson L, Becken M, Daniels J, Antal I, 2001.** New developments in the processing and interpretation of airborne VLF-EM data. 69<sup>th</sup> Annual International Meeting, Society of Exploration Geophysicists, San Antonio. Extended Abstract.
- /9/ **Siripunvaraporn W, Egbert G, 2000.** An efficient data-subspace inversion method for 2-D magnetotelluric data. *Geophysics*, 65, 791–803.
- /10/ **Persson L, 2001.** Plane Wave Electromagnetic Measurements for Imaging Fracture Zones. Uppsala Dissertations from the Faculty of Science and Technology 30. Acta Universitatis Upsalensis, Uppsala 2001.
- /11/ **Thunehed H, Pitkänen T, 2003.** Simpevarp site investigation. Electrical soundings supporting inversion of helicopter borne EM-data. Primary data and interpretation report. SKB P-03-17. Svensk Kärnbränslehantering AB.
- /12/ **Mattsson H, Thunehed H, 2003.** Simpevarp site investigation. Measurements of petrophysical parameters on rock samples during autumn 2002. SKB P-03-19. Svensk Kärnbränslehantering AB.

- /13/ **Mattsson H, Thunehed H, Triumf C A, 2003.** Oskarshamn site investigation. Compilation of petrophysical data from rock samples and in situ gamma-ray spectrometry measurements. SKB P-03-97. Svensk Kärnbränslehantering AB.
- /14/ **Shives R B K, Ford K L, Charbonneau B W, 1995.** Applications of Gamma ray spectrometry/magnetic/VLF-EM Surveys. Geological Survey of Canada Workshop Manual Open File Dossier Public 3061, second edition.
- /15/ **Mattsson H, Triumf C-A, Wahlgren C-H, 2002.** Prediktering av förekomst av finkorniga granitgångar i Simpevarpsområdet. SKB P-02-05. Svensk Kärnbränslehantering AB.

## Appendix A

### **Euler deconvolution of magnetic total field data from the helicopter borne measurements at Simpevarp (in Swedish)**

#### **English summary**

Euler Leonhard (1707-1783) was a Swiss mathematician who did most of his work in St Petersburg. Together with Lagrange he developed the modern mathematics. He also presented papers in mechanics, physics, astronomy, optics, music and navigation.

PC hardware and software development in recent years and the implementation of fast Fourier transform has made it possible to use some of Euler's theoretical work to evaluate potential field data in practice. These solutions probably provide a unique opportunity to study the magnetic data on a routine basis to get objective information strictly correlated to the potential fields. The interpretations can use eighteen century theoretical papers and use these algorithms with the twenty-one century hardware and software.

Thompson D. T. (1982), has implemented Euler's theory for 2D, and Reid A.B. et al. (1990), for 3D. Both articles present many excellent examples.

Euler 3D Deconvolution is a method that makes rapid depth estimations from magnetic and gravity data in grid form using Euler's homogeneity equation. Structural indexes can be used for many various geological situations. "A sill edge, dike, or fault with limited throw is best displayed at an index of 1.0, while a fault with large throw may be best displayed at a zero index" (Reid A.B. et al. 1990).

"Although the structural-index approach to source description does not include irregular boundaries, each solution employs only data within its window, so that irregular sill-like bodies can be well delineated by the Euler method with a index of 1.0, while irregular contacts are well shown with a zero index" (Reid A.B. et al. 1990)

Reproducible and objective solutions, insensitive of magnetic inclination and declination and remanent magnetisation, these Euler solutions provide a powerful tool for analysing the magnetic measurements with the possibility to vary the grid cell size and the window size, which gives opportunities to study different structure sizes. There often are immense aliasing problems with sparse data such as geological structure data of various kinds. Euler 3D Deconvolution is a way to get objective reproducible "structures", with some reasonable constraints, directly from quality potential field data.

The program module, Euler 3D Deconvolution from Geosoft inc, has been used for these dense magnetic data. The OASIS montaj™ terminology and column names are used. To be able to relate the depth solutions to the sea level, we used the airborne radar altimeter showing ground clearance and a topographic model based upon the digital 10 m elevation database, and thus a few columns are added in the ASCII-files.

The various structure indexes, grid cell sizes and window sizes are presented in detail in the Appendix A (in Swedish). The files are listed accordingly to the SKB activity plan AP PS 400-03-10. The results are presented as ASCII-files (Geosoft XYZ-files) and

arcview-tif files. The magnetic data are processed as described in the Application Notes (below) and in chapter 4.1.3, Table 4-4 (main report). A few examples are displayed in Figures 4-5 – 4-7 (main report).

One disadvantage with the numerous Euler solutions is the necessity to discriminate solutions. The main discriminating factor has been only to allow solutions that fall within 3 grid cell sizes from the calculating window. The chosen limit of the error of the depth is 15%.

The 3D visualisation of the many, often more than  $10^6$  Euler solutions, demand a visualisation platform of very good quality. The examples shown in Figures 4-5 to 4-7 (main report) are only fractions of the data sets adjusted for this project.

### **Application Notes from Geosoft Inc**

The apparent depth to the magnetic source is derived from Euler's homogeneity equation (Euler deconvolution). This process relates the magnetic field and its gradient components to the location of the source of an anomaly, with the degree of homogeneity expressed as a “structural index”. The structural index (SI) is a measure of the fall-off rate of the field with distance from the source.

Euler's homogeneity relationship for magnetic data can be written in the form:

$$(x - x_0) \frac{\delta T}{\delta x} + (y - y_0) \frac{\delta T}{\delta y} (z - z_0) \frac{\delta T}{\delta z} = N(B - T)$$

where:

$(x_0, y_0, z_0)$  is the position of the magnetic source whose total field ( $T$ ) is detected at  $(x, y, z)$ .

$B$  is the regional magnetic field.

$N$  is the measure of the fall-off rate of the magnetic field and may be interpreted as the structural index (SI).

The Euler deconvolution process is applied at each target. The method involves setting an appropriate SI value and using least-squares inversion to solve the equation for an optimum  $x_0$ ,  $y_0$ ,  $z_0$  and  $B$ . As well, a square window size must be specified which consists of the number of cells in the gridded dataset to use in the inversion at each selected target location. The window is centred on each of the target locations. All points in the window are used to solve Euler's equation for target depth, inversely weighted by distance from the centre of the window. The window should be large enough to include each target anomaly of interest in the total field magnetic grid, but ideally not large enough to include any adjacent anomalies.

### *Target type*

This defines the target type used in the Euler deconvolution procedure. Mathematically, this parameter (also called "structural index") is a measure of the rate of change of the magnetic anomaly strength with distance from the target.

The following is a list of magnetic bodies with the structural indices:

Magnetic ordnance	3
magnetic sphere	3
magnetic barrel	3
Magnetic ordnance	2.7
Magnetic projectile	2.5
Magnetic cylinder	2
magnetic pipe	2
Magnetic sheet	1
Magnetic sill	1
Magnetic step	0.5
Magnetic contact	0

### *Instrument height*

Enter the instrument sensor height above the ground, in the same units as the X-Y coordinate system. Apparent depths will be reported as depth below ground (in the same units) by subtracting this height from the calculated distance of the sensor to the magnetic sources.

## A.1 Tolkning Helikoptergeofysik

**Leif Kero. Juni 2003. Sveriges Geologiska Undersökning (SGU). Rapport 08-541/2003.**

Tolkning av helikoptergeofysik, magnetiska data, har utförts med Euler dekonvolution på en låghöjdsmätning över Simpevarpsområdet enligt aktivitetsplan AP PS 400-03-10.

Detaljerade höjddata med ett rutnätsmönster på 10 m har erhållits för området och används vid dekonvolveringen.

Programvara för bearbetningarna som används är Oasis Montaj<sup>TM</sup>.

Datafiler som levereras 030611 i form av en CD med en winzip-fil **Slutleverans\_SKB.zip** på 105 537 kB. Det motsvarar 1,47 GB i ej komprimerad form. Papperskopior i A4 är uttagna för de olika variablerna.

Ingående filer är nedanstående:

Grid\_Mag\_Euler\_0\_10x10\_100mgrd.tfw  
Grid\_Mag\_Euler\_0\_10x10\_100mgrd.tif  
Grid\_Mag\_Euler\_0\_10x10\_100mgrd.XYZ  
Grid\_Mag\_Euler\_0\_20x20\_100mgrdup500m\_flyghojd.tfw  
Grid\_Mag\_Euler\_0\_20x20\_100mgrdup500m\_flyghojd.tif  
Grid\_Mag\_Euler\_0\_20x20\_100mgrdup1000m\_flyghojd.tfw  
Grid\_Mag\_Euler\_0\_20x20\_100mgrdup1000m\_flyghojd.tif  
Grid\_Mag\_Euler\_0\_20x20\_100mgrdupp500m\_flyghojd.XYZ  
Grid\_Mag\_Euler\_0\_20x20\_10mgrd\_ns.tfw  
Grid\_Mag\_Euler\_0\_20x20\_10mgrd\_ns.tif  
Grid\_Mag\_Euler\_0\_20x20\_10mgrd\_ns.XYZ  
Grid\_Mag\_Euler\_0\_20x20\_25mgrd.tfw  
Grid\_Mag\_Euler\_0\_20x20\_25mgrd.tif  
Grid\_Mag\_Euler\_0\_20x20\_25mgrd.XYZ  
Grid\_Mag\_Euler\_0\_3x3\_100mgrd.tfw  
Grid\_Mag\_Euler\_0\_3x3\_100mgrd.tif  
Grid\_Mag\_Euler\_0\_3x3\_100mgrd.XYZ  
Grid\_Mag\_Euler\_0\_3x3\_100mgrdup500m\_flyghojd.tfw  
Grid\_Mag\_Euler\_0\_3x3\_100mgrdup500m\_flyghojd.tif  
Grid\_Mag\_Euler\_0\_3x3\_100mgrdup1000m\_flyghojd.XYZ  
Grid\_Mag\_Euler\_0\_3x3\_100mgrdupp500m\_flyghojd.XYZ  
Grid\_Mag\_Euler\_0\_3x3\_10mgrd\_ns.tfw  
Grid\_Mag\_Euler\_0\_3x3\_10mgrd\_ns.tif  
Grid\_Mag\_Euler\_0\_3x3\_10mgrd\_ns.XYZ  
Grid\_Mag\_Euler\_0\_3x3\_10mgrd\_sn.tfw  
Grid\_Mag\_Euler\_0\_3x3\_10mgrd\_sn.tif  
Grid\_Mag\_Euler\_0\_3x3\_10mgrd\_sn.XYZ  
Grid\_Mag\_Euler\_0\_3x3\_25mgrd.tfw  
Grid\_Mag\_Euler\_0\_3x3\_25mgrd.tif  
Grid\_Mag\_Euler\_0\_3x3\_25mgrd.XYZ  
Grid\_Mag\_Euler\_1\_20x20\_10mgrd\_ns.XYZ  
Grid\_Mag\_Euler\_1\_3x3\_25mgrd.tfw

Grid\_Mag\_Euler\_1\_3x3\_25mgrd.tif  
Grid\_Mag\_Euler\_1\_3x3\_25mgrd.XYZ  
Grid\_Mag\_Euler\_2\_20x20\_25mgrd.tfw  
Grid\_Mag\_Euler\_2\_20x20\_25mgrd.tif  
Grid\_Mag\_Euler\_2\_20x20\_25mgrd.XYZ  
Grid\_Mag\_Euler\_3\_20x20\_25mgrd.tfw  
Grid\_Mag\_Euler\_3\_20x20\_25mgrd.tif  
Grid\_Mag\_Euler\_3\_20x20\_25mgrd.XYZ  
Grid\_Mag\_Euler\_05\_3x3\_100mgrd.tfw  
Grid\_Mag\_Euler\_05\_3x3\_100mgrd.tif  
Grid\_Mag\_Euler\_1\_20x20\_10mgrd\_ns.tfw  
Grid\_Mag\_Euler\_1\_20x20\_10mgrd\_ns.tif

Förteckning och beskrivning av delprojektets genomförande av de Euler dekonvolutionfiltreringar som utförts följer nedan.

Den terminologi som beskrivs i kvalitetsdokumentet har använts i redovisningen för både ASCII- och arcview-tif-filer i form av nedanstående uttryck:

#### **Grid\_Mag\_Euler\_strukturindex\_fönsterstorlek\_rutnätsmönsterstorlek\_flygriktning** (flygriktning endast för 10 metersdata)

Kolumnnamnen ingår och data är avgränsade med kommatecknen i ASCII-filerna för att man skall kunna återskapa filerna till valfri digital plattform. De redovisade värdena är relaterade till havsytan som nollvärde och djup med den lägesnoggrannhet och höjdregistrering som föreligger, d.v.s. en 3D-representation. För att försöka kunna redovisa strukturer på större djup har skapats ett raster med bildcellsstorleken 25 samt 100 m och användning av analysfönsterstorlekarna på 3x3, 10x10 och 20x20 bildceller för att framhäva olika stora våglängder.

Då Euler dekonvolution är okänslig för magnetisk inklination, deklination och remanens är den mycket lämplig för denna typ av analyser i 3D.

##### **A.1.1 Beskrivning av kolumnnamnen i ASCII-filerna**

**Neg\_depth** har multiplicerats med -1 för att få negativa värden under havsytan. Djuplösningarna till det valda magnetiska strukturindex i Oasis Montaj™ kommer under kolumnen **Depth** och utgörs av positiva tal.

**Xoff\_30** eller **xoff\_75** och **xoff\_300** har valts för de olika fönsterstorlekarna 10, 25 och 100 m respektive. Det begränsar de lösningar som erhålls till de aktuella fönstren för beräkningarna och tar bort de som ligger utanför det aktuella beräkningsfönstret. Samtliga dessa data finns redovisade i **X\_offset** och **Y\_offset**. Kvalitetsinformationen för lägesnoggrannheten i horisontalplanet finns under kolumnen **dXY**.

Den högsta tillåtna feltoleransen för djupet i djupuppskattningarna är satt till 15%. Dessa felnivåer finns under kolumnen **dZ**.

Läget av lösningarna finns med respektive koordinat i **X\_euler** och **Y\_euler**. Aktuellt beräkningsfönster finns i **X\_Window** och **Y\_Window**. Fönsterstorleken visas under kolumn **WndSize**. **Flygh\_diff\_2** är en korrektion av flyghöjdens avvikelse från nominella 60 m. Hälften av höjdskillnaden mellan verlig flyghöjd och den nominella

har använts för att korrigera Eulerlösningarna (Jacobsen 1987, Pedersen 1991). Den kolumn som har använts för de manuella sorteringsarna är **Mask**.

Ett raster har skapats baserat på flyghöjdsinformation från helikoptermätningen. Från detta raster har erhållits den flyghöjd som föreligger för den koordinat som varje enskilda Eulerlösning erhållit vid beräkningarna. Resultatet är sparad under kolumn **flyghöjd**. Oasis Montaj™ ”sample a grid”-kommando har använts för denna flyghöjdsrasterbild. Denna metodik har även använts för LMV:s höjddata och resultatet finns i kolumn **höjddata**.

**Hoh** är förkortning för höjd över hav och lösningarnas läge i djupled beräknas genom formen  $hoh = hojddata + flygh\_diff\_2 + neg\_depth$ . Därefter har **Xoff\_3xx** och **Yoff\_3xx** använts för att begränsa antalet lösningar och öka kvaliteten på de redovisade lösningarna. Tre gånger aktuell rutmönsterstorlek har genomgående använts för att avgränsa det område som lösningen måste hamna inom för att godkännas. Det har gett den slutliga lösningsmängden i kolumnen med namn **hoh\_xoffyoff\_fönsterstorlek i meter** som är den redovisade mängden träffar med läge och djup i förhållande till havsytans nivå.

### Rasterbilder i Arcview\_tif

Arcview\_tif har skapats med en upplösning på 200 dpi vilket ger filer på drygt 60 MB. Bilderna är framtagna för skalan 1: 20 000 enligt förutsättningarna för projektet. En papperskopia i A4-format för de bifogade ArcView-tif-filerna bifogas.

#### A.1.2 Arbetsmomenten i detalj

Den nedanstående tekniska beskrivningen av genomförandet av projektet måste av nödvändighet bli relativt detaljerad. Till en del är det beroende på utgångsmaterialet som medförde att de nordsydliga och sydnordliga flygrikningarna fick bearbetas separat för genereringen av 10 meters rutnätsmönster, men bearbetningen blev allt mer omfattande allt eftersom alternativa metoder testades för att försöka generera läget och djupet av magnetiska strukturer på större djup. Rutnätsgenerering av ursprungsmaterialet från helikoptermätningen liksom komplettering av de erhållna 10 meters höjddata med mer havsyta för att kunna redovisa alla de data som genereras av Euler dekonvolution har utförts.

Projektion som arbetats i är RT90 2.5 gon V genomgående.

Reduktion till pol, rtp, med inklination 71 grader och deklination 2 grader har valts enligt förutsättningarna för samtliga använda rutnätsmönster.

Rutnätskapande bigrid (Oasis Montaj™) 10 x10 m på erhållna xyz-data har utförts. Dessa 10 m rutnätsmönster har delats upp i en nordsydlig, här med ändelsen **\_ns**, samt en sydnordlig förkortad **\_sn**. Dessa ändelser har endast använts i de levererade xyz- och arcview\_tif-filerna för 10 m rutnätsmönster. Denna uppdelning av helikoptermätningen är gjort på förslag av Sören Byström, SGU, som deltagit i den grupp som arbetat i detalj med mätningen.

Höjddata från flygmätningen visar på olika mätnivå för nordsydliga jämfört med sydnordliga flygrikningar av storleksordningen 10–15 m vid närliggande flygstråk i vissa delar. Detta kan förklara en del av nivåskillnaderna i magnetfältsdata. I princip

borde filtreringarna kunna kompensera denna skillnad i och med att flyghöjden ingår i de efterföljande beräkningarna. I vissa områden verkar så vara fallet, men även motsatsen föreligger. Även effekterna av den stora mäthöjden till mark över kraftledningarna kan inte kompenseras av Eulerbearbetningarna, vilket tydligt kan studeras i lösningarna. De ytligare träffar som erhållits vid kraftledningarna är tydligt flyghödsrelaterade trots ett försök till korrektion av verklig flyghöjd mot den beräkningshöjd som används.

Ett magnetiskt strukturindex lika med 0 har används i de flesta filtreringarna. Detta motsvaras av magnetisk kontakt. Ett antal andra strukturindex såsom 0.5, 1, 2 och 3 har för jämförelse används för några enstaka olika fönsterstorlekar. Magnetisk gång/sill motsvaras av strukturindex lika med 1. Strukturindex 2 motsvarar magnetisk pipa eller horisontell cylinder medan strukturindex=3 motsvarar en magnetisk sfär. Alltför stort index resulterar i överskattat djup och för låga index ger för grunda lösningar rent generellt. Den valda korrektionen för verklig flyghöjd ger i många fall träffar som ligger i nivå med markytan och i en del fall även över markytan, vilket indikerar att strukturindex i dessa delar är för lågt satt. Något optimalt enstaka index som tillfredsställer alla lösningar verkar ej finnas.

De strukturindex som valts, ger vid god kvalitet på lösningarna, d.v.s. när antaganden om magnetisk struktur är bra, linjära träffbilder med många träffar längs ”linjerna”. För strukturindex = 3, (magnetisk sfär), är dock en punktvis ansamling av träffar tecken på ett riktigt antagande. Även för magnetisk pipa som är en del av strukturindex = 2 är de väl centrerade punktvisa träffbilderna ett tecken på rimliga antaganden. Strukturindex = 0 har därför prioriterats för att kunna dokumentera linjära strukturer på olika djup.

Rutnätsmönsterna är valda för att erhålla djupinformation från olika djupavsnitt. De valda fönsterstorlekarna och bildcellsstorlekarna framhäver magnetiska källor på olika djup.

## Djupa strukturer

Några uppräkningar av magnetmätningen har utförts och på det resultatet har används Euler dekonvolution för att på de långvågiga frekvenserna studera de djupare och större strukturerna under det ytliga kortvågiga frekvensinnehållet.

Ett försök att få fram de djup ner till omkring en halv kilometer har utförts genom att räkna upp 100 meters rutnätsmönstret 500 m (markerat **\_100mgrdupp500**) respektive 1000m (markerat **\_100mgrdupp1000**) samt att i filtreringarna ange en nominell flyghöjd till 60 m visar tänkbara lägen och djup till de djupare liggande strukturerna anpassade till havsytans nivå. Ett par exempel på detta redovisas och då har ändelsen **\_flyghöjd** lagts till på slutet av identifikationen. Denna beräkning har endast utförts på 100m rutnätsmönstret då fönsterstorleken bör vara i denna storleksordning för att få relevanta resultat på något större och djupare strukturer (Jacobsen 1987, Pedersen 1991).

## Delmoment vid arbetet med grunddata

### 100 m rutnätsmönster.

Gridskapande bigrid 100 x 100 m ur xyz med Oasis Montaj<sup>TM</sup>

Projektionen är RT90 2.5 gon V genomgående.

Reduktion till pol, rtp, med inklination 71 grader och deklination 2 grader har valts enligt förutsättningarna Uppräkning 100m. Korrektion för att sonden är på 30 meters höjd under helikopterns höjd ger beräkningshöjd 130 m.

Beräkningshöjd 60 m har använts efter uppräkning till 1000 m och filerna med namn Grid\_Mag\_Euler 0\_100mgrdupp1000m\_flyghöjd visar resultatet.

Beräkningshöjd 60 m har använts efter uppräkning till 500 m och har genererat filerna med namn Grid\_Mag\_Euler 0\_100mgrdupp500m\_flyghöjd

#### *25 m rutnätsmönster*

Gridskapande bigrid 25 x 25 m ur xyz med Oasis Montaj<sup>TM</sup>. Projektionen är RT90 2.5 gon V genomgående.

Reduktion till pol, rtp, med inklination 71 grader och deklination 2 grader har valts enligt förutsättningarna

Uppräkning 25 m ger beräkningshöjd 55 m

#### *10 m rutnätsmönster*

Gridskapande bigrid 10x10 m ur xyz med Oasis Montaj<sup>TM</sup>.

Projektionen är RT90 2.5 gon V genomgående.

Reduktion till pol, rtp, med inklination 71 grader och deklination 2 grader har valts enligt förutsättningarna.

Beräkning av nordsydligt **\_ns** och sydnordligt **\_sn** rutnätsmönster

Uppräkning 10m. Korrektion för att sonden är på 30 meters höjd under helikopterns höjd ger beräkningshöjd 40 m.

Flyghöjdsinverkan kan spåras även i Euler-filtreringarna. Tydligast är den vid de stora kraftledningar som föreligger inom mätområdet och i lösningarna med 10 och 25 meters rutnätsmönster.

Raltm\_tot från ursprungsdata från helikoptermätningen har använts och ett rutnätsmönster har skapats. Ur denna flyghöjdsinformation har erhållits den flyghöjd som föreligger för den koordinat som varje enstaka lösning erhållit vid beräkningarna. Denna urvalsmetodik har även använts för LMV:s höjddata och resultatet finns i kolumn **højddata**. Flygh\_diff\_2 visar hälften av den lokala avvikelsen i varje punkt från den nominella flyghöjden 60 m. Trots denna halvering av avvikelsen hamnar en icke försumbar del av lösningarna över markytan, vilket visar att strukturindex = 0 vid dessa snabba flygnivåhöjningar ej är representativ för mätsituationen. Problemställningen med flyghöjdsavvikelsens betydelse vid olika strukturindex bör studeras mer i detalj om effekten skall kunna minimeras framöver.

Därefter har formeln **hoh=højddata+flygh\_diff\_2+neg\_depth** använts. En manuell reducering redovisas i kolumnen med namn **hoh\_xoffyoff\_fönsterstorlek i meter** som är den redovisade mängden träffar med läge och djup i förhållande till havsytans nivå.

## Referenser

- Thompson, D. T., 1982. EULDPH: A new technique for making computer-assisted depth estimates from magnetic data. *Geophysics*, Vol. 47, pp.31-37.
- Reid, A. B., Allsop, J. M., Granser, H., Millett, A. J., Somerton, I. W., 1990. Magnetic interpretation in three dimensions using Euler Deconvolution, *Geophysics*. Vol.55, pp.80-91.
- Jacobsen, B.H., 1987. A case for upward continuation as a standard separation filter for potential field maps. *Geophysics* 52, 1138-1148.
- Pedersen, L.B., 1991. Relations between potential fields and some equivalent sources. *Geophysics* 56, 961 - 971.

## **Appendix B**

### **Specifikationer för fortsatt arbete med tolkningsmetoder för flyg-EM data**

**Hans Thunehed, Geovista 2001. SKB, Djupförvarsteknik. SKB TD-01-12.**

#### **B.1 Inledning**

I en tidigare rapport (Thunehed, 2001) presenterades en utredning om tolkningsmetoder och kommersiellt tillgängliga program för flygmätningar med slingramssystem. slutsatsen i den rapporten var att inga tillgängliga program uppfyller de behov som SKB har för inversion av mätdata till geologiskt relevanta modeller. De grundläggande teorierna för de metoder som är av intresse är dock väl etablerade sedan flera år tillbaka. Programkod finns tillgänglig från Luleå Tekniska Universitet för flera centrala delar av de rutiner som krävs i ett tolkningsprogram.

Nedan presenteras specifikationer för ett inversionsprogram för flyg-EM data som uppfyller SKB:s behov och dessutom ett upplägg för testkörning av programmet innan det ska användas i ett skarpt läge vid platsundersökningar.

#### **B.2 Endimensionell inversion av flyg-EM data**

En av de metoder som förmodligen kommer att användas vid SKB:s platsundersökningar är elektromagnetisk mätning med slingram från helikopter. Med denna metod kan jordtäckets mäktighet och innehåll av silt och lera samt berggrundens allmänna sprickighet karteras. Dessa olika geologiska parametrar kan normalt sett inte utläsas direkt ur uppmätta parametrar utan det är nödvändigt med någon form av numerisk modellering. En sådan process där de geologiskt relevanta parametrarna beräknas i en automatisk eller semiautomatisk process kallas inversion. En enkel men ändå lämplig geologisk modell består av två eller tre horisontella lager med varierande tjocklek och resistivitet. Det understa lagret motsvarar då berggrunden som antas vara homogen inom den volym som undersöks av slingramssystemet (diameter: ca 3 till 4 gånger flyghöjden). Ovanpå detta lager ligger ett lågresistivt lager som motsvarar fuktig jord. För vanlig moräntäckt mark i Sverige är detta lager så tunt att slingramssystemet egentligen endast kan upplösa lagrets integrerade konduktans. Det översta lagret motsvarar luften mellan mätsystemet och marken och resistiviteten är därmed oändlig och tjockleken lika med flyghöjden. Om helikopterns/flygplanets altimeter inte ger tillförlitliga höjddata, på grund av t.ex. vegetation, eller om ett ej försumbart lager med torr jord finns närmast markytan kan dock lagrets tjocklek betraktas som en obekant variabel.

### B.2.1 Iterativ lösning

Den elektromagnetiska responsen för en lagrad jord till ett slingramssystem med horisontella koplanara ramar kan skrivas som en Hankelintegral (Wait, 1982):

$$H_{zz} = \frac{R^3}{\delta^3} \cdot \int_0^\infty \bar{R}(g) g^2 \cdot e^{-gA} \cdot J_0(gB) \cdot dg \quad (1)$$

där

$R$  = ramavstånd,  $\delta$  = skindjup i översta lagret,  $A = 2h/\delta$ ,  $h$  = flyghöjd (inkl ev. torrjordslager),  $B = R/\delta$ .  $R(g)$  är en funktion som beror av modellparametrarna och den kan beräknas med en rekursionsformel.  $J_0$  är en Bessel-funktion av ordning 1. Motsvarande integraler för andra ramgeometrier som t.ex. vertikala koaxiala ramar kan hittas i Wait (1982). Integralen i ekvation (1) kan beräknas effektivt med digitala filter (Ghosh, 1971a; 1971b). För flygmätningar kan förenklingar göras av ekvation (1) som ytterligare snabbar upp beräkningarna (Mundry, 1984).

Vid flygmätning kommer ett antal mätvärden att produceras för varje mätpunkt:

$$V_i = V_i(f_i, R_i, tx_i, rc_i) \quad (2)$$

Varje mätvärde är alltså en funktion av fältets frekvens ( $f$ ), ramavstånd ( $R$ ) och sändarens ( $tx$ ) respektive mottagarens ( $rc$ ) orientering. För varje mätfrekvens erhålls real- och imaginärkomponent av sekundärfältet, d.v.s. två mätvärden. Anta att det totala antalet mätvärden i en punkt är  $M$ . Om inga speciella villkor ställs på modellen måste då antalet modellparametrar,  $N$ , vara mindre än eller möjligent lika med  $M$ . I praktiken bidrar flera mätvärden mycket lite till problemets lösning beroende på att mätfrekvensen är för låg för att ge mätbara sekundärfält, eller för att två ramkonfigurationer med ungefär samma frekvens inte ger någon extra information för en endimensionell modell. En trelagermodell där luften får utgöra det översta lagret (med "okänd" flyghöjd) har fyra modellparametrar ( $N=4$ ):  $p_1 = h$ ,  $p_2 = t_1$ ,  $p_3 = \rho_1$ ,  $p_4 = \rho_2$ . Det vattenmättade jordlagret har alltså resistiviteten  $\rho_1$  och tjockleken  $t_1$  medan berggrunden har resistiviteten  $\rho_2$ . För ett mätsystem med fem frekvenser ( $M=10$ ) innebär det att det formellt sett finns underlag för att bestämma modellparametrarnas värden eftersom  $M > N$ . Av flera skäl är det vettigt att uttrycka modellparametrarna i logaritmisk skala, t.ex.  $p_2 = \ln(t_1)$ . Bland annat medför det att man tvingar alla parametrar att anta positiva värden.

Vi ansätter nu en startlösning för problemet genom att tilldela elementen i vektor  $p$  rimliga startvärden. Med hjälp av ekvation (1) beräknar vi sedan en teoretisk respons:

$$H_i = H_i(f_i, R_i, tx_i, rc_i, p) \quad (3)$$

Vår målsättning är nu att minimera summan:

$$\sum_{i=1}^M \frac{(V_i - H_i)^2}{\sigma_i^2} = \sum_{i=1}^M y_i^2, \quad \underline{y} = (y_1, y_2, \dots, y_M) \quad (4)$$

Eftersom mätvärden kan vara av varierande kvalité normeras vi med variansen  $\sigma^2$ . Vi Taylorutvecklar ekvation (3) med avseende på modellparametrarna och trunkerar serien efter de linjära termerna:

$$H(p + \Delta p) \approx H(p) + B\Delta p \quad (5)$$

B är en matris som innehåller partiella derivator av fältet med avseende på modellparameterna:

$$b_{ij} = \frac{\partial H_i}{\partial p_j} \quad (6)$$

Vi normerar B radvis med variansen på mätdata och får då matrisen A. Minstakvadratlösningen på problemet blir då (t.ex. Inman et al., 1973; Inman 1975):

$$\Delta p = (A^T A)^{-1} A^T y \quad (7)$$

Lösningen  $\Delta p$  utgör en korrektionsvektor som adderas till modellen. Processen upprepas tills en acceptabel lösning erhållits. Ekvation (7) kan antingen lösas med någon vanlig matrisinversionsmetod som t.ex. Cholesky dekomposition eller så kan SVD-metoden användas (t.ex. Johanssen, 1977). I de flesta fall måste lösningen stabiliseras för att processen ska konvergera. SVD-metoden ger som extra resultat en möjlighet att bestämma ett konfidensintervall för de beräknade modellparametrarna.

### B.2.2 A'priori data

Det är inte säkert att resultaten från den inversionsprocess som beskrivs ovan är geologiskt rimlig. Mätfel eller avvikelse från den endimensionella modellen kan få som resultat att någon modellparameter antar orimliga värden. Metoden medger dock att datavektorn V förlängs med andra typer av data (Nissen, 1996; Thunehed, 2000). Det går t.ex. att utnyttja information från andra geofysiska metoder, parametermätningar, borrning eller fältobservationer. Vektorn y måste givetvis också förlängas och dessutom läggs en extra rad till i matrisen A. Ett exempel skulle kunna vara att värdet på jordlagrets tjocklek är känt från en geoteknisk undersökning. Låt oss säga att värdet är 5 m men att den aktuella modellen har ett värde på  $t_1$  som är 4 m. Det innebär att vi lägger till följande:

$$A_{i2} = 1, A_{i1} = A_{i3} = A_{i4} = 0, y_i = \ln(5) - \ln(4)$$

Dessa värden ska dessutom normeras med en uppskattad varians. Det innebär att modellvärdet inte låses utan att lösningen kommer att anpassa sig efter den extra informationen på samma sätt som till övriga mätdata. Om a'priori data baserar sig på observationer en bit ifrån flyglinjen kan alltså variansen sättas till ett högre värde och därmed viktas informationen ned relativt flygmätningarna.

## B.3 Övrig databearbetning

### B.3.1 Nivå- och faskorrigering

Eftersom svensk berggrund i allmänhet är högresistiv kommer de uppmätta sekundärfälten med ett slingramsystem att bli mycket svaga. Det är därför av yttersta vikt att nivå- och fasfel minimeras så långt som möjligt för att inversionen ska ge meningsfulla resultat. Deszcz-Pan et al. (1998) presenterade en metod där stödpunkter på marken utnyttjades för att uppskatta nödvändiga korrektioner. Horisontellt lagrade modeller baserade på inversion av markbaserad geofysik tas fram. Den förväntade responsen för flyg-EM systemet beräknas sedan med ekvation (1). Nivå- och fasfelen för ett flygpass bestäms sedan genom att söka ett minstakvadratfel mellan korrigerade mätdata över stödpunkterna och syntetiska data baserade på modellerna. Vid platsundersökningarna kommer det förmodligen inte att vara möjligt att ha tillräckligt många stödpunkter i mätområdena för att möjliggöra denna typ av beräkning för varje flygpass. Istället föreslås ett förfarande där stödpunkterna läggs längs några väl utvalda tielines. Noggranna korrektioner kan fås längs dessa linjer och korrigerade mätdata kan användas som sekundära stödpunkter vid skärningen med ordinarie flyglinjer. Dessutom föreslås att stödpunkter överflygs i början och slutet av varje flygpass.

### B.3.2 Pseudo-lager modell

Ett populärt sätt att presentera elektriska och elektromagnetiska mätningar är att beräkna en skenbar resistivitet. För de elektriska metoderna är processen trivial. För elektromagnetiska mätningar finns dock inga entydiga lösningar om inte vissa antaganden görs. För flygslingramdata beräknas ofta den skenbara resistiviteten med den s.k. pseudo-lagermetoden (Fraser, 1978). Mätdata för en viss frekvens anpassas till beräknad respons för ett homogent halvrum. Resistiviteten och avståndet till halvrummet väljs så att responsen överensstämmer med uppmätta data. Beräkningarna sker enklast genom interpolation i en tvådimensionell tabell av förberäknade responser. Såvida inte marken är homogen kommer avståndet till halvrummet, d.v.s. den skenbara flyghöjden, inte att överensstämma med den verkliga flyghöjden. Om den flyghöjd som mäts upp med altimetern subtraheras från avståndet så får tjockleken av ett pseudo-lager, d.v.s. ett fiktivt lager som överlagrar det antagna homogena halvrummet. Om resistiviteten ökar med djupet, vilket är normalt i svensk geologi, kommer pseudolagrets tjocklek att vara negativ.

En fördel med pseudo-lagermetoden vid beräkning av skenbar resistivitet är att inga antaganden om flyghöjd behöver göras. Uppmätt höjd med radaraltimeter kan vara påverkad av tät vegetation. En nackdel med pseudo-lagermetoden är dock att både real- och imaginärkomponenten måste användas. För låga mätfrekvenser är signal-brusförhållandet mycket dåligt för realkomponenten om markens resistivitet är hög. Alternativa sätt att beräkna skenbar resistivitet finns som bara utnyttjar den ena av real- och imaginärkomponenterna. En variant som kan komma ifråga är polynomanspassning (Thunehed, 2000).

Den beräknade tjockleken av pseudo-lagret kan användas för att kontrollera datakvalitén. Om mätningar görs över ett större område med inget eller endast tunt jordtäcke och inga större sprickzoner bör ett homogent halvrum vara en god modell av verkligheten. Över ett sådant område bör då den skenbara tjockleken av pseudo-lagret vara lika med noll. Det är dock knappast lämpligt att basera någon form av automatisk

nivåkontroll på denna metod eftersom det trots allt kan förekomma inhomogeniteter i bergmassan som gör att pseudo-lagrets tjocklek avviker från noll.

### B.3.3 Parasektioner

De olika frekvenserna i ett flygslingramssystem har olika djupnedträngning i marken. I de nyaste helikopterburna systemen används mätfrekvenser på över 100 kHz och frekvenser på flera tiotal kHz har använts länge. Den skenbara resistivitet som beräknas för dessa höga frekvenser är representativa för små djup under markytan. De längsta frekvenserna i mätsystemen brukar vara lägre än 1 kHz vilket medför ett betydligt större undersökningsdjup. Undersökningsdjupet är dock alltid en funktion av resistivitetsfördelningen i marken. Sengpiel (1988) och Sengpiel & Siemon (2000) har presenterat metoder för att beräkna djupet till en s.k. centroid som kan ses som en tyngdpunkt för undersökningsvolymen för varje mätfrekvens. Om den skenbara resistiviteten ritas upp som funktion av centroiddjup längs en flyglinje fås en vertikalsektion som motsvarar de pseudosektioner som är mycket populära vid markbaserad elektrisk mätning. I litteraturen benämns dessa sektioner ofta parasektioner eller CDI (conductivity-depth image). Parasektioner bör vara möjliga att framställa från flygmätningar inom platsundersökningarna. Vissa problem kan dock uppstå i högresistiva områden eftersom mätsignalen där kan ligga under brusnivån för de längsta frekvenserna vilket medför att det inte går att beräkna en skenbar resistivitet med god noggrannhet.

## B.4 Specifikationer för programvaruutveckling

I flödesschemat i Bilaga 1 visas ett förslag på arbetsgång för bearbetning av flyg-EM data till kartor i form av rasterfiler för uppmätta fältkomponenter, skenbar resistivitet, skenbar flyghöjd, parasektioner, jorddjupets tjocklek och resistivitet samt berggrundens resistivitet. Schemat är uppdelat i aktiviteter (rektanglar) och datamängder (parallellepipeder). En uppdelning av datamängderna kan dessutom göras i indata och data som produceras i denna process. Ett antal aktiviteter är markerade med feta linjer. För dessa finns ingen färdigutvecklad programvara och därför kommenteras de extra utförligt nedan.

### B.4.1 Indata

Numreringen nedan refererar till motsvarande nummer i Bilaga 1.

1. Rådata (EM) från flygning. Vid flygmätningarna mäts real- och imaginärkomponenten för sekundärfälten upp. Grundläggande bearbetning av dessa data utförs av det företag som utför mätningen. Rådata ska dock vara tillgängliga för kontroll av t.ex. nollnivåavslutningar vid uppstigning till hög höjd (se även: Metodbeskrivning för flygmätning).
2. Digital terrängmodell (50\*50 m). Data från Lantmäteriverkets nationella databas för terränghöjder. Data ska finnas tillgängliga i Geosoft binärt grid-format för hela mätområdet. Dessa data kan ersättas med andra data med högre noggrannhet om sådana finns tillgängliga.
3. Altimeter- och barometerdata från flygning. Mätsystemets höjd över marken behövs som indata för beräkning av syntetiska resoner samt som a' priori data

vid inversionen. Data ska finnas tillgängliga i Geosoft XYZ-format. I första hand används värden från radaraltimeter men om denna påverkas av tät vegetation kan skillnad mellan barometerhöjd och interpolerad höjd från den digitala terrängmodellen användas.

4. **Rådata från elektrisk sondering.** Elektrisk sondering utförs på kontrollpunkter för slingramens nollnivå samt på stödpunkter för inversionen. Mätningen utförs med modifierad Schlumberger-konfiguration (Thunehed, 2000) i två riktningar. Kontrollpunkter läggs längs tie-lines i öppen terräng och där inga större sprickzoner förväntas. Dessutom ska kontrollpunkter finnas tillgängliga för överflygning i början och slutet av varje mätpass. Sonderingsdata sparas i ASCII-tabellformat (För varje avläsning: RT90 X- och Y-koordinater för samtliga elektroder, uppmätt potentialskillnad alternativt kvoten mellan potentialskillnad och utsänd ström, utsänd strömstyrka och uppskattad relativ mätnoggrannhet).
5. **Rådata från X-konfigurationsmätning.** X-konfigurationsmätningar (Thunehed, 2000) utförs för att uppskatta berggrundens bulkresistivitet samt dess anisotropi. Även dessa resultat används som stödpunkter för inversionen. Data sparas i samma format som sonderingsdata.
6. **Information från borrhål, hällkartor mm.** Andra datakällor som kan ge information om jorddjup, jordlagrets resistivitet och berggrundens resistivitet bör utnyttjas som stöd i inversionen. För hällområden kan jorddjupet sättas till noll. Informationen sammanställs i en ASCII-tabellfil med uppgift om RT90 X- och Y-koordinat, värde för  $t_1$ ,  $\rho_1$  och  $\rho_2$  (eventuellt nullvärde för vissa parametrar) samt källa.

#### B.4.2 Producerade data

1. **Bearbetade data (grundläggande bearbetning).** I samband med flygmätningen görs vissa grundläggande bearbetningar av data. Nollnivåjusteringar baserade på uppstigning till hög höjd görs. Dessutom beräknas koordinater i RT90 för mätpunkterna. Data sparas i Geosoft XYZ format (se även: Metodbeskrivning för flygmätning).
2. **Kontroll- och stödpunkter.** Alla uppgifter om jordtäckets och berggrundens bulkresistivitet samt jordtäckets tjocklek samlas i en ASCII tabellfil för att senare sammanställas till a'priori information för inversionen. I tabellen ska ingå: RT90 X och Y-koordinat, resistivitet och tjocklek på jordtäcket (eller null-värde), berggrundens bulkresistivitet (eller null-värde), mätmetod samt källa. De punkter som har uppgifter om samtliga parametrar används som stödpunkter för fas- och nivåkorrektioner.
3. **Syntetiska data för stödpunkter.** För alla stödpunkter som ska användas för fas- och nivåkorrektioner sparas beräknade syntetiska data. Ett individuellt värde lagras för varje överflygning eftersom flyghöjden kan variera. Data lagras i en ASCII tabellfil innehållande: RT90 X- och Y-koordinat, datum, tid, beräknad real- och imaginärkomponent för samtliga ramgeometrier och frekvenser samt en flagga som indikerar om det rör sig om en primär eller sekundär stödpunkt.

4. Nivåkorrigrade data. Data som nivåkorrigeras med hjälp av stödpunkter lagras i Geosoft XYZ-format.
5. Rasterfiler av Re- och Im-komponenter. Interpolerade rasterfiler lagras i Geosoft binärt grid-format med en fil för varje fältkomponent. Maskvidden i rastret bestäms senare men kan typiskt vara 50\*10 m. Dessa rasterfiler lagras i SICADA. Kartor plottas i t.ex. skala 1:20000.
6. Rasterfiler av skenbar resistivitet och flyghöjd. Skenbar resistivitet och flyghöjd beräknad med pseudolagermetoden lagras i Geosoft binärt-gridformat. Maskvidden är densamma som för Re- och Im-komponenter. Filerna lagras i SICADA och kartor plottas i t.ex. skala 1:20000.
7. Parasektioner. Parasektioner framställda enligt Sengpiels (1988) metod eller motsvarande lagras i Geosoft binärt grid-format. Filerna lagras i SICADA.
8. A'priori data. A'priori information om modellparametrar för inversionen lagras i Geosoft binärt grid-format. En rasterfil för varje modellparameter samt en tillhörande rasterfil med uppskattad varians för respektive parameter.
9. Rasterfiler med jorddjup och resistiveter. Resultatet av inversionen lagras i Geosoft binärt grid-format med samma maskvidd som indata (Re- och Im-komponenter). Filerna lagras i SICADA.

#### B.4.3 Aktiviteter

1. Grundläggande databearbetning. Den grundläggande databearbetningen utförs av den organisation som utför flygmätningen i samband med mätningen. I bearbetningen ingår korrigering av nollnivån med hjälp av uppstigning till hög höjd samt eventuellt borttagning av spikar och igenfyllning av saknade data med interpolerade värden. Originaldata ska dock levereras för att alla bearbetningar ska kunna rekonstrueras (se även: Metodbeskrivning för flygmätning).
2. Inversion till lagrad modell. Data från elektriska sonderingar inverteras till horisontellt lagrade modeller med hjälp av t.ex. programmet 4Pole från Luleå Tekniska Universitet. Antalet lager i modellen bör helst vara högst tre (torr jord, våt jord, berg). Resultaten från de två mätriktningarna vägs samman till en modell. Resultatet sparas i en ASCII-fil innehållande RT90 X- och Y-koordinat, lagerparametrar, mätmetod och namn på indatafil. Om avvikelserna från en horisontellt lagrad modell är alltför stora bör punkten inte användas i den vidare databearbetningen.
3. Inversion till anisotrop halvrum. Data från X-konfigurationsmätningar inverteras till ett homogent halvrum med vertikal anisotropi med t.ex. programmet r\_anstrp från Luleå Tekniska Universitet. Om sondering gjorts längs en av utläggets diagonaler inverteras dessa data till en lagrad jord enligt punkt 2 ovan. Resultaten sparas på samma sätt som för punkt 2. Om anisotropoefficienten blir hög bör resultaten från inversionen av flygdata nedan tolkas med viss försiktighet.
4. Sortera information från borrhål mm. Information om jorddjup från borrningar, geotekniska undersökningar, refraktionsseismik, markradarmätningar mm ställs samman. Uppgifter om hällområden eller områden med mycket tunt jordtäcke

hämtas in från geologiska eller topografiska kartor. Resultaten ställs samman enligt punkt 2 där resistiviteterna sätts till ett null-värde. Jordtäckets tjocklek sätts till noll för hällområden.

5. Beräkning av syntetiska data. Syntetiska data för stödpunkter som ska användas till fas- och nivåkorrigering beräknas. Inversionsmodellerna från de elektriska sonderingarna används som indata och sekundärfälten för samtliga ramgeometrier och frekvenser beräknas enligt ekvation (1) eller motsvarande. Eftersom resultatet är beroende av flyghöjden behövs altimeterdata från flygningen. Stödpunkterna placeras i största möjliga utsträckning i områden med öppen terräng för att altimeterdata ska vara tillförlitliga. Som reserv kan dock flyghöjden beräknas som skillnaden mellan barometerhöjd och interpolerad höjd från den digitala terrängmodellen. Eftersom flyghöjden kan variera för olika överflygningar av samma punkt beräknas syntetiska data för varje överflygning. Data sparar i en ASCII tabellfil med uppgift om RT90 X- och Y-koordinater, datum, tid, beräknade fältkomponenter samt en flagga som anger om det rör sig om en primär eller sekundär punkt.

Stödpunkterna förläggs i första hand längs tielines. Fas- och nivåkorrektioner för dessa utförs sedan enligt Desczc-Pan et al. (1998). Proceduren beskrivs under punkt 6 nedan. Korrigrade data för skärningspunkter med ordinarie flyglinjer sparar som sekundära stödpunkter. Manuell kontroll görs av dessa punkter så att skärningspunkter som ligger vid anomalier plockas bort från listan. En korrektion för eventuell skillnad i flyghöjd mellan flygning längs tielines och ordinarie flyglinjer måste göras. Förmodligen kan detta göras genom att ett höjdberoende beräknas approximativt som höjdberoendet för ett homogent halvrum med en resistivitet lika med den skenbara resistiviteten. Om detta inte fungerar kan data inverteras till en lagrad modell enligt punkt 12 nedan. Om flyghöjden skiljer kraftigt mellan flygning längs en tieline och ordinarie flyglinje över en skärningspunkt bör den dock inte användas för korrektioner.

Inget existerande datorprogram finns för beräkning av syntetiska data enligt beskrivningen ovan. Programkod för beräkning av ekvation (1) och liknande integraler finns tillgänglig från Luleå Tekniska Universitet. Den modifikation som krävs av detta program är anpassning till in- och utdata. Den arbetsinsats som krävs för detta bedöms som mycket måttlig. En förenkling av ekvation (1) kan göras för att snabba upp beräkningarna vid flygmätning (Mundry, 1984). Denna modifikation bör dock inte göras eftersom den förväntade vinsten är marginell.

6. Beräkning av fas- och nivåkorrektioner. Mätdata jämförs med beräknade syntetiska data för stödpunkter. En medelvärdesbildning av mätdata görs längs en sträcka längs flyglinjen vars längd är valbar. Fas- och nivåfel beskrivs med hjälp av fyra parametrar. Storleken av dessa fyra parametrar bestäms genom minsta-kvadratanpassning av mätdata till syntetiska data enligt Deszcz-Pan et al. (1998). Nivåfelen beräknas separat för varje flygpass medan fasfelet gäller för en hel dag. Dessutom beräknas ett förstärkningsfel som är gemensamt för hela mätningen. Korrektionerna appliceras på data och de korrigerade data sparar i Geosoft XYZ-format.

Inget datorprogram finns tillgängligt för denna bearbetning. De matematiska operationer som används i processen är dock tämligen triviala så den beräknade insatsen för att skriva ett program bedöms som måttlig. Programmet ska presentera

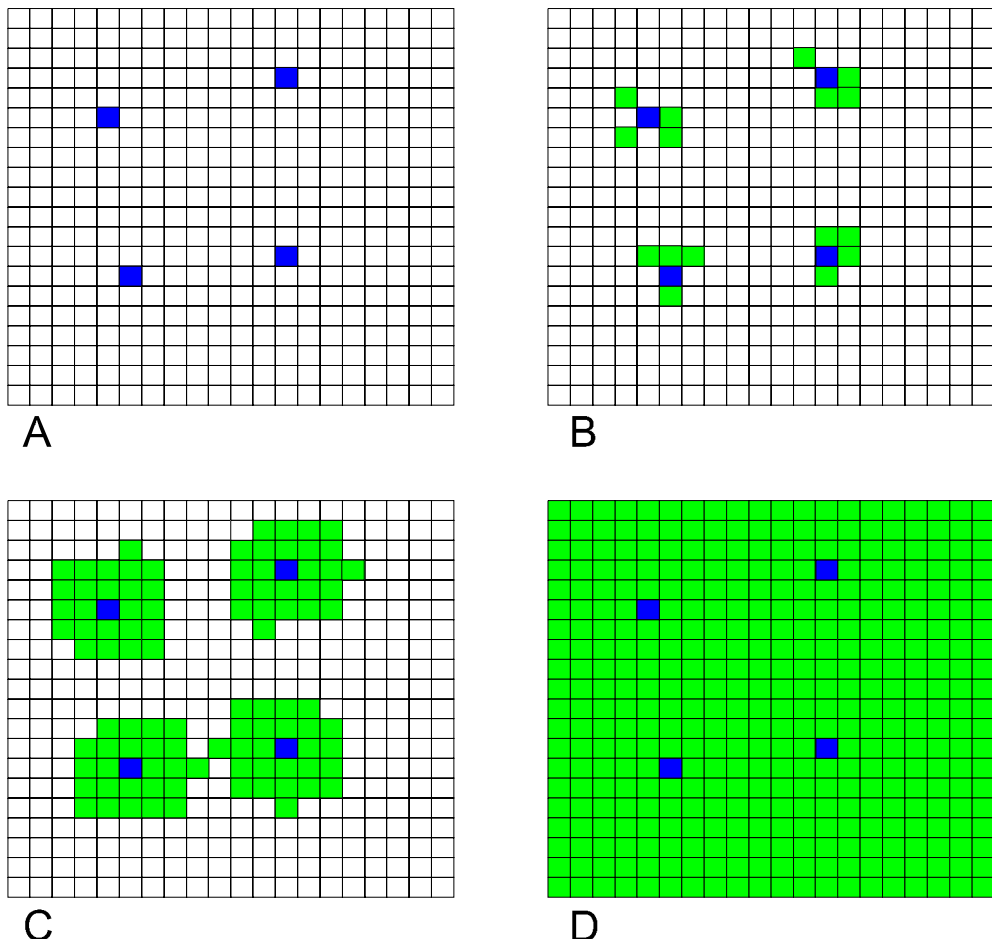
residualfelen för de olika stödpunkterna så att punkter som misstänks ge dåliga resultat kan plockas bort. Residualfelen ger dessutom en uppfattning om hur noggrann bestämningen av fas- och nivåläge är.

7. Framställning av rasterfiler. Mätdata interpoleras till ett regelbundet raster med en viss maskvidd. I denna process tas spikar bort och eventuellt görs lågpassfiltrering längs flyglinjerna. Filerna lagras i Geosoft binärt grid-format (se även: Metodbeskrivning för flygmätningar). Uppenbara nivelleringsfel kan korrigeras manuellt.
8. Beräkning av skenbar resistivitet och flyghöjd. Skenbar resistivitet och flyghöjd beräknas enligt Fraser (1978) för de olika mätfrekvenserna. Detta är ett bearbetningssteg som utförs mer eller mindre rutinmässigt av de flesta som utför flyg-EM mätningar. Någon kommersiell programvara för ändamålet har vi dock inte hittat. Beräkningarna är dock tämligen enkla och kan baseras på interpolation i tvådimensionella tabeller. Ett nytt program för ändamålet kan därför skrivas. Resultatet sparar i Geosoft binärt grid-format med samma maskvidd som indata. Filerna sparar i SICADA.
9. Framställning av parasektioner. Parasektioner kan framställas på beställning men det kan också vara rimligt att t.ex. en sektion framställs för var femte profil och sparas undan. Centroiddjup för de olika mätfrekvenserna beräknas med hjälp av formler i Sengpiel (1988) eller Sengpiel & Siemon (2000). Sektionerna i form av rasterfiler kan sedan interpoleras fram med t.ex. programmet Surfer (Golden Software). Ny programvara behöver då bara framställas för att plocka ut skenbar resistivitet ur färdiga rasterfiler och att beräkna centroiddjup med enkla metoder. Ett makro för att automatisera hanteringen med Surfer behövs också.
10. Kontroll av nivellering. Rasterfilerna med skenbar flyghöjd bör ange samma värde som den verkliga flyghöden över områden med mycket tunt jordtäcke under förutsättning att berggrundens är någorlunda homogen. Om så inte är fallet kan eventuellt en justering av nollnivån göras. Denna bör dock inte basera sig på någon automatik eftersom en manuell bedömning av nivelleringskorrektionen förmödlig är nödvändig.
11. Sammanställning av a'priori data. A'priori data för inversionen utgörs av förhandsinformation om flyghöjd, jordtäckets tjocklek och resistivitet samt berggrundens bulkresistivitet. Rasterfiler framställs där t.ex. jordtäckets tjocklek beräknas för alla rasternoder som ett vägt medelvärde av alla uppgifter om jordtäckets tjocklek inom området. Viktningen görs med hänsyn till avståndet till mätpunkter. En varians uppskattas också för varje rasternod så att a'priori information om områden som ligger långt ifrån någon mätpunkt viktas ned i den kommande inversionen. Beräkningarna kan förmödligi göras direkt i någon kommersiell programvara som t.ex. Surfer. För information om flyghöden används altimeterdata utom i de fall där man kan misstänka en påverkan från tät vegetation. I sådana fall kan skillnad mellan barometerhöjd och terränghöjd läggas in. Någon form av uppskattning av flyghöjdens varians bör göras. Där måste man också väga in att den del av jordtäcket som ligger ovanför grundvattennivån kommer att inkluderas i detta lager vid inversionen.
12. Inversion. Målsättningen med inversionen är att beräkna jorddjupets tjocklek och resistivitet samt berggrundens resistivitet i varje rasternod. Dessutom

kommer flyghöden att vara en fri parameter eftersom altimeterdata kan vara påverkade av vegetation. Eventuell torr jord närmast markytan kommer i praktiken att inkluderas i flyghöden. Trots att antalet lager i modellen är endast två (+ luften) finns det egentligen ingen anledning att begränsa programkoden till så få lager. Inversionen kommer att basera sig på en den dämpade iterativa metod som är väl beprövad för såväl elektriska som elektromagnetiska mätningar (ekvation (2) till (7); t.ex. Inman et al., 1973; Inman, 1975; Johanssen, 1977). Modellparametrarnas varians uppskattas genom att matrisinversionen utförs med Singular Value Decomposition (SVD, Johanssen, 1977).

Eftersom antalet mätfrekvenser är relativt litet i ett helikoptersystem och dessutom den förväntade signalstyrkan i många fall kommer att ligga nära brusnivån måste begränsningar sättas på modellen för att parametrarna ska vara geologiskt rimliga. Detta görs genom att a'priori geologiska data adderas till datamatrisen vid varje mätpunkt (Nissen, 1986; Thunehed, 2000). De a'priori data som används blir avståndsviktade medelvärdena av jorddjupsbestämningar och inversionmodeller från elektriska sonderingar. Medelvärdena normeras och viktas därmed med en uppskattad varians. Dessutom används uppmätt flyghöjd som a'priori data för flyghöjd + torr jord, eventuellt adderas ett litet värde. Exakt hur denna varians ska beräknas måste man förmodligen prova sig fram till med testdata. Inversionen bör inte ske rad- och/eller kolumnvis utan istället används soneringspunkter etc. som fröpunkter (Figur B4-1). Inversion görs först i dessa punkter där tillförlitliga a'priori data finns. Sedan görs beräkningar för punkter på gradvis större avstånd från fröpunkterna tills så småningom hela området är täckt. Vitsen med detta förfarande är att inversionsresultatet i en punkt kan användas dels som startlösning för nästa punkt och dessutom som a'priori data. Normering och viktning för dessa a'priori data görs då med hjälp av uppskattad varians från SVD. Totalt kommer då följande data att användas i inversionen:

- Uppmätta sekundärfält normerade med mätnoggrannhet. Viktningen av dessa data kommer alltid att vara så hög att de får en avgörande inverkan på inversionsresultatet.
- Avståndsviktat medelvärde av jorddjupsbestämningar, soneringsresultat mm. Normering sker med hänsyn till avståndet till mätpunkterna. Viktningen kommer att vara sådan att mycket liten hänsyn tas till dessa data på avstånd större än t.ex. några hundra meter.
- Medelvärde av modellparametrar för redan inverterade angränsande punkter. Viktning sker med hänsyn till uppskattad varians. Genom att använda angränsande pixlar som a'priori data fås en filtrerande effekt som undertrycker effekten av mätbrus. Viktningen får dock inte vara för kraftig i förhållande till mätdata eftersom detta kommer att sudda ut laterala variationer i t.ex. jorddjup.
- Altimeterdata (alternativt barometerhöjd – terränghöjd) används som a'priori data för flyghöjd + torr, högresistiv jord. Ett litet värde adderas som motsvarar förväntad tjocklek av jord ovan grundvattenytan. Viktning görs med hänsyn till altimeterns mätnoggrannhet och eventuellt kan data viktas ned områdesvis med hänsyn till information om vegetation.



**Figur B4-1.** I mätområdet finns ett antal punkter där jorddjup och/eller resistiviteter bestämts med andra metoder (A). Denna information används som *a'priori* data för inversionen. Punkterna används också som fröpunkter, d.v.s. dessa punkter inverteras först. Sedan inverteras närliggande punkter (B) på större och större avstånd (C) tills hela området är täckt (D).

Delar av programkoden för ett inversionsprogram finns redan tillgänglig. Beräkning av integralen i ekvation (1) kan göras med kod från Luleå Tekniska Universitet. Kod för SVD finns t.ex. i Numerical Recipes (Press et al., 1988). De partiella derivatorna i ekvation (5) till (7) måste beräknas. Detta bör göras genom att funktionen  $R(g)$  i ekvation (1) deriveras analytiskt med kedjeregeln och sedan konvolveras med ett digitalt filter. Ny kod måste skrivas för den analytiska deriveringens medan konvolveringen med filtret kan inkorporeras i beräkningen med ekvation (1). Förutom ovanstående krävs ny kod för att hantera in- och utdata samt fröpunkter. Totalt sett innebär detta viss programmeringsinsats men ändå inte större än att det skulle vara genomförbart till acceptabel kostnad.

Resultatet av inversionen sparas i Geosoft binärt grid-format. För varje parameter skapas dels ett raster med parameterns uppskattade värde och dels ett raster med den uppskattade noggrannheten. Om det visar sig att noggrannheten i någon del av undersökningsområdet är otillräcklig är det möjligt att i efterhand göra fler markbaserade mätningar för att utöka antalet kontrollpunkter.

#### B.4.4 Programkod

Den programkod som finns tillgänglig för att t.ex. beräkna ekvation (1) är skriven i ANSI Fortran77/90. All ny kod bör skrivas i samma språk. Kompilering och länkning kan ske i t.ex. MS Fortran PowerStation 4.0. Användargränssnittet bör göras så enkelt som möjligt. Förslagsvis genom att programmen framställs som konsolapplikationer. Dessa är 32-bitars program som kan utnyttja tillgängligt minne i MS Windows men som startas från kommandoraden i ett DOS-fönster. Programmen utformas för att underlätta batchkörningar.

### B.5 Förslag till testprogram

Ett antal parametrar som påverkar den metodik som beskrivs ovan är svåra att förutsäga. Det gäller t.ex. helikoptersystemets mät noggrannhet och hur denna påverkar resultaten. Alternativa modeller för att uppskatta fas- och nivåfel från stödpunkter på marken måste testas. Dessutom måste en lämplig modell för att vikta a' priori data gentemot mätdata utarbetas. För att undvika krångel vid den skarpa situationen i samband med platsundersökningen är det dessutom lämpligt att den nya programvaran testats med verkliga mätdata.

Mätningar med helikopter-EM pågår för närvarande i Jämtland. Mätningarna kommer förmödlig att slutföras någon gång under våren 2001 och i och med detta blir data tillgängliga. Vi rekommenderar därför att elektriska sonderingar görs i detta område för att kunna användas som stödpunkter. Eftersom flygmätningarna inte anpassats till stödpunkter med bl.a. val av tielines går det förmödlig inte att applicera den föreslagna metodiken fullt ut på dessa data men det bör i alla fall vara möjligt att genomföra ett test.

### Referenser

- Deszcz-Pan M., Fitterman D.V., Labson V.F., 1998.** Reduction of inversion errors in helicopter EM data using auxiliary information. Expl. Geoph. 29, 142-146.
- Fraser D.C., 1978.** Resistivity mapping with an airborne multicoil electromagnetic system. Geophysics, 43, 144-172.
- Ghosh, D.P., 1971a.** The application of linear filter theory to the direct interpretation of geoelectrical resistivity sounding measurements. Geoph. Prosp., 19, 192-217.
- Ghosh, D.P., 1971b.** Inverse filter coefficients for the computation of apparent resistivity standard curves for a horizontally stratified earth. Geoph. Prosp., 19, 769-775.
- Inman, J.R., Ryu, J., Ward, S.H., 1973.** Resistivity inversion. Geophysics, 38, 1088-1108.
- Inman J.R., 1975.** Resistivity inversion with ridge regression. Geophysics, 40, 798-817.
- Johansen, H.K., 1977.** A man/computer interpretation system for resistivity sounding over a horizontally stratified earth. Geoph. Prosp., 25, 667-691.

- Mundry, E., 1984.** On the interpretation of airborne electromagnetic data for the two-layer case: Geophys. Prosp., 32, no. 02, 336-346.
- Nissen J., 1986.** Versatile programs for geoelectromagnetic interpretations. Ph.D. thesis. Luleå University of Technology.
- Sengpiel K-P., 1988.** Approximative inversion of airborne EM data from a multilayered ground. Geoph. Prospecting, 36, 446-459.
- Sengpiel K-P., Siemon B., 2000.** Advanced inversion methods for airborne electromagnetic exploration. Geophysics, 65, 1983-1992.
- Thunehed H., 2000.** Mapping and characterisation of Swedish bedrock by DC resistivity and transient electromagnetic measurements. Ph.D. Thesis. Luleå University of Technology.
- Thunehed, H., 2001.** Inventering av elektromagnetiska tolkningsmetoder och tolkningsverktyg för flyg-EM data. SKB TD-01-11.
- Wait J.R., 1982.** Geo-electromagnetism. Academic Press Inc.

